UCLA
UCLA Electronic Theses and Dissertations

Title

Performance Evaluation Under Modeling Uncertainty: A Unified Approach Using Spherically Invariant Random Processes

Permalink

Author

Yang, Cheng-An

Publication Date

2015

Peer reviewed|Thesis/dissertation

Università of California

Los Angeles

Performance Evaluation Under Modeling Uncertainty: A Unified Approach Using Spherically Invariant Random Process

A dissertation submitted in partial satisfaction

of the requirements for the degree

Doctor of Philosophy in Electrical Engineering

by

Cheng-An Yang

2015

Abstract of the Dissertation

Performance Evaluation Under Modeling Uncertainty: A Unified Approach Using Spherically Invariant Random Process

by

Cheng-An Yang

Doctor of Philosophy in Electrical Engineering

University of California, Los Angeles, 2015

Professor Kung Yao, Chair

In this dissertation, we considered the exceedingly general spherically invariant random process (SIRP) as a unifying framework for studying the wireless communication fading channels. In addition, we studied the important issue of modeling uncertainty, where only limited knowledge of the underlying fading channel statistics is known. The moment space methodology was proposed to characterize the uncertainty range of the system performance. Since performance evaluation for wireless communication systems frequently involve Monte Carlo simulation, we introduce the Super-Efficient Monte Carlo simulation methodology and the concept of Approximate Super-Efficiency (ASE) to improve the convergence rate of Monte Carlo simulation. While conventional Monte Carlo simulation yields the convergence rate $1/N$, our Super-Efficient Monte Carlo simulation has a superior convergence rate $1/N^2$ for integrands of the Super-Efficient type, and $1/N^\alpha$ for ASE algorithm, where $\alpha \in [1,2]$. Finally, we studied the downlink throughput maximization problem in cellular networks. Inspired by the multi-armed bandit problem, we proposed several algorithms to solve the online throughput maximization problem, and provided convergence analysis. The proposed algorithms achieved up to 99% of the performance upper bound within 1000 time steps.

The dissertation of Cheng-An Yang is approved.

Henry Huang

Lieven Vandenberghe

Izhak Rubin

Kung Yao, Committee Chair

University of California, Los Angeles

2015

To my family.

TABLE OF CONTENTS

xiii

Acknowledgments

 I would like to thank my supervisor Prof. Kung Yao for his guidance and support of my PhD. Prof. Yao not only introduced me the fascinating research topics like Super-efficient Monte Carlo simulation and the moment bound problem, but also gave me lots of freedom to explore other research topics that interest me. I could not have been able to finish my study without his support.

I would like to thank my committee members, Prof. Izhak Rubin, Prof. Lieven Vandenberghe and Prof. Henry Huang, who gave me constructive comments and suggestions.

I would like to thank Dr. Ralph Hudson, who always has good ideas about how to solve difficult problems in practical manners. I admire his engineering insight greatly.

I would like to thank Prof. Ezio Biglieri and Prof. Ken Umeno. It was a great honor to co-author several papers with them. (Chapter 2 and 3 are based on our paper [1]. Chapter 4 and 5 are based on our paper [2].) I was greatly inspired by their innovative ideas and deep understanding of the field.

I would like to thank my colleagues Hung-Bin Chang, Chun-Hao Liu and Yu-Yu Lin for valuable discussions.

I would like to thank my family for their support and encouragement.

Finally, I would like to thank my wife Han-Hsin Chang, who is always by my side and be the strongest support for me.

Vita

2004–2007	B.S. (Electronic Control Engineering), National Chiao Tung University, Hsinchu, Taiwan.
2007–2009	M.Sc. (Communication Engineering), Chalmers University of Technology, Gothenburg, Sweden.
2011–2015	Ph.D. Candidate (Electrical Engineering), University of California, Los Angeles (UCLA), USA.

Publications

C.-A. Yang, K. Yao, K. Umeno, and E. Biglieri, "Using deterministic chaos for Superefficient Monte Carlo simulations," *Circuits and Systems Magazine, IEEE*, vol. 13, no. 4, pp. 26–35, 2013.

C.-A. Yang, K. Yao, and E. Biglieri, "Wireless fading communication system performance evaluations via SIRP and SDP methods," in *Signal Processing Systems (SiPS), 2013 IEEE Workshop*, pp. 7–12, IEEE, 2013.

C.-A. Yang, K. Yao, and E. Biglieri, "Modeling wireless channels under spherical invariance assumptions," in *Information Theory and Applications Workshop (ITA), 2014*, pp. 1–5, Feb 2014.

C.-A. Yang, K. Yao, and E. Biglieri, "A study on the statistical modeling of fading and its effects on system performance using SIRP and SDP methods,"

in *Acoustics, Speech and Signal Processing (ICASSP), 2014 IEEE International Conference*, pp. 4284–4288, May 2014.

C.-A. Yang, K. Yao, and E. Biglieri, "Superefficient Monte Carlo simulations," in *Simulation Technologies in Networking and Communications: Selecting the Best Tool for the Test* (S. K. Al-Sakib Khan Pathan, Muhammad Mostafa Monowar, ed.), ch. 3, pp. 69–93, CRC Press, Taylor & Francis, October 2014.

E. Biglieri, K. Yao and C.-A. Yang, "Fading models from spherically invariant processes," *IEEE Transactions on Communications*, to appear, 2015.

C.-A. Yang, and K. Yao, "A Multi-Armed Bandit Approach to Throughput Maximization in Cellular Networks," *IEEE Transactions on Communications*, to be submitted, 2015.

CHAPTER 1

Introduction

The cellular network has been one of the most successful and widely used communication technology of the past three decades. As smartphones and tablets become ubiquitous over the past several years, these mobile devices generate an explosive growth of data traffic over the cellular network not seen in previous generations. The industry estimated that there will be a thousandfold increase of mobile data traffic within 10 years. To accommodate such a challenging demand, more sophisticated data transmission schemes with high spectral efficiency is needed. Among possible solutions, including ultra-wideband (UWB) radio and massive multiple-input multiple-output systems (MIMO) has received great attention due to it's potential to serve multiple users with high data rate.

However, these new technologies also introduce new challenges. One fundamental and primary issue is the modeling of the mechanism of radio propagation channel. For example, due to the superior angular resolution of the massive-MIMO systems, there are more separable multipaths being seen by the antenna array. As a result, the energy intercepted by each angular bin decreases. Thus the usual assumption that each angular bin receives the combination of a large number of multipath contributions is no longer valid. Hence we can not invoke the central limit theorem to argue that the channel statistic is Gaussian.

The UWB channels are also fundamentally different from the conventional channels. This is because larger bandwidth results in shorter delay bins, which reduces the number of multipath components per bin. As a result, the channel

statistics is no longer governed by the central limit theorem. Since the performance of these important technologies depend critically on the underlying channel statistics, thus a flexible, reliable and versatile mathematical model is called for.

1.1   Spherically Invariant Random Process

In this dissertation, we propose the use of the exceedingly general spherical invariant random process (SIRP) as a modeling tool for various wireless communication systems. It is well known that the performance of wireless communications is strongly affected by power fades. Under various propagation scenarios, several models for the probability distribution of the fading envelope have been proposed, and are used for performance prediction and design.

Fading models may be categorized into two broad classes: those derived from physical considerations (a typical example is Rayleigh fading), and those containing a number of parameters whose values can be obtained by empirical fitting of observed data. A rich collection of fading models can be found in [3, 4], where envelope and signal-to-noise ratio distributions are shown along with the corresponding moment-generating functions.

In this dissertation we focus on a class of fading processes obtained as envelopes of a generalization of Gaussian processes which exhibit a property called "spherical invariance." Spherically Invariant Random Processes (SIRPs) inherit many analytically tractable properties from Gaussian processes. They have been advocated as relevant to the modeling of atmospheric noise, speech processes, radar clutters, impulsive noise, etc. (see, e.g., [5, 6] and references within), and most of the popular fading models turn out to be special cases of SIRPs. We aims at justifying the ubiquity of spherically invariant distributions in modeling fading effects, and advocating their use for system analysis. Among the reasons motivating their applicability are their generality, flexibility, and the fact that, under

suitable constraints, they maximize differential entropy, as it occurs for Gaussian processes under the only constraint of bounded variance. Moreover, the fact that a vast majority of fading models used in practice turn out to be special cases of SIRP models suggests some underlying structural property that SIRP processes can capture.

1.2   Model Uncertainty

From a practical point of view, even if a general statistical channel model is available, the exact set of parameters for the model may not be accurately known. This makes determining the system performance very challenging. A possible way of solving this problem is to assume a pdf belonging to the model, and analyze the performance of the system using it. This procedure carries a fundamental danger, that of not optimizing the real-life system but rather an inaccurate model of it, which occurs unless one makes sure that the optimum of the approximation is actually an approximation of the optimum.

A more reasonable approach we take here consists of determining the interval of performance parameters caused by the uncertainty in the channel model. This interval is determined by using in the calculations only the (usually limited) statistical information available about the channel model. More specifically, we use the moment space methodology to characterize the uncertainty range of the system performance. Using the SIRP decomposition, we transformed the infinite dimensional optimization problem into a univariate moment problem, which can be solved by performing a series of numerical integrations.

1.3 Super-Efficient Monte Carlo Simulation

For the purpose of performance evaluation, numerical integration is needed to evaluate complicated mathematical expressions. Monte Carlo simulation is a general technique for estimating integrals. We investigated and improves the Super-Efficient Monte Carlo methodology, which was first proposed by Umeno [7].

Monte Carlo (MC) simulation methods are widely used to solve complex engineering and scientific problems. Unlike other deterministic methods, MC methods use statistical sampling to produce approximate solutions. As the processed sample size N growths, the uncertainty of the solution is reduced. It is well known that the mean-square approximation error decreases as $1/N$. However, for large problems like high-dimensional integrations and computationally intensive simulations, MC methods may take months or even years to obtain a solution with acceptable tolerance. The Super-Efficient (SE) Monte Carlo simulation method, originated by Umeno, produces a solution whose approximation error decreases as fast as $1/N^2$. However, it only applies to a small class of problems possessing certain properties. We describe an approximate SE Monte Carlo simulation method that is applicable to a wider class of problems than the original SE method, and yields a convergence rate as fast as $1/N^\alpha$ for $1 \leq \alpha \leq 2$.

1.4 Downlink Throughput Maximization

As an application to the moment space methodology introduced earlier, we study the problem of downlink throughput maximization in cellular networks. The purpose of this study is twofold: to investigate the throughput maximization problem for mobile user equipment (UE) and find effective online algorithms to achieve the optimal performance with minimal learning cost. Specifically, we formulate the throughput maximization problem as a linear fractional program under the

independent channel condition, and derive an explicit solution for both the unconstrained and block error rate (BLER) constrained case. We propose using the Multi-Armed Bandit (MAB) approach to cleverly adjusting the Channel Quality Indicator (CQI) and maximize the average throughput. We derive a performance upper bound and show that the algorithm converges to the optimal solution almost surely. To achieve the optimal online performance without the prior knowledge of the channel statistics, we propose Multi-Armed Bandit (MAB) based algorithms which learn the problem data by cleverly adjusting the Channel Quality Indicator (CQI) used by the network for scheduling of data transmission, and maximize the average throughput. In the unconstrained case, we prove that the maximal throughput can be achieved by reporting a single CQI, which is problem-dependent and needs to be learned online. By adopting the MAB framework, we not only exploit the throughput maximizing CQI with high probability but also minimize the learning cost. In the BLER constrained case, we prove that the throughput maximizing CQI distribution has two atoms and derive an explicit formula for the distribution. We propose a novel Greedy-LP algorithm to solve the BLER constrained problem and show that it converges almost surely. Simulation results confirm the effectiveness of the proposed algorithms. Both the unconstrained and BLER constrained algorithms are shown to achieve up to 99% of the optimal throughput over a broad range of common channel models.

1.5 Notation

We use boldface and lowercase letters to denote vectors (like $\boldsymbol{a}, \boldsymbol{b}, \boldsymbol{x}, \boldsymbol{y}$). Matrices are denoted by boldface and uppercase letters, such as $\boldsymbol{A}$ and $\boldsymbol{B}$. Random variables and vectors are denoted by capital letters. The probability density function (pdf) and cumulative density function (cdf) of X are denoted by f_X and F_X, respectively. The random variable X is distributed as f_X is denoted by $X \sim f_X$.

The expectation operator is denoted by $\mathbf{E}(.)$. The variance operator is denoted by $\mathrm{Var}\,[.]$. $\mathbb{R}$ is the set of real numbers, $\mathbb{Z}$ is the set of integers and $\mathbb{N}$ is the set of natural numbers.

CHAPTER 2

Spherically Invariant Random Process

It is well known that the performance of wireless communications is strongly affected by power fades. Under various propagation scenarios, several models for the probability distribution of the fading envelope have been proposed, and are used for performance prediction and design. Fading models may be categorized into two broad classes: those derived from physical considerations (a typical example is Rayleigh fading), and those containing a number of parameters whose values can be obtained by empirical fitting of observed data. A rich collection of fading models can be found in [3, 4], where envelope and signal-to-noise ratio distributions are shown along with the corresponding moment-generating functions. In this paper we focus on a class of fading processes obtained as envelopes of a generalization of Gaussian processes which exhibit a property called "spherical invariance." Spherically Invariant Random Processes (SIRPs) inherit many analytically tractable properties from Gaussian processes. They have been advocated as relevant to the modeling of atmospheric noise, speech processes, radar clutters, impulsive noise, etc. (see, e.g., [5, 6] and references within), and most of the popular fading models turn out to be special cases of SIRPs. Our paper aims at justifying the ubiquity of spherically invariant distributions in modeling fading effects, and advocating their use for system analysis. Among the reasons motivating their applicability are their generality, flexibility, and the fact that, under suitable constraints, they maximize differential entropy, as it occurs for Gaussian processes under the only constraint of bounded variance. Moreover,

the fact that a vast majority of fading models used in practice turn out to be special cases of SIRP models suggests some underlying structural property that SIRP processes can capture. From a practical viewpoint, (a) SIRP models can be parametrized through the use of the H-function representation of their probability density function (pdf), thus simplifying the generation of a mathematical model from experimental data, (b) Computer simulation of SIRP fading need only the generation of a Gaussian process and a scalar pseudorandom variable with a suitable pdf, and (c) The calculation of relevant performance parameters is made easier if a SIRP fading model is available.

This paper is organized as follows: Section 2.1 summarizes, in a tutorial fashion, the main facts about SIRPs, and shows that they are entropy maximizers. Section 2.2 focuses on the envelope of a SIRP and its use as a fading model. In particular, it is shown how the use of Mellin transforms allows one to construct a fading model and simplify performance evaluation. A parametric model for the pdf of SIRP fading is derived, and it is shown how most practical fading models turn out to be spherically invariant. A closer look at the performance of digital transmission systems affected by a SIRP fading is taken in Section 3.1, where we derive upper and lower bounds to system performance when we have a limited knowledge of SIRP statistics. In Section 3.2 we derive the best and worst fading processes for a given signal-to-noise ratio under the assumption of spherical invariance, and in Section 3.3 we conclude the paper.

2.1 Definitions and key properties

SIRPs are characterized by some properties commonly associated with Gaussian processes. Specifically, it is well known that mean-square estimation problems on Gaussian processes have linear solutions, and Gaussian processes are closed under linear operations. Vershik showed that these two properties do not uniquely

characterize Gaussian processes, while they do characterize SIRPs [5, 8, 9]. Let $Y(t)$ be a second-order process with mean $m(t)$ and covariance function $\sigma(t, s)$. Then $Y(t)$ is a SIRP if all random variables (RVs) in the closed linear span of $Y - m$ (i.e., the subspace of square-integrable linear functions over $Y - m$) having the same variance have the same distribution. A random vector $\boldsymbol{X}$ is spherically invariant if there exist a function g and a positive definite matrix $\boldsymbol{R}$ such that its pdf can be written as

$$f_X(\boldsymbol{x}) = g(\boldsymbol{x}^T \boldsymbol{R} \boldsymbol{x}). \tag{2.1}$$

Notice that, deriving structural properties of SIRPs, we can restrict ourselves to zero-mean, white processes. In fact, the affine map $\boldsymbol{y} = \boldsymbol{A}\boldsymbol{x} + \boldsymbol{\mu}$ transforms a zero-mean vector with independent, unit-variance components into one with mean $\boldsymbol{\mu}$ and covariance matrix $\boldsymbol{A}\boldsymbol{A}^T$.

It is useful to observe that a SIRP can be characterized as a mixture of Gaussian processes, and determined by a mean $\mu(t)$, a covariance function $R(t, s)$, and a pdf in $\mathbb{R}^+ \triangleq [0, \infty)$. Specifically, for a Gaussian process with covariance function $v^2 R(t, s)$, the density of a corresponding SIRP is given by the expected value of the pdf of the Gaussian process taken with respect to v. A SIRP $\{Y(t), -\infty < t < \infty\}$ has an nth-order pdf of the form [5]

$$f_{\boldsymbol{Y}}(\boldsymbol{y}) = C_n \int_0^\infty \frac{1}{v^n} e^{-(1/2)(\boldsymbol{y}-\boldsymbol{\mu})^T (v^2 \boldsymbol{R})^{-1} (\boldsymbol{y}-\boldsymbol{\mu})} f_V(v) \, dv, \tag{2.2}$$

where $\boldsymbol{y} \in \mathbb{R}^n$, $C_n = (2\pi)^{-n/2} |\boldsymbol{R}|^{-1/2}$ is a normalization constant, $\boldsymbol{\mu}$ is the mean vector, and $\boldsymbol{R}$ is the positive definite covariance matrix.

Eq.(2.2) shows that the nth order pdf of a SIRP is the statistical average of the nth order pdf of a Gaussian process taken with respect to an arbitrary nonnegative-valued univariate RV V whose pdf is $f_V(v)$ (in [10], it is shown that the distribution of V need not be supported on the nonnegative real line, and that the second-order property or the nonsingularity property, assumed in [5, 9], need

not be imposed). This implies that the spherically invariant process $Y(t)$ has a simple representation in the form of a Gaussian process with random variance: formally,

$$\{Y(t) = VZ(t), -\infty < t < \infty\}, \tag{2.3}$$

where $\{Z(t), -\infty < t < \infty\}$ is a Gaussian process independent of V.[1] Thus, a SIRP is completely characterized by its mean value, its covariance function, and its univariate pdf (or characteristic function). This first-order pdf can be either prescribed or obtained from experimental data (see, e.g., [11]. A graphical test for the spherical invariance of a random process has been advocated in [12]). In [11], it is shown how higher-order pdfs can be derived from the first-order pdf.

2.1.1 Properties of SIRPs

For completeness, here we briefly summarize some of the known additional basic properties of SIRPs, and indicate its generalizations.

- For SIRPs, the linear mean-square estimator is optimum in the class of all mean-square estimators. [5].

- Under certain conditions, the class of SIRPs is closed under deterministic linear operations. [5].

- The form of the likelihood-ratio detector of a known deterministic signal in additive spherically invariant noise is a correlation receiver or matched filter. [5].

- The concept of spherically invariant distributions can be extended to mea-

---

[1]Notice that representation (2.3) implies that a SIRP can be ergodic only if V is a constant, i.e., the process is Gaussian. Otherwise, no individual realization of the process can offer information about the statistics of V. Notice also the (overly critical) statement in [8], "The fact that a spherically invariant process which is ergodic is also normal sheds doubt on the physical significance of non-normal spherically invariant processes." See below, Section 2.6.1, for a discussion.

sures on Hilbert spaces. [13]

- Nonlinear estimation and discrimination of SIRPs is studied in [14, 15].

- Statistical inference issues on elliptically contoured random processes are examined in [16].

2.1.2 SIRPs maximize the differential entropy

The maximum-entropy principle states that, if a random process model is to be built from incomplete information, one with the largest entropy should be chosen among those consistent with prior information [17]. Consider an absolutely continuous (AC) random vector $\boldsymbol{X}$, i.e., one taking on an uncountable set of values and such that the probability that its realization belongs to a given set can be computed as a multiple integral over its joint pdf. The (differential) entropy of a vector $\boldsymbol{X}$ with pdf $f(\boldsymbol{x})$ is defined as [18, p. 224]

$$h(\boldsymbol{X}) \triangleq - \int f(\boldsymbol{x}) \log(f(\boldsymbol{x})) \, d\boldsymbol{x}. \tag{2.4}$$

With a slight abuse of notation, (2.4) is sometimes written as $h(f)$. This function is concave.

In [18, Theorem 9.6.5], it is proved that, under the constraint that $\boldsymbol{X}$ has a given covariance matrix, the multivariate Gaussian distribution of $\boldsymbol{X}$ maximizes the entropy over all distributions with the same covariance. We shall now prove the more general statement that, under a spherically invariant constraint, the entropy is maximized by a spherically invariant distribution.

Let $\boldsymbol{R} = \boldsymbol{\Gamma}\boldsymbol{\Gamma}^T$ be the Cholesky decomposition of the positive definite matrix $\boldsymbol{R}$, and define the group

$$G \triangleq \left\{ \boldsymbol{T} = (\boldsymbol{\Gamma}^T)^{-1}\boldsymbol{O}\boldsymbol{\Gamma}^T \mid \boldsymbol{O} \in O(n) \right\}, \tag{2.5}$$

where $O(n)$ is the compact group of orthogonal matrices on $\mathbb{R}^n$. We say that a function f is G-invariant if

$$f(\boldsymbol{Q}\boldsymbol{x}) = f(\boldsymbol{x}) \tag{2.6}$$

for all $\boldsymbol{Q} \in G$ and $\boldsymbol{x}$ in the domain of f. With these definitions, the entropy function h turns out to be G-invariant. Consider next a constraint on $\boldsymbol{X}$ with the form $\mathbf{E}(C(\boldsymbol{X})) \leq 0$. This constraint is G-invariant if $\mathbf{E}(C(\boldsymbol{X})) \leq 0$ implies $\mathbf{E}(C(\boldsymbol{Q}\boldsymbol{X})) \leq 0$ for all $\boldsymbol{Q} \in G$. We are now ready to formulate and prove the following:

Theorem 1. *Let* $\mathbf{E}(C(\boldsymbol{X})) \leq 0$ *be a G-invariant constraint. If the entropy maximization problem*

$$\max_{\boldsymbol{X} \in \mathrm{AC}} \quad h(\boldsymbol{X}) \tag{2.7}$$

$$\text{s.t.} \quad \mathbf{E}(C(\boldsymbol{X})) \leq 0 \tag{2.8}$$

has a maximizer $\boldsymbol{X}^*$, *and* $C(\boldsymbol{X}^*)$ *is integrable, then* $\boldsymbol{X}^*$ *can be selected to be spherically invariant.*

Proof

Since G is a compact group, then Haar's theorem [19, p. 250 ff.], [20, p. 68 ff.] shows that a unique invariant probability measure ν exists such that

$$\nu(\boldsymbol{T}D) = \nu(D) \tag{2.9}$$

for all $\boldsymbol{T} \in G$ and for all measurable $D \subset G$.

Suppose now that $\boldsymbol{X}^*$ is the optimal solution of Theorem 1. The random variable

$$\overline{\boldsymbol{X}^*} \triangleq \int_G \boldsymbol{T}\boldsymbol{X}^* \, d\nu(\boldsymbol{T}) \tag{2.10}$$

is well-defined almost everywhere and integrable, because

$$\left\| \int_G \boldsymbol{T}\boldsymbol{X}^* \, d\nu(\boldsymbol{T}) \right\| \leq \int_G \|\boldsymbol{T}\boldsymbol{X}^*\| \, d\nu(\boldsymbol{T}) \leq \int_G \|\boldsymbol{X}^*\| \, d\nu(\boldsymbol{T}) = \|\boldsymbol{X}^*\|. \qquad (2.11)$$

Let f^* denote the pdf of $\boldsymbol{X}^*$. Then the pdf of $\overline{\boldsymbol{X}^*}$ is given by

$$\overline{f^*}(\boldsymbol{x}) = \int_G f^*(\boldsymbol{T}^{-1}\boldsymbol{x}) \, d\nu(\boldsymbol{T}). \qquad (2.12)$$

We will show that $\overline{\boldsymbol{X}^*}$ is the maximizer of (2.7) and it is spherically invariant.

1. $\overline{\boldsymbol{X}^*}$ is feasible: in fact

$$\mathbf{E}(C(\overline{\boldsymbol{X}^*})) = \int_{\mathbb{R}^n} C(\boldsymbol{x}) \int_G f^*(\boldsymbol{T}^{-1}\boldsymbol{x}) \, d\nu(\boldsymbol{T}) \, d\boldsymbol{x} \qquad (2.13)$$

$$= \int_G \underbrace{\left(\int_{\mathbb{R}^n} C(\boldsymbol{x}) f^*(\boldsymbol{T}^{-1}\boldsymbol{x}) \, d\boldsymbol{x} \right)}_{\mathbf{E}(C(\boldsymbol{T}\boldsymbol{X})) \leq 0} \, d\nu(\boldsymbol{T}) \leq 0. \qquad (2.14)$$

   (By Fubini-Tonelli theorem, the order of integration can be inverted in (2.13) and (2.14) because $C(\boldsymbol{X}^*)$ is integrable.)

2. $\overline{\boldsymbol{X}^*}$ is optimal: in fact, from Jensen's inequality [18, p. 25] and the concavity of h, it follows that

$$h(\overline{f^*}) = h\left(\int_G f^*(\boldsymbol{T}^{-1}\boldsymbol{x}) \, d\nu(\boldsymbol{T}) \right) \geq \int_G h(f^*(\boldsymbol{T}^{-1}\boldsymbol{x})) \, d\nu(\boldsymbol{T}) = \int_G h(f^*(\boldsymbol{x})) \, d\nu(\boldsymbol{T}) = h(f^*).$$

3. $\overline{\boldsymbol{X}^*}$ is invariant under G: in fact

$$\boldsymbol{Q}\overline{\boldsymbol{X}^*} = \int_G \boldsymbol{Q}\boldsymbol{T}\boldsymbol{X}^* \, d\nu(\boldsymbol{T}) = \int_G \boldsymbol{S}\boldsymbol{X}^* \, d\nu(\boldsymbol{Q}^{-1}\boldsymbol{S}) = \int_G \boldsymbol{S}\boldsymbol{X}^* \, d\nu(\boldsymbol{S}) = \overline{\boldsymbol{X}^*}.$$
$$(2.15)$$

$\square$

Example 1. *Being a function of $\boldsymbol{x}^T\boldsymbol{R}^{-1}\boldsymbol{x}$, the multivariate Student-t distribution*

$$f(\boldsymbol{x}) = \frac{\Gamma((\nu+n)/2)}{\sqrt{(\pi\nu)^n|\boldsymbol{R}|}\Gamma(\nu/2)}\left(1 + \frac{1}{\nu}\boldsymbol{x}^T\boldsymbol{R}^{-1}\boldsymbol{x}\right)^{-(n+\nu)/2} \tag{2.16}$$

is spherically invariant. It turns out to be the entropy maximizer subject to a G-invariant constraint (2.5) *on the expected value* $\mathbf{E}(\log)\left(1 + \frac{1}{\nu}\boldsymbol{x}^T\boldsymbol{R}^{-1}\boldsymbol{x}\right)$ *[21].*

2.2 Modeling fading envelopes using SIRPs

Consider now narrowband processes and their envelopes. A narrowband Gaussian process $Y(t)$ can be expressed in the form

$$Y(t) = Y_I(t)\cos(2\pi f_0 t) - Y_Q(t)\sin(2\pi f_0 t), \tag{2.17}$$

where $Y_I(t)$ and $Y_Q(t)$ are independent low-pass Gaussian processes. Its envelope $R_Y(t) \triangleq (Y_I(t)^2 + Y_Q(t)^2)^{1/2}$, has a Rice pdf. If $Y(t)$ is a SIRP, then (2.3) holds, and its envelope can be given the form

$$R_Y(t) = (Y_I(t)^2 + Y_Q(t)^2)^{1/2} = ((VZ_I(t))^2 + (VZ_Q(t))^2)^{1/2} = VR_Z(t), \tag{2.18}$$

where $R_Z(t)$, the envelope of a Gaussian process, has a Rice pdf.[2] To simplify our notation, assuming stationarity we suppress the variable t, and denote the original envelope of the Gaussian process by R and the fading SIRP envelope by X. Thus,

$$X = VR, \tag{2.19}$$

where V is the same nonnegative-valued univariate RV as above, whose pdf is $f_V(v)$. Eq. (2.19) shows how the envelope of a SIRP process can be represented as

---

[2]In the special case of a zero-mean $Y(t)$, and hence zero-mean $Z(t)$, $R_Z(t)$ has a Rayleigh pdf.

that of a Rice (or Rayleigh) process with random variance. Various applications of this principle are examined in [5, 22, 23].[3]

With V and R in (2.19) two independent nonnegative-valued univariate RVs, the pdf of X satisfies

$$f_X(x) = \int_0^\infty (1/v) f_R(x/v) f_V(v)\, dv, \quad 0 < x < \infty, \tag{2.20}$$

showing that the pdf of X in (2.20) is a mixture or compound density, resulting from compounding f_R with f_V [24].

Remark 1. *Eq. (2.19) can be used as the basis for computer simulation of spherically invariant fading processes. If a simulator of a Gaussian process is available, it suffices to multiply its envelope by a suitable random variable to generate an exceedingly wide array of envelope statistics.*

Remark 2. *We may approximate (2.20) using a discrete mixture, i.e., its discrete parametric version*

$$f_X(x \mid \Theta) = \sum_{i=1}^M \alpha_i f_R(x \mid \theta_i), \tag{2.21}$$

where the vector $\Theta \triangleq (\alpha_1, \ldots, \alpha_M, \theta_1, \ldots, \theta_M)$ summarizes the parameters α_i and θ_i of the discrete mixture. These are such that such that $\sum_{i=1}^M \alpha_i = 1$ and each $f_R(x \mid \theta_i)$ is a Rice pdf. The EM algorithm can be used to estimate the parameters of the mixture [25–27].

Using (2.20), we have the following theorem.

Theorem 2. *A sufficient condition for a fading envelope RV X to be SIRP is that its pdf $f_X(x)$ be given by the integral in (2.20), where $f_R(r)$ is a Rician pdf, and $f_V(v)$ is the pdf of a RV V independent of R and defined on $\mathbb{R}^+$.*

---

[3]Ref. [5] examines SIRP modeling of radar clutters, whose scattering issues are similar to those of wireless fading.

Example 2. *The Suzuki envelope X has the pdf [28]*

$$f_X(x) = \int_0^\infty \frac{1}{\sigma} \left(\frac{x}{\sigma} \exp(-(x/\sigma)^2/2) \right) \left[\frac{1}{\sqrt{2\pi}\,\beta\sigma} \exp(-(\ln(\sigma))^2/(2\beta^2)) \right] d\sigma \,, \ 0 \le x < \infty \,,$$

(2.22)

where the term between round brackets in (2.22) is the normalized Rayleigh pdf evaluated at x/σ, while that between square brackets is the lognormal pdf

$$f(\sigma) = \frac{1}{\sqrt{2\pi}\beta\sigma} \exp\left(-\frac{(\ln(\sigma))^2}{2\beta^2} \right), 0 \le \sigma < \infty \,.$$

(2.23)

Integral (2.22) has the same form as that of (2.20). Thus, from Theorem 2, we can conclude that the Suzuki fading envelope RV is SIRP. The Sukuki pdf models the NLOS short-term fast Rayleigh multipath effects with its standard deviation σ randomized by the long-term slow shadowing lognormal pdf effects. □

Example 3. *The Suzuki Extended Type I envelope X [28] has pdf*

$$f_X(x) = \int_0^\infty \frac{1}{\sigma} \left(\frac{x}{\sigma\sigma_1^2} \exp\left(-\frac{(x/\sigma)^2 + s^2}{2\sigma_1^2} \right) I_0 \left(\frac{xs}{\sigma\sigma_1^2} \right) \right) \left[\frac{1}{\beta\sigma\sqrt{2\pi}} \exp\left(-\frac{(\ln(\sigma))^2}{2\beta^2} \right) \right] d\sigma,$$

(2.24)

where $0 \le x < \infty$. The term between round brackets in (2.24) is the normalized Rice pdf evaluated at x/σ, and that between square brackets is the lognormal pdf of (2.23). Again, the integral of (2.24) has the same form as that of (2.20). Thus, from Theorem 2, we can conclude that the Suzuki Extended Type I envelope RV is SIRP. The Suzuki Extended Type I pdf models the LOS short-term fast Rician multipath effects with its standard deviation σ randomized by the long-term slow shadowing lognormal pdf effects. □

Example 4. *The "Half-Cauchy-like" fading envelope random variable X has pdf*

$$f_X(x) = \frac{2ax}{(1 + 2x^2)^{3/2}}, \quad 0 \le x < \infty, \ 0 < a.$$

(2.25)

Direct integration shows that $f_X(x)$ in (2.25) can be expressed as

$$f_X(x) = \int_0^\infty \frac{1}{v}(f_R)(\frac{x}{v}) \, f_V(v) \, dv, \quad 0 \leq x < \infty \tag{2.26}$$

where $f_R(x/v)$ is the normalized Rayleigh pdf evaluated at x/v, and the pdf $f_V(v)$ is given by

$$f_V(v) = \sqrt{\frac{2}{\pi}} v^{-2} \exp\left(-\frac{1}{2v^2}\right), \, 0 < v < \infty, \tag{2.27}$$

which is positive-valued on $\mathbb{R}^+$ and integrates to one. Since (2.26) is of the form of (2.20), from Theorem 2 we have that the "Half-Cauchy-like" fading envelope RV X is SIRP. We note that the "Half-Cauchy-Like" pdf does not have a bounded second moment. $\square$

Eq. (2.20) may be used to define what is called the *Mellin convolution* between densities f_R and f_V, i.e., we may write

$$f_X(x) = (f_R \star f_V)(x). \tag{2.28}$$

Now, it can be shown [29] that the Mellin convolution is commutative and associative, so that $g \star h = h \star g$, and $(f \star g) \star h = f \star (g \star h)$. This allows us to state, in the form of a theorem, the closure property of SIRP envelopes:

Theorem 3. *If the pdf of X has the form (2.28), where R is a SIRP envelope and V is a positive random variable, then X is also a SIRP envelope.*

Remark 3. *An implicit assumption made in Theorem 3 is that X, R, and V are mutually independent. This allows one to avoid the subtle issue of the joint dependency among these three random variables.*

Example 5. *The gamma–lognormal fading envelope r.v. X [30] has a pdf given*

17

by

$$f_{Ga-\log}(x) = \int_0^\infty \frac{1}{\sigma} \left(\frac{m^m (x/\sigma)^{m-1}}{\Gamma(m)} \exp(-mx/\sigma) \right) \left[\frac{1}{\beta\sigma\sqrt{2\pi}} \exp\left(-\frac{(\ln(\sigma))^2}{2\beta^2} \right) \right] d\sigma,$$
(2.29)

for $0 \leq x < \infty$. *The term in* *(2.29)* *within square brackets is the lognormal pdf* *(2.23)*, *while that within round brackets is the following gamma pdf:*

$$f(x) = \frac{1}{\Gamma(m)} m^m x^{m-1} \exp(-mx), \, 0 \leq x < \infty, \,.$$
(2.30)

evaluated at (x/σ). *Later, we shall prove (Example 8) that a gamma-distributed process is a SIRP. Thus, from Theorem 3 we can conclude the Gamma-lognormal pdf is a SIRP pdf. The Gamma-lognormal pdf models the NLOS short-term fast Gamma statistical multipath effects with its standard deviation* σ *randomized by the long-term slow shadowing lognormal pdf effects.* $\square$

2.3   The Mellin transformation

Convolution (2.28) can be transformed into a product if Mellin transforms are used. The Mellin transform [29, 31, 32] $\hat{f}_X(s) = \mathcal{M}[f_X(x)]$ of the univariate pdf $f_X(x)$ defined in $\mathbb{R}^+$ is defined as

$$\hat{f}_X(s) \triangleq \mathbb{E}[X^{s-1}] = \int_0^\infty f_X(x) x^{s-1} \, dx.$$
(2.31)

The integral above is defined for any Lebesgue-integrable function, and converges in a vertical strip of the complex plane. The inverse Mellin transform is given by

$$f_X(x) = \frac{1}{2\pi j} \int_{c-j\infty}^{c+j\infty} \hat{f}_X(s) x^{-s} \, ds, \qquad c \in \mathbb{R}, x \in \mathbb{R}^+.$$
(2.32)

Raising both sides of (2.19) to power $s-1$, and taking expectations after using

the independence of V and R, we obtain from (2.31)

$$\hat{f}_X(s) = \hat{f}_V(s)\hat{f}_R(s), \tag{2.33}$$

or, equivalently,

$$\hat{f}_V(s) = \frac{\hat{f}_X(s)}{\hat{f}_R(s)}, \tag{2.34}$$

and hence

$$f_V(x) = \mathcal{M}^{-1}\left\{\frac{\hat{f}_X(s)}{\hat{f}_R(s)}\right\}. \tag{2.35}$$

Thus, if the Mellin transforms $\hat{f}_R(x)$ and $\hat{f}_X(x)$ are computed, the inverse transform of their ratio yields $f_V(x)$.

Example 6. *(Nakagami-m fading) Consider the Nakagami-m density*

$$f_X(x) = \frac{2m^m}{\Gamma(m)\Omega^m}x^{2m-1}\exp\left(-\frac{m}{\Omega}x^2\right). \tag{2.36}$$

With R a Rayleigh fading envelope, we obtain from direct calculation:

$$f_V(v) = \frac{2\left(\frac{m}{\Omega}\right)^m}{\Gamma(m)\Gamma(1-m)}v^{2m-1}\left(1-\frac{m}{\Omega}v^2\right)^{-m}, \qquad v \in \left(0, \sqrt{\Omega/m}\right). \tag{2.37}$$

$\square$

Example 7. *(κ-μ fading and shadowed fading) A model which has been recently introduced [33] is that of κ-μ fading. More recently, the κ-μ distribution was generalized to encompass shadowing in the line-of-sight (LOS) signal component [34]. This model describes the short-term signal variations of a faded signal in the presence of line-of-sight components. The physical model underlying this distribution includes Rayleigh, Rice, and Nakagami-m models as special cases, and the distribution itself provides a better fit to experimental data than other traditional fading models. Ref. [35] shows that the κ-μ distribution is a version of the generalized*

Rice distribution described in [36].

The κ-μ density is given by

$$f_X(x) = \frac{x}{\sigma^2}\left(\frac{x}{d}\right)^{\mu-1}\exp\left(-\frac{x^2+d^2}{2\sigma^2}\right)I_{\mu-1}\left(\frac{dx}{\sigma^2}\right), \quad 0 \le x < \infty, \qquad (2.38)$$

where $I_{\mu-1}$ denotes the modified Bessel function of the first kind, σ^2 denotes the variance of the non-LOS component, and d^2 is the total power of the LOS components. The Mellin transform of $f_X(x)$ is given by

$$\hat{f}_X(s) = \left(2\sigma^2\right)^{(s-1)/2}\frac{\Gamma\big((s-1)/2+\mu\big)}{\Gamma(\mu)}{}_1\tilde{F}_1\left(-\frac{s-1}{2};\mu;-\frac{d^2}{2\sigma^2}\right), \qquad (2.39)$$

and converges in the strip $\Re[s] > \max(-\mu, 1-2\mu)$ (here, ${}_1\tilde{F}_1$ denotes the regularized confluent hypergeometric function). While in this paper we show that a large number of important fading processes are spherically invariant, we were neither able to prove nor disprove the fact that a process with a κ-μ density is actually a SIRP. $\qquad\square$

2.4 Parameterizing SIRP Using Fox H-function

Examples 6 and 7 refer to cases where Mellin transforms can be obtained in closed form with relative ease. A tool allowing one to deal with more general situations can be derived through the use of Fox H-function representation of densities (see, e.g., [37]). Due to its generality, H-function has found a number of applications in fading analysis: for example, it has be used to generate closed-form expressions of capacities and probabilities of digital transmission over faded

channels in [3, 4, 38, 39]. The Fox H-function is defined as follows:

$$H(z) = H_{p,q}^{m,n} \left[z \, \middle| \, \begin{array}{c} \{(a_1, A_1), \quad \ldots \quad , (a_p, A_p)\} \\ \{(b_1, B_1), \quad \ldots \quad , (b_q, B_q)\} \end{array} \right] \tag{2.40}$$

$$\triangleq \mathcal{M}^{-1} \left\{ \frac{\prod_{j=1}^{m} \Gamma(b_j + B_j s) \prod_{j=1}^{n} \Gamma(1 - a_j - A_j s)}{\prod_{j=m+1}^{q} \Gamma(1 - b_j - B_j s) \prod_{j=n+1}^{p} \Gamma(a_j + A_j s)} \right\},$$

where the nonnegative integers $\{m, n, p, q\}$ satisfy $0 \leq m \leq q$ and $0 \leq n \leq p$, and a_j, b_j, A_j, and $B_j > 0$, are complex numbers such that no poles of the gamma function $\Gamma(b_j - B_j s)$ coincide with the poles of $\Gamma(1 - a_j + A_j s)$. In (2.40), products whose upper index is zero or less than the lower index are set equal to 1.

Now, assume that the densities f_X and f_R have expressions as H-functions, viz.,

$$f_X(x) = k_1 H_{p_1,q_1}^{m_1,n_1} \left[c_1 x \, \middle| \, \begin{array}{c} \{(a'_1, A'_1), \cdots, (a'_{p_1}, A'_{p_1})\} \\ \{(b'_1, B'_1), \cdots, (b'_{q_1}, B'_{q_1})\} \end{array} \right], \tag{2.41}$$

where k_1 and c_1 are some positive constants, and

$$f_R(x) = k_2 H_{p_2,q_2}^{m_2,n_2} \left[c_2 x \, \middle| \, \begin{array}{c} \{(a''_1, A''_1), \cdots, (a''_{p_2}, A''_{p_2})\} \\ \{(b''_1, B''_1), \cdots, (b''_{q_2}, B''_{q_2})\} \end{array} \right], \tag{2.42}$$

where k_2 and c_2 are also some positive constants. Then, the mixing $f_V(x)$ pdf is given explicitly by

$$f_V(x) = k H_{p,q}^{m,n} \left[cx \, \middle| \, \begin{array}{c} \{(a_1, A_1), \cdots, (a_p, A_p)\} \\ \{(b_1, B_1), \cdots, (b_q, B_q)\} \end{array} \right], \qquad 0 \leq x < \infty, \tag{2.43}$$

where the parameters of $H_{p,q}^{m,n}[.]$ are related to the parameters of $H_{p_1,q_1}^{m_1,n_1}[.]$ and

$H_{p_2,q_2}^{m_2,n_2}[.]$ as follows:

$$k = \frac{k_1}{k_2}, \ c = \frac{c_1}{c_2}, \ m = m_1 + p_2 - n_2, \ n = n_1 + q_2 - m_2, \ p = p_1 + q_2, \ q = q_1 + p_2,$$

$$(2.44)$$

$$\{a_1, \cdots, a_p\} = \left\{ \{a'_1, \cdots, a'_{n_1}\}, \{b''_{m_2+1}, \cdots, b''_{q_2}\} \right\}, \left\{ \{a'_{n_1+1}, \cdots, a'_{p_1}\}, \{b''_1, \cdots, b''_{m_2}\} \right\},$$

$$(2.45)$$

$$\{A_1, \cdots, A_p\} = \left\{ \{A'_1, \cdots, A'_{n_1}\}, \{B''_{m_2+1}, \cdots, B''_{q_2}\} \right\}, \left\{ \{A'_{n_1+1}, \cdots, A'_{p_1}\}, \{B''_1, \cdots, B''_{m_2}\} \right\},$$

$$(2.46)$$

$$\{b_1, \cdots, b_q\} = \left\{ \{b'_1, \cdots, b'_{m_1}\}, \{a''_{n_2+1}, \cdots, a''_{p_2}\} \right\}, \left\{ \{b'_{m_1+1}, \cdots, b'_{q_1}\}, \{a''_1, \cdots, a''_{n_2}\} \right\},$$

$$(2.47)$$

$$\{B_1, \cdots, B_q\} = \left\{ \{B'_1, \cdots, B'_{m_1}\}, \{A''_{n_2+1}, \cdots, A''_{p_2}\} \right\}, \left\{ \{B'_{m_1+1}, \cdots, B'_{q_1}\}, \{A''_1, \cdots, A''_{n_2}\} \right\}.$$

$$(2.48)$$

The proof is straightforward but lengthy, and will be omitted here.

The above can be summarized in the form of the following theorem:

Theorem 4. *The random variable X models a SIRP envelope if f_X and f_R admit an H-function representation. In this case V has a pdf admitting the H-function representation* (2.43).

Remark 4. *It is possible that a pdf does not admit an H-function representation, so that Theorem 4 cannot be used to prove that it is the pdf of a SIRP. For example, the authors were unable to derive an H-function representation for the Suzuki Extended Type I pdf, which was proved to be the pdf of a SIRP in Example 3.*

Example 8. *Let X be a RV with a generalized Gamma distribution, so that*

$$f_X(x) = \frac{\beta a^{\alpha/\beta}}{\Gamma(\alpha/\beta)} x^{\alpha-1} e^{-ax^\beta} = \frac{a^{1/\beta}}{\Gamma(\alpha/\beta)} H_{0,1}^{1,0} \left[a^{1/\beta} x \left| \frac{\text{----------}}{\{((\alpha-1)/\beta, 1/\beta)\}} \right. \right], \qquad 0 \le x < \infty.$$

Next, take as R a Rayleigh-distributed random variable, so that

$$f_R(x) = 2a_2'' x \exp(-a_2'' x^2) = \sqrt{a_2''} H_{0,1}^{1,0} \left[\sqrt{a_2''} x \, \Big|_{\{(1/2, 1/2)\}}^{------} \right], \qquad 0 < x < \infty, \ 0 < a_2''. \tag{2.49}$$

The pdf (2.49) includes as special cases seven well-known densities, each corresponding to a SIRP envelope. The corresponding densities of V are listed in Table I.

$\square$

Some of the densities f_V derived above are well known, while others are not. However, in all cases, upon explicit evaluation, all the densities described by H-functions take nonnegative values on $\mathbb{R}^+$ and integrate to 1, which makes them valid pdfs on $\mathbb{R}^+$. Notice also that, if a symbolic computation program is used, one may express H-functions as Meijer G-functions, as indicated for example in [40]. An efficient Mathematica® program for the evaluation of H-functions is presented in [41, Appendix].

2.5 Mellin transforms and asymptotics

In certain instances, one does not need to derive the pdf of a random variable if its Mellin transform is known. One of these instances occurs for narrowband transmission at high SNR, where the diversity d offers a useful indication of the channel performance, and this can be evaluated through the parameters of the following approximation of the pdf of SNR:

$$f_{\mathsf{snr}}(x) = gx^b + o(x^{b+\epsilon}), \tag{2.50}$$

as $x \to 0^+$, where $\epsilon > 0$ and g, b are positive constant. As shown in [42] (see also [43, Chapter 4], and [44] for a generalization), whenever the error probability

$f_X(x)$	$f_V(v)$	a_1	α_1	β_1	k_1	c_1	b_1	B_1
Gamma	$\frac{c^3 v^2}{2\sqrt{\pi}}\exp -c^2v^2/4$			1	$1/\Gamma(\alpha_1)$	a_1	(α_1-1)	1
Rayleigh	$\delta(v-1)$		2	2	$\sqrt{a_1}$	$\sqrt{a_1}$	$1/2$	$1/2$
Weibull	$\frac{c}{\sqrt{\pi}}\exp(-c^2v^2/4)$		$\alpha_1=\beta_1$		a_1^{1/α_1}	a_1^{1/α_1}	$(\alpha_1-1)/\alpha_1$	$1/\alpha_1$
Nakagami-m	$\frac{2c\sqrt{cv}(1-(cv)^2)^{-3/4}}{\Gamma(1/4)\Gamma(3/4)}$	m/Ω	$2m$	2	$\sqrt{m}/\Omega/\Gamma(m)$	$\sqrt{m}/\Omega$	$(2m-1)/2$	$1/2$
Chi-Squared	$\frac{cK_{1/4}((cv)^2/8)\exp(-c^2x^2/8)}{\pi^{3/2}\sqrt{2}}$	$1/2$	$\nu/2$	1	$1/(2\Gamma(\nu/2))$	$1/2$	$(\nu/2-1)$	1
Half-Gaussian	$\frac{c}{\sqrt{\pi}}\exp(-c^2v^2/4)$		1	2	$\sqrt{a_1}/\Gamma(1/2)$	$\sqrt{a_1}$	0	$1/2$
One-sided exponential	$\frac{c}{\sqrt{\pi}}\exp(-c^2v^2/4)$		1	1	a_1	a_1	0	1

Table 2.1: Various nonegative-valued univariate pdfs as special cases of generalized Gamma functions and H-function parameters.

of a transmission scheme over the additive white Gaussian noise channel can be approximated by the expression

$$P_{AWGN}(e) \approx \kappa Q \left(\sqrt{2\gamma \, \mathsf{snr}} \right), \tag{2.51}$$

with $Q(\cdot)$ the Gaussian tail function, snr the energy-per-bit to noise-spectral-density ratio, κ the *error coefficient*, and γ the *asymptotic power efficiency*, then over a fading channel with fading amplitudes R known at the receiver the average error probability can be written, as $\mathsf{snr} \to \infty$, in the form

$$P(e) \approx \mathbb{E}_{X^2} \left[\kappa Q \left(\sqrt{2\gamma X^2 \mathsf{snr}} \right) \right] \sim \kappa g \frac{\Gamma(t + 3/2)}{2\sqrt{\pi}(t+1)} \left(\gamma \, \mathsf{snr} \right)^{-(b+1)}, \tag{2.52}$$

where $\sim$ denotes asymptotic behavior as snr grows to infinity. The parameter $d \triangleq b+1$, which quantifies the smoothness of $f_{X^2}(x)$ at the origin, is the diversity, while the coefficient g determines the shift of the the error-probability curve relative to a baseline curve.

Now, if the Mellin transform $\hat{f}_{X^2}(s)$ is known, d and g can be directly computed from it. In fact we have, as $x \to 0^+$,

$$f_{X^2}(x) \sim [\operatorname{Res} \hat{f}_{X^2}(s)]_{s=\hat{s}} \, x^{-\Re \hat{s}}, \tag{2.53}$$

where Res denotes the residue at a pole, and $\Re \hat{s}$ is the left boundary of the convergence strip of $\hat{f}_{X^2}(s)$ (see [45] for technical details about the validity of (2.53)). Using definition (2.31), the Mellin transform $\hat{f}_{X^2}(s) = \mathbb{E} X^{2(s-1)}$ can be obtained from $\hat{f}_X(s)$ with the simple transformation $s \to 2s - 1$.

Example 9. *Consider the Nakagami-m density* (2.36) *with* $\Omega = 1$:

$$f_X(x) = \frac{2m^m}{\Gamma(m)} x^{2m-1} e^{-mx^2}, \tag{2.54}$$

which yields

$$f_{X^2}(x) = \frac{m^m}{\Gamma(m)} x^{m-1} e^{-mx}, \qquad (2.55)$$

and hence, as $x \to 0^+$,

$$f_{X^2}(x) \sim \frac{m^m}{\Gamma(m)} x^{m-1}, \qquad (2.56)$$

and diversity $d = m$. The Mellin transform of (2.54) is, from direct calculation,

$$\hat{f}_X(s) = \frac{1}{\Gamma(m)} m^{(1-s)/2} \Gamma\big((s-1)/2 + m\big), \qquad (2.57)$$

from which we have

$$\hat{f}_{X^2}(s) = \frac{1}{\Gamma(m)} m^{(1-s)} \Gamma\big((s-1) + m\big). \qquad (2.58)$$

This converges for $\Re s > 1 - m$ with residue at $s = 1 - m$ equal to $m^m / \Gamma(m)$, hence yielding (2.56), as it should. $\qquad \square$

2.6 Performance calculations based on first-order densities

Here we make the assumption that the transmission system operates on a channel affected by SIRP fading, that the signal observed by the receiver is the sum of a faded data signal and of a white Gaussian noise, and that its performance can be described by the expected value η of a known function $h(\cdot)$ of the RV X. Using (2.19), we can write

$$\eta \triangleq \mathbb{E}_X[h(X)] = \mathbb{E}_V[H(V)], \qquad (2.59)$$

where

$$H(V) \triangleq \mathbb{E}_R[h(VR) \mid V]. \qquad (2.60)$$

26

Important examples of performance parameters are (a) error probability of uncoded binary antipodal modulation with equally likely symbols and (b) outage probability. The first parameter is representative of system performance when no error-control coding is used, while the second one reflects the performance when a near-optimal code is used.

2.6.1   A word of caution

Observe that one must be careful in describing the conditions under which the performance parameters are defined, because the SIRP underlying the fading envelope cannot be ergodic—otherwise it would be Gaussian (in fact, it is not possible to derive the distribution of V from the observation of a single realization of $X(t)$). Appropriate assumptions of deep interleaving must be added, for example when error probabilities are evaluated by taking the expectation with respect to V (see below). In this case, we may assume that the process is "locally SIRP," in the sense that $V = V(t)$ is slowly varying. With this model, if $V(t)$ and $R(t)$ are jointly stationary and ergodic, then $X(t)$ is also stationary and ergodic [46, Proposition 3.36], without the need for $V(t)$ to be a constant process.

2.6.2   Binary error probability

The binary error probability with antipodal signals, coherent reception, and channel-state information known at the receiver, is given by [43, Chapter 4]

$$P(e \mid V) = \mathbb{E}_R Q\left(\sqrt{2V^2 R^2 \mathsf{snr}}\right), \tag{2.61}$$

so that

$$h(x) = Q\left(x\sqrt{2\mathsf{snr}}\right). \tag{2.62}$$

With Rayleigh fading, (2.61) yields

$$P(e \mid V) = H(V) = \frac{1}{2}\left(1 - \sqrt{\frac{V^2\mathsf{snr}}{1 + V^2\mathsf{snr}}}\right),\tag{2.63}$$

while in the Rice case we have the implicit expression, which does not seem to be amenable to closed form:

$$P(e \mid V) = 2(1+K)e^{-K}\int_0^\infty r\exp\left\{-(1+K)r^2\right\} I_0\left(2r\sqrt{K(1+K)}\right) Q\left(\sqrt{2V^2r^2\mathsf{snr}}\right) dr.$$

where K denotes the Rice factor [43, p. 28].

2.6.2.1 Outage probability

On a nonergodic channel affected by fading with random envelope X and additive white Gaussian noise, the *information outage probability* is the probability that the transmission rate ρ, measured in bits per channel use, exceeds the instantaneous mutual information of the channel. This is given by

$$p_{out} = \mathbb{P}\left[\log_2(1 + X^2\mathsf{snr}) < \rho\right].\tag{2.64}$$

This is the information-theoretical limit which cannot be exceeded by the word error probability of any coded scheme, and hence can be utilized for estimating the error probability of transmission scheme using a nearly optimum error-control code. From (2.64) we have

$$p_{out} = \mathbb{P}\left[X \in \mathcal{I}\right],\tag{2.65}$$

where

$$\mathcal{I} \triangleq \left(0, \sqrt{(2^\rho - 1)/\mathsf{snr}}\right),\tag{2.66}$$

and hence

$$h(x) = \begin{cases} 1, & x \in \mathcal{I} \\ 0, & \text{otherwise.} \end{cases} \qquad (2.67)$$

Thus, we have [43, p. 86]

$$p_{out}(V) = \mathbb{P}\left(R < \sqrt{\frac{2^\rho - 1}{V^2 \mathsf{snr}}} \right), \qquad (2.68)$$

which, in the Rayleigh case, yields

$$p_{\text{out}}(V) = H(V) = 1 - \exp[-(2^\rho - 1)/V^2 \mathsf{snr}], \qquad (2.69)$$

and, in the Rice case,

$$p_{out}(V) = 1 - Q\left(\sqrt{2K}, \sqrt{\frac{(2^\rho - 1)}{V^2 \mathsf{snr}}} \right), \qquad (2.70)$$

where $Q(\,\cdot\,,\,\cdot\,)$ denotes the Marcum Q-function [47, p. 775].

2.6.3 Statistics of fading time intervals

The design of certain features of a wireless system, and the analysis of its performance, may depend on the statistics on fading time intervals. For example, the statistics of burst errors yields useful information for the design of error-control codes and interleavers. These statistics are known for Rayleigh, Rice, lognormal, Nakagami, and κ-μ fading distributions (see [48, 49] and references therein).

One of these statistics is the rate (in crossings per second) at which the envelope $X(t)$ crosses the level x in the positive or negative-going direction. The level crossing rate (LCR) of the stationary differentiable envelope process $X(t)$ is given by

$$L_X(x) = \int_{-\infty}^{\infty} \dot{x} f_{X,\dot{X}}(x, \dot{x}) \, d\dot{x}, \qquad (2.71)$$

where $f_{X,\dot{X}}$ is the joint pdf of X and $\dot{X}$. The average fade duration (AFD) of $X(t)$ is the average time spent by the envelope below level x, and is given by

$$T_X(x) \triangleq \frac{F_X(x)}{L_X(x)}, \tag{2.72}$$

where F_X is the cumulative distribution function of X.

In our context, consider again the process $X(t) = \sqrt{X_I^2(t) + X_Q^2(t)}$, with $X_I(t)$ and $X_Q(t)$ independently distributed, with common autocorrelation function

$$\rho(\tau) \triangleq \mathbb{E}\left(X(t)X(t+\tau)\right), \tag{2.73}$$

and assume that $|\rho''(0)|$ exists. Then the conditional crossing rate is

$$L_{X|V}(x \mid v) = \int_{-\infty}^{\infty} |\dot{x}| \, f_{X,\dot{X}|V}(x, \dot{x} \mid v) \, d\dot{x} = \frac{1}{v^2} \int_{-\infty}^{\infty} |\dot{x}| \, f_{R,\dot{R}|V}(x/v, \dot{x}/v \mid v) \, d\dot{x}. \tag{2.74}$$

When R has a Rayleigh distribution, $\dot{R}$ is $\sim \mathcal{N}(0, |\rho''(0)|)$ and independent of R. Therefore,

$$L_{X|V}(x \mid v) = \sqrt{\frac{2|\rho''(0)|}{\pi}} f_R(x/v), \tag{2.75}$$

and hence, averaging over the pdf of V:

$$L_{X|V}(x) = \sqrt{\frac{2|\rho''(0)|}{\pi}} \int_0^\infty f_R(x/v) f_V(v) \, dv. \tag{2.76}$$

Similarly, we can obtain the AFD of a SIRP fading envelope as

$$T_X(x) = \frac{\int_0^\infty F_R(x/v) f_V(v) \, dv}{L_X(x)}. \tag{2.77}$$

CHAPTER 3

Modeling Uncertainty Under SIRP Assumption

3.1 Bounds to system performance

When the distribution f_V of V is completely known, we can compute the performance parameter η in (2.59) by exact calculation or numerical integration, or approximate it by Monte Carlo computer simulation. However, in many situations the exact distribution of V is unknown, as we only have limited knowledge about it [50, 51]. In these conditions, we can evaluate upper and lower bounds η_{max} and η_{min} that are consistent with our prior information about V. We are interested in *sharp* bounds, i.e., bounds that can be actually achieved by probability distributions satisfying the set of constraints describing our knowledge of the fading process, and hence cannot be further tightened without altering the constraints. More precisely, we will determine the performance range that can be obtained if (a) the fading model is inaccurately chosen, or (b) the propagation conditions are expected to vary in time by a wide margin, and adaptive techniques are not sufficient to allow a single propagation model to be valid in a variety of conditions. In both situations, it is useful to study how the performance parameter η ranges as the channel model runs through an *uncertainty set*. This set may reflect (a) the inaccuracy in determining the mathematical channel model from measured data, or (b) the wide uncertainty in the knowledge of the actual operating conditions. Based on this approach, the robustness of system design to channel modeling can be assessed.

Our approach to case (a) (Subsection 3.1.1) is based on the evaluation of the degradation suffered by a system when a small discrepancy, measured by the Kullback–Leibler (K–L) divergence between a nominal and the actual probability distribution of the fading, is caused by model uncertainty. In particular, we derive upper and lower bounds to performance parameters as the fading envelope distribution ranges in a set having a prescribed K–L divergence from the nominal distribution. This approach was taken in [50] without the SIRP constraint. For case (b) (Subsection 3.1.2), we assume that some low-order moments of the fading envelope distribution are known, and derive upper and lower bounds to performance parameters as the distribution varies among those having the prescribed moments. To do this, classical moment-bound theory [52], and some its recent developments centered on semidefinite programming (see, e.g., [53]), are used.

3.1.1 Using Kullback–Leibler divergence

Here we assume that a fading model has been chosen in accordance to the SIRP assumption, and hence by using (2.19). For a given choice of the pdf of R, the model is picked by choosing a pdf of V. We study the effect of an inaccurate choice of the latter pdf, while maintaining the SIRP model assumption. To do this, let us denote as f_{V_0} the nominal density chosen, and as f_V a pdf with K–L divergence from f_{V_0} given by

$$D(V\|V_0) \triangleq \int f_V(v) \log \frac{f_V(v)}{f_{V_0}(v)}\, dv. \qquad (3.1)$$

The problem to be solved is

$$\max_{f_V} \int_0^\infty H(v) f_V(v)\, dv,$$

$$\text{s.t.} \quad \int_0^\infty \log \frac{f_V(v)}{f_{V_0}(v)} f_V(v)\, dv \le d,$$

$$\int_0^\infty f_V(v)\, dv = 1,$$

where $H(\cdot)$ was defined in (2.60), and f is the pdf of V (condition $f_V(v) \ge 0$ should be added unless automatically satisfied). Duplicating the derivation in [50], the optimizing $f_V(v)$ is obtained in the form

$$f_V^\star(v) = f_{V_0}(v) \frac{e^{H(v)/s^\star}}{\xi(s^\star)}, \tag{3.2}$$

where

$$\xi(s) \triangleq \int_0^\infty e^{H(v)/s} f_{V_0}(v)\, dv, \tag{3.3}$$

s is the solution of

$$\frac{\xi'(s)}{\xi(s)} - s \log \xi(s) = ds, \tag{3.4}$$

and

$$\xi'(s) \triangleq \frac{d\xi(s)}{d(1/s)} = \int_0^\infty H(v) e^{H(v)/s} f_{V_0}(v) dv. \tag{3.5}$$

The resulting maximum value of $\mathbb{E}\, H$ is given by

$$\eta_{max} = \frac{\xi'(s^\star)}{\xi(s^\star)}. \tag{3.6}$$

Example 10. *Assume that the nominal density for X is Nakagami-m. With R a Rayleigh random variable, the density of V_0 is given by (2.37). Choosing outage probability as the performance parameter, $H(V)$ is given by (2.69). Numerical results are shown in Fig. 3.1, 3.2, and 3.3.*

Fig. 3.1 and 3.2 show the densities of V and R, respectively, associated with
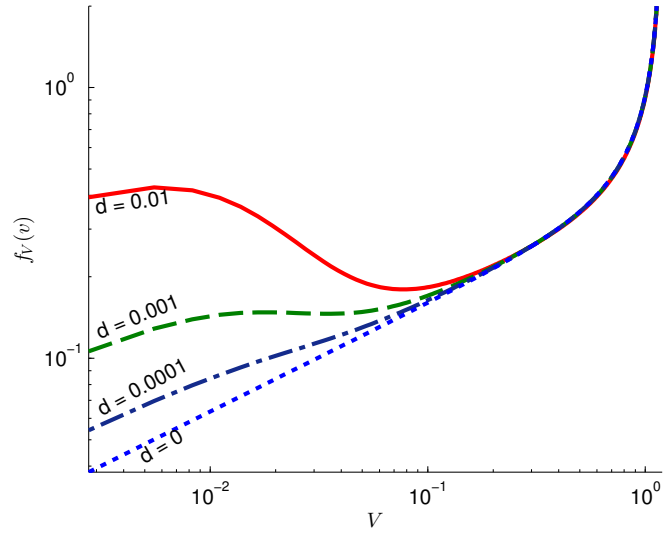
Figure 3.1: Worst $f_V(v)$ for different values of d and nominal Nakagami-m density with $m = 0.7$ (snr $= 30$ dB).
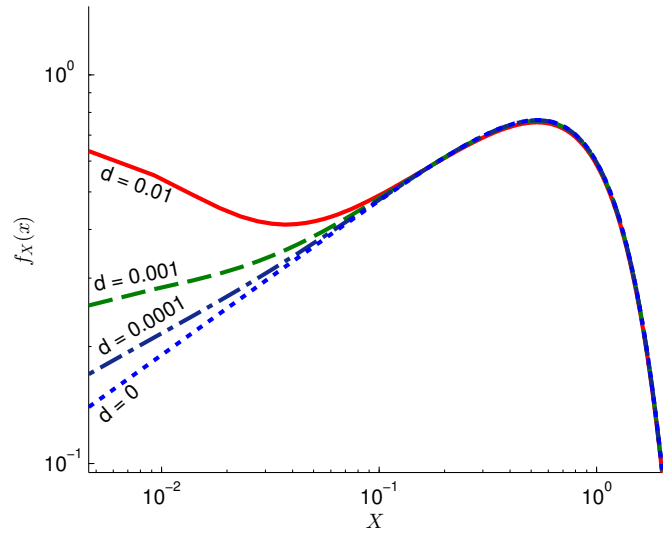
Figure 3.2: Worst $f_X(x)$ for different values of d and nominal Nakagami-m density with $m = 0.7$ (snr $= 30$ dB).

the nominal Nakagami-m density with $m = 0.7$. The curves with $d = 0$ are the nominal densities, while the other curves show the densities having divergence d from the nominal one and yielding the largest outage probability. Fig. 3.3 shows the resulting outage probabilities.
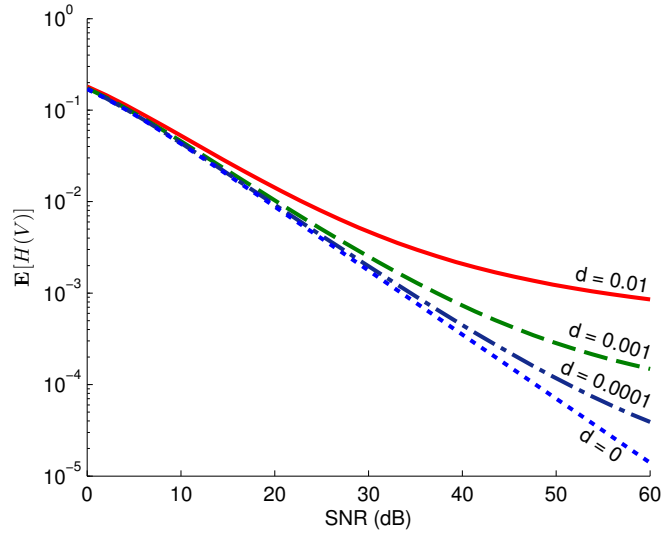
Figure 3.3: Worst outage probability for different values of d and nominal Nakagami-m density with $m = 0.7$.

*It can be observed how, for small values of **snr**, system performance is essentially determined only by **snr**, reflecting the fact that the effect of model uncertainty is "masked" by the effect of additive noise, while for high **snr** the performance loss is mainly due to model uncertainty.* □

3.1.2 Moment constraints

The problem of finding the sharpest bounds when the information on V consists of the values of some of its moments is called the *Generalized Moment Problem* (GMP). As expected, the tightness of the bounds depends on how any moments of V are available: the more they are, the tighter the bounds will be. In this section, we show how moment bounds can be computed under the assumption that the process whose envelope yields V is SIRP. Mathematically, the GMP for the lower

bound has the form

$$(P) \qquad \inf_{V \geq 0} \quad \mathbf{E}(H(V))$$

$$\text{s.t.} \quad \mathbf{E}(\boldsymbol{F}(V)) = \boldsymbol{b},$$

$$\mathbf{E}(\boldsymbol{G}(V)) \leq \boldsymbol{c},$$

where $\boldsymbol{F}(V)$ and $\boldsymbol{G}(V)$ are vector-valued functions known as generalized moment functions, and $\boldsymbol{b}$, $\boldsymbol{c}$ are constant vectors. This problem can be efficiently solved using semidefinite programming algorithms [53].

Notice that it is possible to obtain bounds even when the moments are only known within an interval (see [54] and the references within).

3.1.3 Introducing constraints on second-order statistics

Based on the parameters introduced in Section 2.6.3, moment problems that include LCR or AFD can be solved. For example, one may look for the SIRP envelope maximizing or minimizing the LCR given a set of moment constraints, or maximizing or minimizing the AFD. [1] Yet another problem consists of optimizing a performance parameter under the constraint that AFD does not exceed a given value.

3.2 Best and worst spherically invariant fading processes

If we look for the "best" and the "worst" fading pdfs with no constraints other than their moments, the solution turns out to be discrete (see, e.g., [55] and references within). Now, discrete pdfs for the fading envelope can hardly be motivated in the practice, and hence one may want to focus on a class of pdfs with a strong

---

[1] In this case the moment problem becomes of the fractional type, and hence transformable to a linear problem.

physical motivation. SIRP is one such class.

To this end, we may formulate the following GMP

$$(P') \qquad \inf_{f_X \in \mathcal{S}} \quad \mathbf{E}(h(X))$$

$$\text{s.t.} \quad \mathbf{E}(\boldsymbol{f}(X)) = \boldsymbol{b},$$

$$\mathbf{E}(\boldsymbol{g}(X)) \leq \boldsymbol{c},$$

(as well as the corresponding sup problem) where h is some performance metric such as bit error rate (2.62) and outage probability (2.64), and $\mathcal{S}$ is the collection of all SIRP fading distributions. Moreover, $\boldsymbol{f}(x) \triangleq [f_0(x), \ldots, f_n(x)]^T$, $\boldsymbol{g}(x) \triangleq [g_0(x), \ldots, g_m(x)]^T$, $\boldsymbol{b} \triangleq [b_0, \ldots, b_n]^T$, $\boldsymbol{c} \triangleq [c_0, \ldots, c_m]^T$ describe the moment constraints. Due to the probability density constraint, we assume $f_0 = 1$ and $b_0 = 1$ throughout. The GMP (P') is an infinite dimensional optimization problem over the set of SIRP distributions.

Due to property (2.20), under the assumption that the underlying fading process is SIRP, our problem can be formulated as in (P), where $H(V) = \mathbf{E}(h(X) \mid V)$, $\boldsymbol{F}(V) = \mathbf{E}(\boldsymbol{f}(X) \mid V)$ and $\boldsymbol{G}(V) = \mathbf{E}(\boldsymbol{g}(X) \mid V)$. This is a univariate moment problem with domain $\mathbb{R}^+$, which is known as the Stieltjes-type of moment problem, and can be reduced to a semidefinite program (SDP).

This approach is equivalent to Popescu's approach to the convex class of distribution constraints [53]. It follows from (2.20) that the class of SIRP fading densities is convex, and generated by the collection of Rice densities indexed by their variance. Here we reduce ourselves to considering the only constraint of unit second moment, reflecting the signal-to-noise ratio snr.

Assume R to have a Rice density with parameters ν and σ. We write $R \sim$

$\mathcal{R}(\nu, \sigma)$, and the density function is

$$f_R(r) = \frac{r}{\sigma^2} \exp\left\{-\frac{r^2 + \nu^2}{2\sigma^2}\right\} I_0\left(\frac{r\nu}{\sigma^2}\right). \tag{3.7}$$

Observing that

$$\mathcal{R}(\nu, \sigma) = \sigma \mathcal{R}(\nu/\sigma, 1), \tag{3.8}$$

we write the SIRP decomposition in the form

$$X = VR = \underbrace{(\sigma V)}_{V'} \underbrace{(R/\sigma)}_{\mathcal{R}(\nu/\sigma, 1)}, \tag{3.9}$$

which indicates that we incur in no loss of generality if we assume $R \sim \mathcal{R}(\nu/\sigma, 1)$. Introducing the "Rice factor" ($K = 0$ yields the Rayleigh density) $K \triangleq \frac{\nu^2}{2\sigma^2}$, we have

$$f_R(r) = 2r(1 + K) \exp\left\{-(1 + K)r^2 - K\right\} I_0\left(2r\sqrt{K(1 + K)}\right). \tag{3.10}$$

In our calculations, we fix K and vary the overall SNR, so that our generalized moment problem becomes

$$(P'') \qquad \inf_{f_X \in \mathcal{F}} \quad \mathbf{E}(h(X))$$

$$\text{s.t.} \quad \mathbf{E}(X^2) = \frac{N_0}{\mathcal{E}}\mathsf{snr},$$

where

$$\mathcal{F} \triangleq \{f_X : X = VR, V \geq 0, R \sim \mathcal{R}(\sqrt{2K}, 1)\}. \tag{3.11}$$

3.2.1 Deriving the bounds

To derive the bounds we shall make use of the following result, which can be derived from classical moment-bound theory [52] and generalizes a finding in [55].

Consider the expectation $\mathbb{E}_X h(X)$, where $h(\,\cdot\,)$ is monotonic in the interval $[0, A]$, and $\mathbb{E}\, X$ is known. Using Jensen's inequality, we have that:

- If $h(X)$ is decreasing and convex $\cup$, then $\mathbb{E}_X h(X)$ takes its *minimum* value if X is deterministic, i.e., $X = \mathbb{E}\, X$, and its *maximum* value if the distribution of X has only two mass points, one at 0 (with probability close to 1) and the other one at "infinity" (with probability close to zero).

- If $h(X)$ is increasing and concave $\cap$, then $\mathbb{E}_X h(X)$ takes its *maximum* value if X is deterministic, i.e., $X = \mathbb{E}\, X$, and its *minimum* value if the distribution of X has only two mass points, one at 0 (with probability close to 1) and the other one at "infinity" (with probability close to zero).

When the function $h(\,\cdot\,)$ is nonmonotonic, numerical SDP techniques should be used.

Error probability, unrestricted case   From (2.61), since $Q(\sqrt{x})$ is decreasing and convex $\cup$, we have that the maximum value of $P(e)$ is 0.5, while its minimum value is achieved for $V^2 R^2 = 1$, i.e., $P(e) = Q\left(\sqrt{2\,\mathsf{snr}}\right)$, corresponding to an AWGN channel.

Error probability, zero-mean SIRP process   From (2.63), since $P(e \mid V)$ is decreasing and convex $\cup$, we have that the maximum value of $P(e)$ is 0.5, while its minimum value is achieved for $V^2 = 1$ (V deterministic), so that that if the SIRP process has mean zero the best fading envelope is Rayleigh, yielding

$$P(e) = \frac{1}{2}\left(1 - \sqrt{\frac{\mathsf{snr}}{1 + \mathsf{snr}}}\right). \tag{3.12}$$

The gap between the upper and lower bound is rather large because the pdf of V is arbitrary. A more realistic setting is to assume V is unimodal [56, p.

158] with mode $\sqrt{\text{snr}}$. The unimodal constraint on the pdf of V is intuitively reasonable, since we can model a delta function for the pdf of V as the limit of some narrower and narrower unimodal distributions. Fig. 3.4 shows the feasible region of the (P') with the additional unimodal constrain on the pdf of V. The
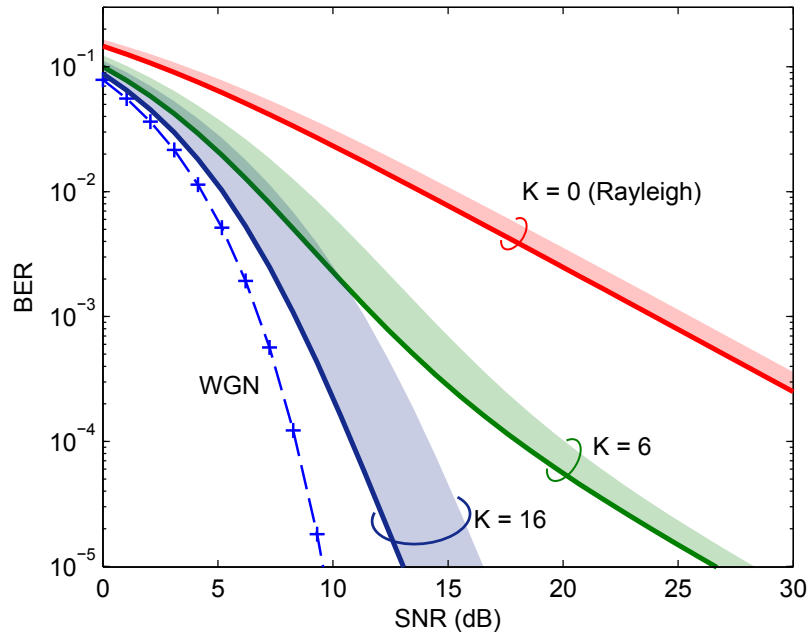
Figure 3.4: The feasible region of the GMP (P') and (P'') with objective function $P(e)$ is represented by the shaded area. The upper and lower bound can be found at the upper and lower boundary of the feasible region, respectively. The BER of Rician fading with factor $K = 0, 6$ and 16 are represented by solid lines.

Rayleigh fading case is represented by the solid line.

Error probability, nonzero-mean SIRP process Without the unimodal constraint, for a given value of K, the worst fading corresponds again to $P(e) = 0.5$, while the best fading is achieved for a deterministic V, thus yielding a Rice fading envelope.

By introducing the unimodal constraint on the pdf of V, the gap between the upper and the lower bound becomes tighter as shown in Fig. 3.4. The feasible region of (P'') is represented by the shaded area. Note that the lower bound

coincide with the Rician fading cases (solid lines) because the objective function is convex $\cup$ in V.

As expected, as $K \to \infty$ the best channel tends to the additive white Gaussian channel, so that

$$P(e) = Q\left(\sqrt{2\,\mathsf{snr}}\right). \tag{3.13}$$

Outage probability, unrestricted case   The function $h(x)$ defined in (2.67) can be written as the limit, as $\xi \to \infty$, of the decreasing concave $\cap$ function

$$h_{\mathrm{c}}(x) = 1 - x^{\xi/\sqrt{(2^\rho - 1)/V^2 \mathsf{snr}}}. \tag{3.14}$$

Thus, we can see that the maximum value of the outage probability is $p_{out} = 1$, achieved at $V^2 = 0$. The minimum value is achieved at $V^2 = 1$, corresponds to an unfaded channel, and takes values

$$p_{out} = \begin{cases} 0, & \text{if } \rho < C \\ 1, & \text{if } \rho > C, \end{cases} \tag{3.15}$$

where $C \triangleq \log_2(1 + \mathsf{snr})$ is the capacity of the AWGN channel.

Outage probability, Rayleigh R   With the unimodal constraint on the pdf of V, fig. 3.5 shows the feasible region of the GMP and upper and lower bounds to p_{out} for $\rho = 9$ bits per dimension pair. The outage probability for the Rayleigh case is represented by the solid line.

Outage probability, Rice R   Fig. 3.5 shows the feasible region of the GMP with the unimodal constraint. The outage probability for the Rician case with $K = 16$ is represented by the solid line.
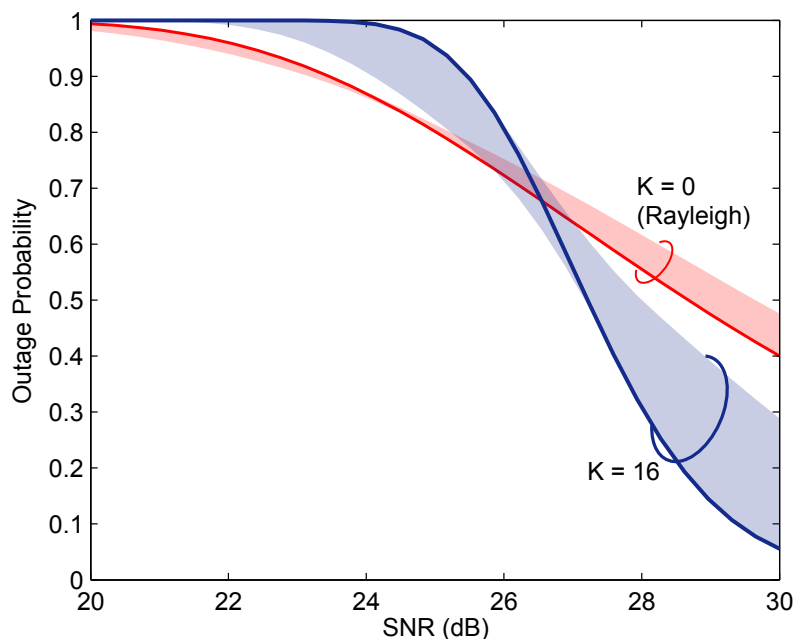
Figure 3.5: The upper and lower bound of BER and outage probability. The feasible region of the GMP (P') and (P'') with objective function p_{out} is represented by the shaded area. The upper and lower bound can be found at the upper and lower boundary of the feasible region, respectively. The outage probability of Rician fading with factor $K = 0$ and 16 are represented by solid lines.

3.3 Conclusions

We have examined the use of spherically invariant random processes to model fading in wireless communications. After proving that these processes are differential-entropy maximizers, we have described a mathematical technique allowing evaluation of the performance of digital communication over a channel affected by spherically invariant fading. Next, we have shown how sharp upper and lower moment bounds to system performance can be obtained when only a few moments of the fading process are known, and have derived the best and worst spherically invariant fading distributions for a given performance parameter and a given signal-to-noise ratio.

CHAPTER 4

Super-Efficient Monte Carlo Simulation

Ulam and von Neumann first formulated the Monte Carlo (MC) simulation methodology as one using random sequences to evaluate high-dimensional integrals [57]. Since then, MC simulations have been used in many applications to evaluate the performance of various systems that are not analytically tractable. The simplest, yet most important, form of MC simulation is used to approximate the integral

$$I = \int_{\Omega} A(x)dx, \tag{4.1}$$

where the integrand $A(x)$ is defined on the domain $\Omega = [a, b]$ for some real number $a < b$. To do this, we first choose a probability density function (pdf) $\rho(x) \neq 0$ in Ω, and define the function

$$B(x) := \frac{A(x)}{\rho(x)}, \tag{4.2}$$

The integral (4.1) is approximated by calculating the N-sample average

$$\frac{1}{N} \sum_{i=1}^{N} B(X_i) \approx \mathrm{e}b(x_j) = i, \qquad j = 1, 2, \dots, n. \tag{4.3}$$

where n is the sample size, x_i's are independent identically distributed ($i.i.d.$) random samples whose common pdf is $\rho(x)$, and $\mathbf{E}(.)$ denotes the expectation operator with respect to $\rho(x)$. By the strong law of large numbers, the summation (4.3) converges almost surely to i if the random samples are independent.

Furthermore, the variance of the approximation decreases at rate $1/n$. that is,

$$\text{Var}\left[\frac{1}{n}\sum_{i=1}^{n} b(x_i)\right] = \frac{1}{n}\text{Var}\left[b(x_j)\right], \qquad j = 1, 2, \ldots, n. \tag{4.4}$$

Note that (4.4) holds regardless of the dimension of the domain ω of the integrand $a(x)$, which make Monte Carlo simulation suitable for performing multidimensional integrations. Umeno's super-efficient Monte Carlo (SEMC) algorithm [7] is a variation of standard MC based on chaotic sequences, and exhibits a superior rate of convergence. Umeno and Yao's approximate SEMC [58] removes some restriction in the original method to make the concept of super-efficiency applicable to more general situations. In the following sections, we review the pseudo-random number generation used in conventional MC simulation, and describe the concept of chaotic sequences and chaotic MC simulation. The correlation between samples of the chaotic sequence gives rise to the super-efficient convergence rate, which makes chaotic MC simulation super-efficient. We illustrate how to generate chaotic sequences from the practical point of view, and how to apply super-efficient simulation methods to a wide class of integrands using the notion of approximate SEMC. In the last section, we provide some concluding remarks and point to the directions for future research.

4.1   Pseudo-Random Number and Chaotic Sequence

A fundamental question of implementing Monte Carlo simulation is how to generate random samples. It turned out that the generation of truly random sequences in a controlled manner is a nontrivial problem. Fortunately, in many applications it suffices to use pseudo-random (PR) sequences [59]. A PR sequence is generated deterministically by some transformations, and it appears to be random from the statistical point of view [60]. For example, the sequence of linear congruential PR

numbers (LCPRN) $x_0, x_1, \ldots$ is produced by the recursion

$$x_{n+1} = (ax_n + c) \mod m, \tag{4.5}$$

where $0 < a < m$, $0 \leq c < m$ and $0 \leq x_0 < m$ is the seed of the sequence [57]. When the parameters a, c, m and x_0 are properly selected, the linear congruential recursion can produce a sequence of period m. LCG is one of the oldest and a popular algorithm for generating PR sequences due to its simplicity and well-understood properties. Although a LCPRN sequence passes many randomness tests, LCG has some serious defects. Most notably, it exhibits correlation between successive samples. The Mersenne Twister algorithm [61] is a better choice for generating high quality PR numbers for reducing this correlation. For example, Matlab uses the Mersenne Twister algorithm as the default uniform random number generator starting from its version 7.4 in 2007 [62]. We can think of the process of generating the PR sequence as applying a deterministic transformation on some state variable repeatedly. More precisely, let Ω denote the collection of all possible states the of PR generator and $T : \Omega \mapsto \Omega$ denote the transformation. We select a seed or initial state $x_0 \in \Omega$ and generate the sequence $(x_1, x_2, \ldots)$ by

$$x_{i+1} = T(x_i), i = 0, 1, \ldots. \tag{4.6}$$

The output of the PR generator can be written as $y_i = g(x_i)$ for some suitable output function g.

Another way of generating PR sequences is through dynamical systems. Formally, a measure-preserving dynamical system is the quadruple $(\Omega, \mathcal{A}, \mu, T)$, where Ω is the state space, $\mathcal{A}$ is the σ-algebra on Ω, μ is a probability measure on $\mathcal{A}$ and T is a mapping from Ω to itself such that

$$\mu(T^{-1}(E)) = \mu(E) \tag{4.7}$$

for all measurable $E \in \mathcal{A}$. A mapping T that satisfies (4.7) is called a measure-preserving transformation. The initial state x_0 of a dynamical system at time 0 is a point in the domain Ω, and the evolution of the state is governed by a mapping T such that $x_{i+1} = T(x_i)$ for $i = 0, 1, \ldots$. The sequence $(x_1, x_2, \ldots)$ with seed $x_0 \in \Omega$ is called the orbit of the dynamical system under T. The "time average" of the integrand $B(x)$ with respect to the orbit is defined as

$$\langle B(x_i) \rangle_N := \frac{1}{N} \sum_{i=1}^{N} B(x_i). \tag{4.8}$$

A natural question to ask is whether (4.8) will converge or not as $N \to \infty$. More importantly, will it converge to the ensemble average I? Birkhoff theorem [63] says that, the time average of an integrable function $B(x)$ will converge to an integrable function $\bar{B}(x)$ almost surely, and $\mathbf{E}(B(X)) = \mathbf{E}(\bar{B}(X))$, where the expectation is taken with respect to the measure μ. In general $\bar{B}(x)$ is a function of the initial seed x_0. If a measure-preserving dynamical system has the property that every integrable function $B(x)$ has a constant time average, then it is called an ergodic dynamical system. By Birkhoff theorem, this constant must agree with the ensemble average I. That is,

$$\langle B(x_i) \rangle_N \to \mathbf{E}(B(X)) \quad \text{pointwise as } N \to \infty. \tag{4.9}$$

In this chapter, we will focus on a special type of ergodic system, which has "chaotic" behavior in the sense of Auslander-Yorke [64] that 1) it has a dense orbit in the space Ω, and 2) the orbits are unstable, meaning that orbits arising from different x_0, even if arbitrarily close to each other, grow apart exponentially. For example, the doubling map

$$T_d(x) = \begin{cases} 2x & \text{if } 0 \leq x < 0.5, \\ 2x - 1 & \text{if } 0.5 \leq x < 1, \end{cases} \tag{4.10}$$

defined on $\Omega = [0, 1)$ is known to be chaotic. The invariant pdf $\rho(x)$ is the uniform distribution on Ω, that is $\rho(x) = 1$ on $0 \leq x < 1$ and 0 elsewhere. The doubling map is related to many other chaotic dynamical systems, like the Chebyshev dynamical system. The Chebyshev dynamical system of order p is defined on the domain $\Omega = [-1, 1]$ with the mapping

$$T_p(y) = \cos(p \arccos(y)), \tag{4.11}$$

where p is a positive integer. The mapping $T_p(y)$ is in fact the pth order Chebyshev polynomial of the first kind. The Chebyshev dynamical system of order 2 is related to the doubling map via the relation

$$y_i = \cos(2\pi x_i), \tag{4.12}$$

where $x_i = T_d(x_{i-1})$.

4.2 Chaotic Monte Carlo Simulation

A chaotic MC simulation is a MC simulation with a PR sequence replaced by a chaotic sequence [7]. Furthermore, specifically, let T be a chaotic mapping, and $\rho(x)$ its invariant pdf. We first draw a seed x_0 from the invariant pdf $\rho(x)$, and use the chaotic mapping T to generate the sequence $x_1, x_2, \ldots, x_N$ by $x_i + 1 = T(x_i)$ for $i = 0, 1, \ldots, N - 1$, where N is the number of samples. The "time-average"

$$\langle B(x_i) \rangle_N = \frac{1}{N} \sum_{i=1}^{N} B(x_i) \rightarrow I \tag{4.13}$$

will converge to the integral I defined in (4.1) as N approaches infinity [63].

4.2.1 Statistical and Dynamical Correlation

The greatest distinction between conventional and chaotic MC simulation is that the chaotic sequence has correlation between samples. For conventional MC simulation, good PR number generators produce near iid samples. Correlation between samples is generally considered to be a bad thing, because it may decrease the convergence rate of the simulation. However, if we select the chaotic mapping carefully, the correlation between samples may actually improve the convergence rate for certain integrands. In the following, we show how the correlation can affect the variance of the approximation error. For measure-preserving dynamical systems, any measurable function $B(x)$ on Ω forms a stationary random process $\{B(x_k)\}_{k \in \mathbb{N}}$, where $B(x_k) = B(T^k(x_0))$. For simplicity, denote $B(x_k)$ by B_k and $\langle B(x_i) \rangle_N$ by $\langle B \rangle_N$. Define the autocorrelation function

$$R(k) = \mathbf{E}((B_{k+i} - I)(B_i - I)), \tag{4.14}$$

where the expectation is taken with respect to the invariant pdf $\rho(x)$, and $i = 1, 2, \ldots$ is arbitrary because $B(x_k)$ is stationary. The variance of the approximation error $\langle B \rangle_N - I$ is given by

$$\sigma_N^2 := \mathbf{E}(((\langle B \rangle_N - I)^2) = \frac{1}{N}\mathrm{Var}\,[B] + \frac{2}{N^2}\sum_{k=1}^{N}(N - k)R(k). \tag{4.15}$$

The first term on the right-hand side in (4.15) is called the statistical correlation, which depends on the integrand $B(x)$ and the pdf $\rho(x)$. The second term is called the dynamical correlation, which depends on the integrand as well as on the chaotic sequence [7]. Clearly, for iid random samples $x_1, x_2, \ldots$, we have $R(k) = 0$, and hence (4.15) reduces to the conventional case (4.4), where the convergence rate is $1/N$. If there are positive correlations between samples, the variance of the approximation error σ_N^2 will increase. On the other hand, negative correlations

between samples might decrease σ_N^2. It is therefore natural to ask what is the best achievable convergence rate of chaotic MC simulation. This leads to the notion of super-efficiency of the chaotic MC simulation detailed in next section.

4.2.2 Super-Efficient Chaotic MC Simulation

Rewrite the variance of the approximation error (4.15) as

$$\sigma_N^2 = \frac{1}{N} \underbrace{\left(\mathrm{Var}\,[B] + 2 \sum_{k=1}^{N} R(k) \right)}_{\eta} - \frac{2}{N^2} \sum_{k=1}^{N} k R(k). \tag{4.16}$$

This shows that the convergence rate of σ_N^2 has two contributors, one decaying as $1/N$ and the other as $1/N^2$. Eventually the convergence rate will be dominated by $1/N$, which suggests that the chaotic MC simulation has the same performance as the standard MC simulation. However, if the dynamical system introduces the right amount of negative correlation such that $\eta = 0$, the convergence rate becomes $1/N^2$, which is a huge improvement over the conventional MC simulation. To obtain $\eta = 0$, and hence convergence rate $1/N^2$, one should suitably combine the sequence correlation with the integrand [7]. We say the chaotic MC simulation is Super-Efficient (SE) if the variance of the approximation error decays as $1/N^2$ for $N \to \infty$. Umeno [7] also showed that the condition $\eta = 0$ for super-efficiency is necessary as well as sufficient.

Example 11. *Consider the integrand defined on p.1447 of [7]*

$$A(x) = \frac{-8x^4 + 8x^2 + x - 1}{\pi \sqrt{1 - x^2}}. \tag{4.17}$$

It satisfies the SE condition under Chebyshev dynamical systems (4.11) of order $p = 2$ and $p = 4$. Fig. 4.1 shows the results of applying the chaotic MC simulation to find the integral of $A(x)$ using Chebyshev chaotic mappings, and compares their

convergence rates with the conventional MC simulation using uniform PR samples.
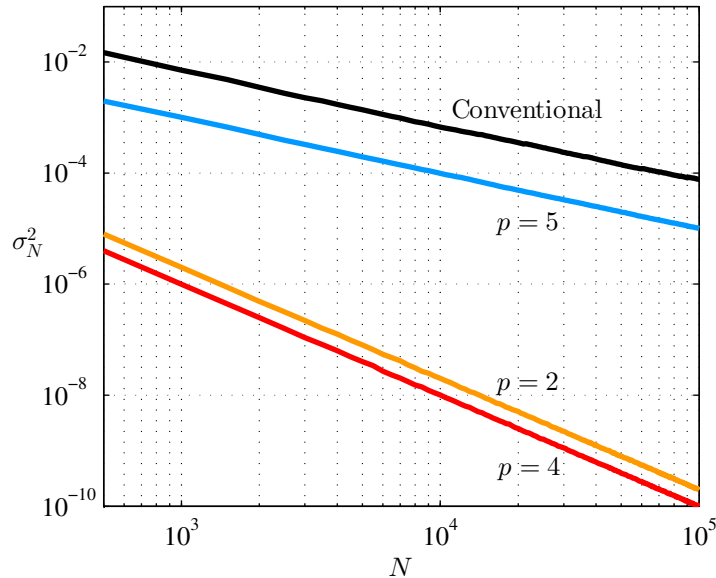
Figure 4.1: Variance of the approximation error σ_N^2 versus the sample size N. We compare the convergence rate of the chaotic MC simulation using Chebyshev mapping of order $p = 2$, 4 and 5, and the conventional MC simulation.

The numerical results verify that the chaotic MC simulation is super-efficient when $p = 2$ and $p = 4$. On the other hand, both conventional and chaotic MC simulation with $p = 5$ have convergence rate $1/N$ Using the properties of the Chebyshev polynomials, it can be shown that the variances σ_N^2 under $p = 2$ and $p = 4$ are $2/N^2$ and $1/N^2$, respectively, which indicate super-efficiency. On the other hand, the case $p = 5$ yields a nonzero η in (4.16). In next section, we present a very powerful characterization of super-efficiency.

4.2.3 Condition for Super-Efficiency

The super-efficiency condition $\eta = 0$ arising from (4.16) does not explicitly suggest any way to achieve it. Umeno [7] first gave a characterization of super-efficiency in terms of the coefficients of the generalized Fourier series of the modified integrand $B(x) = A(x)/\rho(x)$ for Chebyshev and piecewise linear dynamical systems,

but the results in [7] did not made clear whether those conclusions are also applicable to other dynamical systems. Yao [58] established the connection between Super-Efficiency and the Lebesgue spectrum of ergodic theory [63], which puts the super-efficient condition derived in Umeno's work in a general framework, and generalizes Umeno's result to a wide range of dynamical systems, namely those with a Lebesgue spectrum. This observation helps us explain the super-efficiency systematically and hopefully leads to practical algorithms as detailed in section 5. In this section, we briefly introduce the concept of Lebesgue spectrum and the important characterization of super-efficiency in terms of Lebesgue spectrum.

Definition 1. *Let Λ be an index sets and $\mathbb{N}_0 = \{0, 1, 2, \ldots\}$. A dynamical system with mapping T is said to have countable one-sided Lebesgue spectrum if there exists an orthogonal basis containing the constant function $\mathbb{1}$ and the collection of functions $\{f_{\lambda,j}(x) \,|\, \lambda \in \Lambda, j \in \mathbb{N}_0\}$ such that*

$$f_{\lambda,j}(T(x)) = f_{\lambda,j+1}(x) \tag{4.18}$$

for all λ and j, where the index λ labels the classes and j labels the functions within each class.

The Koopman operator induced by the transformation T is defined as $U_T f(x) := f(T(x))$. It is an isometry and it becomes unitary when T is invertible [65]. We may rewrite (4.18) as $U_T f_\lambda, j = f_{\lambda,j+1}$, which means U_T has invariant subspaces $W_\lambda = \text{span}(f_{\lambda,0}, f_{\lambda,1}, \ldots)$ generated by $f_{\lambda,0}$'s. Therefore, the "least element" of the invariant subspace W_λ is the generating vector $f_{\lambda,0}$. Note that the dynamical system has one-sided Lebesgue spectrum if and only if it is exact (see e.g. [63] and [66]). If a dynamical system has Lebesgue spectrum, then it is strongly mixing [63] and hence chaotic in the sense of Auslander-Yorke [64]. All the dynamical systems we consider in this chapter have Lebesgue spectrum. Since $\{\mathbb{1}\} \cup \{f_{\lambda,j}(x) \,|\, \lambda \in \Lambda, j \in \mathbb{N}_0\}$ forms a complete orthogonal basis on the square in-

tegrable functions $L^2(\Omega)$, the generalized Fourier series expansion of an integrand $B(x)$ can be written as

$$B(x) = b_{0,0} + \sum_{\lambda \in \Lambda} \sum_{j \in \mathbb{N}_0} b_{\lambda,j} f_{\lambda,j}(x). \tag{4.19}$$

where $b_{0,0}$ is the coefficient corresponding the constant function $\mathbb{1}$, which is just the integral I of $B(x)$.

Theorem 5. *Consider a dynamical system which has Lebesgue spectrum $\{f_{\lambda,j}(x) \mid \lambda \in \Lambda, j \in \mathbb{N}_0\}$ indexed by the sets Λ. The associated chaotic MC simulation is super-efficient if and only if*

$$d_\lambda := \sum_{j=0}^{\infty} b_{\lambda,j} = 0 \quad \text{for all } \lambda \in \Lambda, \tag{4.20}$$

where

$$B(x) = b_{0,0} + \sum_{\lambda \in \Lambda} \sum_{j \in \mathbb{N}_0} b_{\lambda,j} f_{\lambda,j}(x) \tag{4.21}$$

is the Generalized Fourier series of $B(x) = A(x)/\rho(x)$.

Proof. The autocorrelation function (4.14) can be written as

$$R(n) = \mathbf{E}\left(\sum_{\lambda \in \Lambda} \sum_{j=0}^{\infty} b_{\lambda,j} f_{\lambda,j}(T^n x) \sum_{\nu \in \Lambda} \sum_{i=0}^{\infty} b_{\lambda,i} f_{\lambda,i}(x) \right) \tag{4.22}$$

$$= \sum_{\nu,\lambda \in \Lambda} \sum_{i,j=0}^{\infty} b_{\lambda,j} b_{\lambda,i} \, \mathbf{E}(f_{\lambda,j+n}(x) f_{\lambda,i}(x)) \tag{4.23}$$

$$= \sum_{\lambda \in \Lambda} \sum_{j=0}^{\infty} b_{\lambda,j} b_{\lambda,j+n}. \tag{4.24}$$

From (4.16), η can be expressed as

$$\eta = \sum_{\lambda \in \Lambda} \left(\sum_{j=0}^{\infty} b_{\lambda,j}^2 + 2 \sum_{k=1}^{N} \sum_{j=0}^{\infty} b_{\lambda,j} b_{\lambda,j+k} \right) = \sum_{\lambda \in \Lambda} \left(\sum_{j=0}^{\infty} b_{\lambda,j}^2 + 2 \sum_{j=0}^{\infty} \sum_{i=j+1}^{j+N} b_{\lambda,j} b_{\lambda,i} \right). \tag{4.25}$$

As N goes to infinity,

$$\eta = \sum_{\lambda \in \Lambda} \left(\sum_{j=0}^{\infty} b_{\lambda,j}^2 + 2\sum_{i>j}^{\infty} b_{\lambda,j} b_{\lambda,i} \right) = \sum_{\lambda \in \Lambda} \left(\sum_{j=0}^{\infty} b_{\lambda,j} \right)^2. \tag{4.26}$$

Therefore $\eta = 0$ if and only if $\sum_{j=0}^{\infty} b_{\lambda,j} = 0$ for each $\lambda \in \Lambda$. $\qquad\square$

Thus, the explicit condition for super-efficiency is that the sum of coefficients in each class λ be zero. We say that an integrand $A(x)$ is Super-Efficient (under the dynamical system with mapping T and invariant pdf ρ) if (4.20) holds for $B(x) = A(x)/\rho(x)$.

Example 12. *Consider a variant of the integrand* (4.17)

$$A(x) = \frac{-8x^4 + 8x^2 + (1+\epsilon)x - 1}{\pi\sqrt{1-x^2}} = B_\epsilon(x)\rho(x). \tag{4.27}$$

Under the Chebyshev dynamical system (4.11), $B_\epsilon(x)$ *can be expanded as*

$$B_\epsilon(x) = (1+\epsilon)T_1(x) - T_4(x). \tag{4.28}$$

If $p = 2$, the coefficients of the generalized Fourier series are $b_{1,0} = 1 + \epsilon$, $b_{1,2} = -1$ and zero otherwise. The sum of coefficients are $d_1 = \epsilon$ and $d_\lambda = 0$ for $\lambda \neq 1$. Therefore $A(x)$ is super-efficient if and only if $\epsilon = 0$. When $\epsilon \neq 0$ we have "mismatched" SE MC simulation, which appears to be super-efficient for small N but gradually loses super-efficiency as N increases [67]. See Fig. 4.2.

From the previous example, it is now clear why the integrand $A(x)$ in (4.17) under the chaotic mappings T_2 and T_4 (but not T_5) are super-efficient. More specifically, the modified integrand under the Chebyshev dynamical system can be written as $B(x) = T_1(x) - T_4(x)$. When $p = 2$ and $p = 4$, the sum of coefficients in the class $\lambda = 1$ is $d_1 = 1 - 1 = 0$, and all other d_λ's are zero. Hence, the chaotic
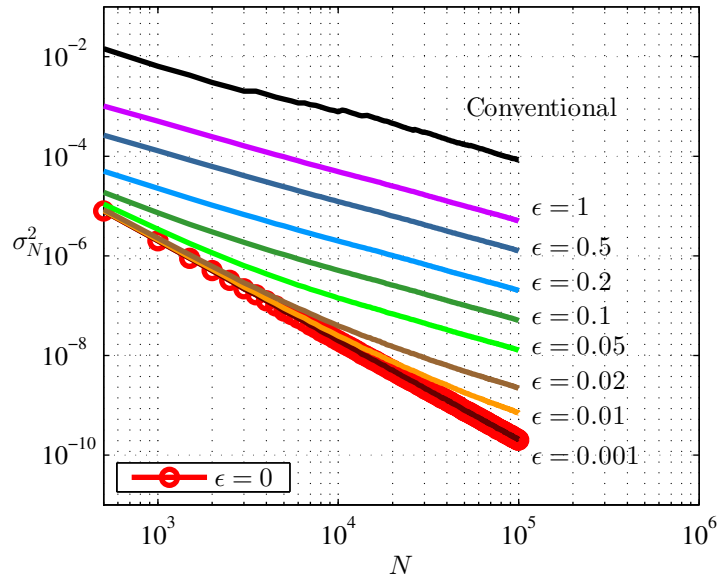
Figure 4.2: The variance of the approximation error σ_N^2 versus the number of samples N. The slope of the conventional MC simulation curve is -1, indicating its $1/N$ behavior. On the other hand, the slope of the super-efficient MC simulation is -2 because σ_N^2 decays like $1/N^2$. Between these two extremes are the mismatched SE MC simulations with different size of ϵ. For $\epsilon = 0.001$, the curve is almost identical to the super-efficient curve. As ϵ becomes larger, the slope of the mismatched SE MC simulations gradually increase as N becomes larger.

MC simulations under both chaotic mappings T_2 and T_4 are super-efficient. On the other hand, when $p = 5$, the chaotic MC simulation has the same convergence rate as the conventional MC simulation, because $d_1 = 1$ does not satisfy the super-efficiency condition.

4.2.4 Multi-dimensional Dynamical Systems

Note that the characterization of super-efficiency (4.20) holds regardless of the dimension of the domain Ω as long as the system has Lebesgue spectrum. Nevertheless, high-dimensional dynamical systems arise naturally through the product of multiple one-dimensional dynamical systems. In this section, we show that the Lebesgue spectrum of the product dynamical system has a special structure, and we derive the corresponding necessary and sufficient condition for super-

efficiency. For simplicity, we consider two one-dimensional dynamical systems $(\Omega_1, \mathcal{A}_1, \mu_1, T_1)$ and $(\Omega_2, \mathcal{A}_2, \mu_2, T_2)$. The product dynamical system $(\Omega, \mathcal{A}, \mu, T)$ is defined as the product probability space $(\Omega_1 \times \Omega_2, \mathcal{A}_1 \otimes \mathcal{A}_2, \mu_1 \otimes \mu_2)$ with the mapping $T(x, y) = T_1(x) T_2(y)$. It is not difficult to show that the product space is also a measure-preserving dynamical system [66]. Suppose both the dynamical systems $(\Omega_1, \mathcal{A}_1, \mu_1, T_1)$ and

$$(\Omega_2, \mathcal{A}_2, \mu_2, T_2)$$

have Lebesgue spectrum with basis function $\mathcal{B}_1 = \{\mathbb{1}\} \cup \{f^{(1)}_{\lambda_1, j_1}(x) \,|\, \lambda_1 \in \Lambda_{1, j_1} \in \mathbb{N}_0\}$ and $\mathcal{B}_2 = \{\mathbb{1}\} \cup \{f^{(2)}_{\lambda_2, j_2}(y) \,|\, \lambda_2 \in \Lambda_{2, j_2} \in \mathbb{N}_0\}$, respectively. The complete orthogonal basis on $(\Omega_1 \times \Omega_2, \mathcal{A}_1 \otimes \mathcal{A}_2, \mu_1 \otimes \mu_2)$ is $\mathcal{B} = \mathcal{B}_1 \times \mathcal{B}_2$, which can be written explicitly as

$$\{\mathbb{1}\} \cup \{f^{(1)}_{\lambda_1, j_1}(x)\} \cup \{f^{(2)}_{\lambda_2, j_2}(y)\} \cup \{f^{(1)}_{\lambda_1, j_1}(x) f^{(2)}_{\lambda_2, j_2}(y)\} \quad \text{for } \lambda_1 \in \Lambda_1, \lambda_2 \in \Lambda_{2, j_1, j_2} \in \mathbb{N}_0. \tag{4.29}$$

Because of the constant function $\mathbb{1}$, the expression for $\mathcal{B}$ in (4.29) becomes very messy. It gets even more cumbersome for higher dimensional spaces. For notational convenience, we define the redundant functions

$$f_{0, j}(x) := 1 \quad \text{for all } j = 0, 1, 2, \ldots. \tag{4.30}$$

This way, the constant function $\mathbb{1}$ can be indexed by $(0, j)$ for any non-negative j. To make sense of this definition, we require that $b_{0, j} = 0$ for all $j > 0$ and $b_{0, 0} = I$ is the integral of $B(x)$.

Clearly, the action of U_T on the basis function is

$$U_T f^{(1)}_{\lambda_1, j_1}(x) f^{(2)}_{\lambda_2, j_2}(y) = f^{(1)}_{\lambda_1, j_1}(T_1(x)) f^{(2)}_{\lambda_2, j_2}(T_2(y)) = f^{(1)}_{\lambda_1, j_1+1}(x) f^{(2)}_{\lambda_2, j_2+1}(y) \tag{4.31}$$

for all $\lambda_1 \in \Lambda_1, \lambda_2 \in \Lambda_2$ and $j_1, j_2 \in \mathbb{N}_0$. That is, the index of the basis function changes from $(\lambda_1, \lambda_{2, j_1, j_2})$ to $(\lambda_1, \lambda_{2, j_1+1, j_2+1})$ after applying U_T. From (4.31) we

found that the least element in each invariant subspace associated with U_T have the form

$$f^{(1)}_{\lambda_1, j_1}(x) f^{(2)}_{\lambda_2, j_2}(y), \quad j_1, j_2 \in \mathbb{N}_0, \text{ and } j_1 j_2 = 0. \tag{4.32}$$

That is, at least one of the index j_1 and j_2 of the least element must be zero so that no other function can precede it under U_T. See Fig. 4.3.
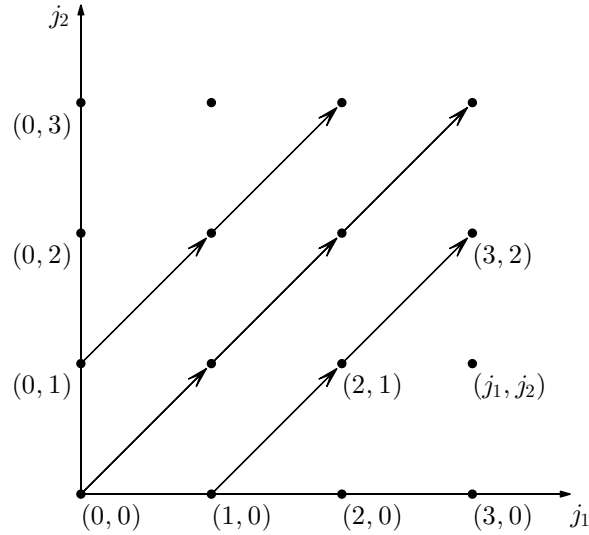
Figure 4.3: An illustration of the Lebesgue spectrum for 2D systems. Given λ_1 and λ_2, each circle represents an basis function indexed by $(\lambda_1, \lambda_2, j_1, j_2)$. Applying T on the basis function increases both of j_1 and j_2 by 1. The least elements are on the boundary. They generate the invariant subspace.

Therefore we define the index set $\Lambda = \Lambda_1 \times \Lambda_2$ and $J = \{(j_1, j_2) \in \mathbb{N}_0 : j_1, j_2 \in \mathbb{N}_0, j_1 j_2 = 0\}$ to index the least elements in each of the invariant subspaces associated with U_T. The generalized Fourier expansion of an integrable function $B(x, y)$ is given by

$$B(x, y) = \sum_{\lambda \in \Lambda} \sum_{\mathbf{j} \in J} \sum_{k=0}^{\infty} b_{\lambda, \mathbf{j}+k\mathbf{1}} f_{\lambda, \mathbf{j}+k\mathbf{1}}(x, y), \tag{4.33}$$

where $\mathbf{1}$ denotes the vector with all unity components. Similarly, for d-dimensional

space, we define

$$\Lambda = \prod_{i=1}^{d} \Lambda_i \tag{4.34}$$

and

$$J = \{(j_1, j_2, \ldots, j_d) \in \mathbb{N}_0^d \ : \ j_1 j_2 \ldots j_d = 0\}. \tag{4.35}$$

The necessary and sufficient condition for super-efficiency is given by

$$d_{\lambda,\mathbf{j}} = \sum_{k=0}^{\infty} b_{\lambda,\mathbf{j}+k\mathbf{1}} = 0 \tag{4.36}$$

for each $\lambda \in \Lambda$ and $\mathbf{j} \in J$.

Example 13. *2D Walsh system. The Walsh system is a complete orthonormal set associated with the doubling map* (4.10). *The Rademacher system on the unit interval equipped with Lebesgue measure is a set of orthonormal functions*

$$\{x \mapsto r_n(x) = \mathrm{sgn}(\sin(2^{n+1}\pi x) \,|\, x \in [0, 1), n \in \mathbb{N}\}, \tag{4.37}$$

where sgn *is the signum function. Note that the Rademacher system is not complete. The complete orthonormal basis is the given by the Walsh-Paley system*

$$\{W_n(x) : [0, 1) \mapsto \{-1, 1\} \,|\, n \in \mathbb{N}_0\}, \tag{4.38}$$

where $W_0(x) = 1$ and $W_n(x) = r_{\nu_1}(x)r_{\nu_2}(x)\cdots r_{\nu_m}(x)$, where

$$n = 2^{\nu_1} + 2^{\nu_2} + \cdots + 2^{\nu_m} \tag{4.39}$$

is the binary representation of n and $\nu_1 < \nu_2 < \cdots < \nu_m$. To show that the

Walsh-Paley system satisfies (4.18), *observe that* $r_n(T_d(x)) = r_{n+1}(x)$ *and*

$$W_n(T(x)) = r_{\nu_1}(T(x))r_{\nu_2}(T(x)) \cdots r_{\nu_m}(T(x)) \tag{4.40}$$

$$= r_{\nu_1+1}(x)r_{\nu_2+1}(x) \cdots r_{\nu_m+1}(x) \tag{4.41}$$

$$= W_{2n}(x). \tag{4.42}$$

Therefore the complete orthonormal basis is given by

$$f_{\lambda,j}(x) := W_{\lambda 2^j}(x). \tag{4.43}$$

Because of the simple structure of the Walsh function, there is a fast way of evaluating it. Let $x = 0.b_1 b_2 \ldots b_p$ *be the first p-bit binary representation of a number* $x \in [0, 1)$. *Then*

$$W_n(x) = -1^{\oplus_{i=1}^{p}(b_i \wedge d_{p-i+1})}, \tag{4.44}$$

where $\wedge$ *is the logic AND and* $\oplus$ *is the exclusive-OR.*

Consider the integrand

$$B(x,y) = W_1(x)W_2(y) + 0.5 W_6(x)W_1(y) - (1-\epsilon)(W_2(x)W_4(y) + 0.5 W_{12}(x)W_2(y)) \tag{4.45}$$

on the product space $[0,1)^2$. *By* (4.43) *we can verify that*

$$d_{\lambda_1,j_1} = b_{\lambda_1,j_1} + b_{\lambda_1,j_1+1} = 1 - (1-\epsilon) = \epsilon, \qquad \boldsymbol{\lambda}_1 = (1,1), \boldsymbol{j}_1 = (0,1), \tag{4.46}$$

$$d_{\lambda_1,j_1} = b_{\lambda_2,j_2} + b_{\lambda_2,j_2+1} = 0.5 - 0.5(1-\epsilon) = 0.5\epsilon, \quad \boldsymbol{\lambda}_2 = (3,1), \boldsymbol{j}_2 = (1,0), \tag{4.47}$$

which satisfies super-efficient condition (4.36) *if* $\epsilon = 0$. *See Fig. 4.4.*
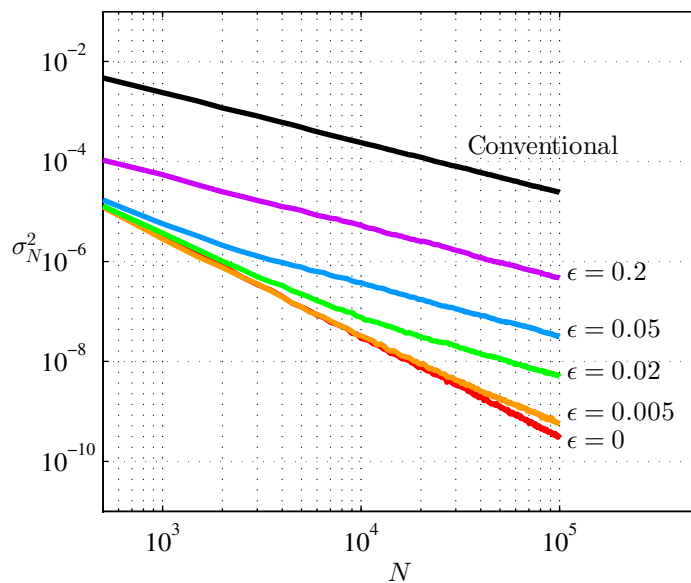
Figure 4.4: The variance of the approximation error σ_N^2 versus the number of samples N. The slope of the conventional MC simulation curve is -1, indicating $\alpha = 1$ behavior. On the other hand, the slope of the super-efficient MC simulation is -2. The ϵ indicates the degree of mismatch of the super-efficiency. As ϵ becomes larger, the slope of the mismatched SE MC simulations gradually increase as N becomes larger.

CHAPTER 5

Approximate Super-Efficient Monte Carlo Simulation

Applying chaotic MC simulation on super-efficient integrands yields superior convergence rate of $1/N^2$ in contrast to the conventional convergence rate $1/N$. However, most integrands are not SE. This implies that chaotic MC simulation has no advantage over conventional MC simulation in general. While most integrands do not satisfy the SE condition, Yao proposed the Approximate Super-Efficient (ASE) algorithm [58] that modifies the integrand so that it is approximately SE, and by applying chaotic MC simulation on the modified integrand, we get a much faster convergence rate of $1/N^\alpha$ for convergence exponent α between 1 and 2 (a concept equivalent to ASE was proposed by Umeno in 2002 [68]. A crucial step here consists of adding to $B(x)$ a function that has zero mean. This will not change the integral of $B(x)$ [58]. Therefore, if we know the sum of coefficients d_λ in (4.20) for each class λ, then the new integrand

$$B'(x) = B(x) - \sum_{\lambda \in \Lambda} d_\lambda f_{\lambda,0}(x) \tag{5.1}$$

will be super-efficient without changing the integral of $B(x)$ (recall the basis functions $f_{\lambda,j}(x)$'s have zero mean for all λ and j). We call the function $d_\lambda f_{\lambda,0}(x)$ the compensator associated with class λ. By subtracting compensators from $B(x)$, we introduce negative dynamical correlation, and make the chaotic MC simulation nearly super-efficient. In practice, since we do not know the sum of coefficients, it

is not possible to construct infinitely many compensators to achieve perfect super-efficiency. The idea of ASE algorithm is to approximate the sum of coefficients d_λ by its K_λ-term partial sum

$$\hat{d}_\lambda \approx b_{\lambda,0} + b_{\lambda,1} + \ldots + b_{\lambda,K_\lambda} \tag{5.2}$$

using conventional MC or chaotic MC simulations, where L_λ is some (hopefully not too large) positive integer. Then we form the modified integrand

$$\tilde{B}(x) = B(x) - \sum_{\lambda \in \Lambda_\omega} \hat{d}_\lambda f_{\lambda,0}(x), \tag{5.3}$$

where the index set Λ_ω contains ω classes. If the sum of coefficients $\tilde{d}_\lambda = d_\lambda - \hat{d}_\lambda$ of $\tilde{B}$ is close to zero, and $\tilde{\eta} = \sum_{\lambda \in \Lambda} \tilde{d}_\lambda = \epsilon > 0$ is small, then from (4.16) the variance of the approximation error can be written as

$$\sigma_N^2 = \frac{\epsilon^2}{N} + \frac{\zeta}{N^2} \tag{5.4}$$

for some ζ. The effective convergence rate can be expressed as $1/N^\alpha$, where $\alpha \in [1, 2]$ is referred to as the convergence exponent, and it is defined as the negative slope of the N-σ_N^2 curve (see Fig. 5.1).

$$\alpha := -\frac{\mathrm{d}\sigma_N^2}{\mathrm{d}N} \frac{N}{\sigma_N^2}. \tag{5.5}$$

The conventional MC simulation has $\alpha = 1$ and the Super-Efficient MC simulation has $\alpha = 2$. For ASE algorithm, α will decrease as the sample size N increases. Indeed, when N increases, α will gradually decrease to 1, because the term ϵ^2/N will eventually dominate the convergence rate. The more accurate the estimates $\hat{d}_\lambda$'s are, the slower α decreases to 1 (Fig. 5.1).
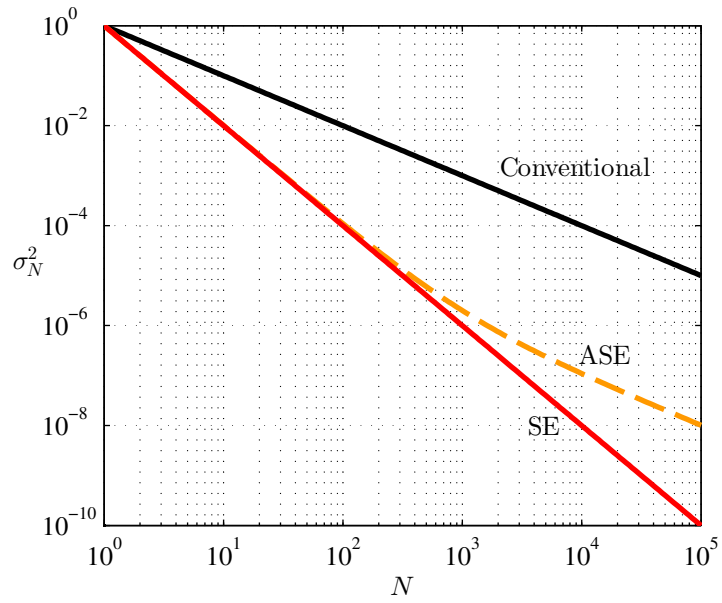
Figure 5.1: Illustration of the convergence rate of σ_N^2 versus the sample size N. The convergence exponent α is the negative slope of the curve. Conventional MC simulation has $\alpha = 1$. SEMC simulation has $\alpha = 2$. ASE algorithm has $\alpha \approx 2$ when N is small, and will gradually decrease to $\alpha \approx 1$ when N becomes large. Note that even though decay exponent α of the ASE algorithm ultimately goes to 1, the error variance σ_N^2 is significantly smaller than the conventional case.

5.0.5   Fixed-Accuracy ASE Algorithm

Yao first proposed the following two-stage ASE algorithm [58] (see Algorithm 1).

Algorithm 1: Approximate Super-Efficient Algorithm

   // Stage I: Estimate d_λ for each λ

1 for $\lambda \in \Lambda_\omega$ **do**

2 $\hat{d}_\lambda \leftarrow \langle F_\lambda^{(K)}(x_i)B(x_i)\rangle$

3 end

4 $\tilde{B}(x) := B(x) - \sum_{\Lambda_\omega} \hat{d}_\lambda f_{\lambda,0}(x)$;   // Define the ASE integrand

5 $x \sim \rho$;   // Draw a seed from the invariant pdf

6 $S \leftarrow 0, D_\lambda \leftarrow 0$ for each $\lambda \in \Lambda_\omega$;   // Initialize accumulators

   // Stage II: Chaotic MC simulation

7 while $\#iteration < N$ **do**

8 $x \leftarrow T(x)$;   // Compute the next state

9 $S \leftarrow S + \tilde{B}(x)$;

10 end

11 return S/N;

---

1. Approximate the sum of coefficients $\hat{d}_\lambda$'s in (5.2) using n-sample conventional or chaotic MC simulation for each $\lambda \in \Lambda_\omega$.

2. Subtract the compensators from the integrand $B(x)$ to form $\tilde{B}(x)$ as defined in (5.3), and apply chaotic MC simulation on $\tilde{B}(x)$.

Note that we need to spend n samples to estimate d_λ for each $\lambda \in \Lambda_\omega$ in stage 1. The quality of the estimates will affect how well the chaotic MC simulation performs in the second stage. To illustrate this point, we apply ASE using different sizes of n, and compare their performance in the following example.

Example 14. *Consider the Chebyshev dynamical system of order $p = 2$ and the*

integrand [67]

$$A(x) = (1 - x^2)\exp(-x^2) = B(x)\rho(x). \tag{5.6}$$

Unlike the previous examples, where the integrand $B(x)$ could be expressed as finite sum of basis functions, the integrand (5.6) has infinitely many terms in its generalized Fourier series expansion. We choose $\Lambda_\omega = \{1, 3, 5, 7, 9\}$ and $K_\lambda = 5$. We perform chaotic MC simulation for $N = 10^6$ samples using conventional, ASE and Progressive ASE (PASE) MC algorithms (to be defined shortly), see Fig. 5.2.
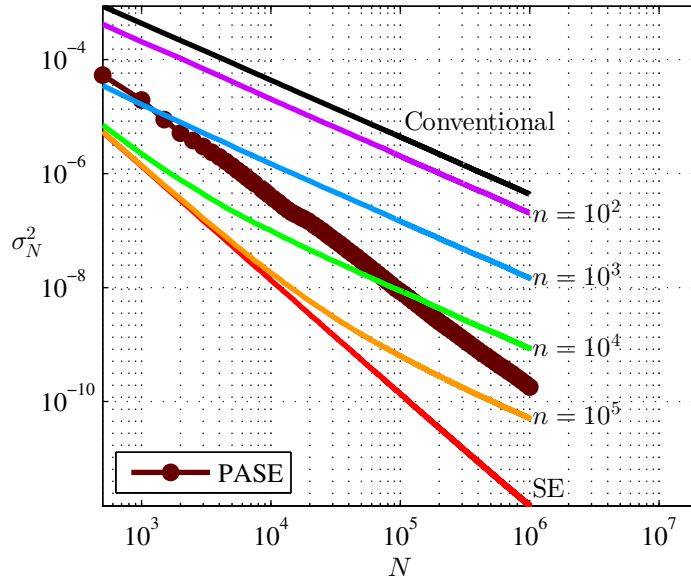
Figure 5.2: Variance of approximation error σ_N^2 versus the number of samples N. Throughout the entire simulation, both the conventional and super-efficient MC simulation constantly has $1/N$ and $1/N^2$ behavior, respectively. The ASE MC simulations have $1/N^2$ behavior at first, but gradually degrade to $1/N$. ASE simulations with larger values of n have better accuracy than the estimates $\hat{d}_\lambda$'s, and lose super-efficiency later. The Progressive ASE simulation has $1/N$ behavior at first but gradually improves to $1/N^2$, because the estimates $\hat{d}_\lambda$'s get more accurate as N increases.

As a benchmark, we compute the sum of coefficients using accurate numerical integration for the super-efficient case. For ASE MC simulations, we use different number of samples n to estimate d_λ's to demonstrate the effect of inaccurate estimates and convergence rate. For Progressive ASE MC simulation we estimate

64

d_λ's at the same time as the chaotic MC simulation runs.

To better visualize the decay exponent α, we use least square method to find the slope of the curves in Fig. 5.3 (recall that α is the negative slope of the curve in the log-log plot).
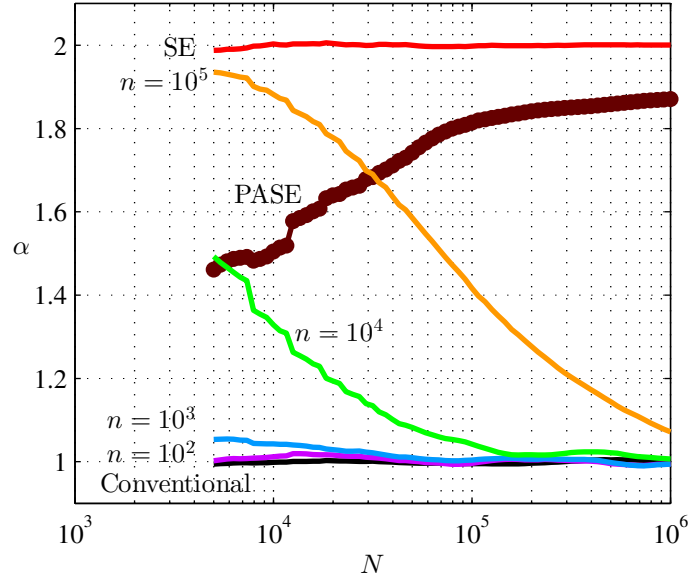
Figure 5.3: To see the decay exponent α more clearly, we use least square method to find the slope of the curves in Fig. 5.2. The decay exponent for the super-efficient MC simulation is 2 for the entire simulation. On the other hand, the exponent for the conventional MC simulation is 1. For the ASE MC simulation with sample size $n = 100,000$, it is super-efficiency at $N = 10^4$ but the decay exponent gradually decreases to 1.1 in the end of the simulation. With ASE MC, simulations with lower sample size n have smaller decay exponents, all of which decrease to 1 very fast. On the other hand, the PASE simulation has decay exponent around 1.4 in the beginning and gradually increases to nearly 1.9 in the end, indicating that the quality of the estimates d_λ's is getting better.

From (4.16), if the integrand is nearly super-efficient, then the decay exponent α will be around 2. For conventional MC simulation, $\alpha = 1$.

Note that for ASE simulations, we need to spend n random samples in the first stage for each class in Λ_L. The effective number of samples for ASE simulations should take those extra samples into consideration. On the other hand, the Progressive ASE algorithm (see next section) does not have this overhead, and

its convergence rate is improving as N increases because the estimates of d_λ are getting more and more accurate.

5.0.6 Progressive ASE Algorithm

ASE simulation is approximately super-efficient for moderate sizes of N. However, from (5.4) it is clear that ASE simulation will eventually lose the $1/N^2$ convergence rate as long as $\epsilon \neq 0$. In [67], Biglieri suggested computing $\hat{d}_\lambda$'s iteratively to improve the accuracy of the estimation . As opposed to the original ASE algorithm, which has fixed accuracy for the entire simulation, we proposed a Progressive ASE (PASE) algorithm that keeps improving the accuracy of $\hat{d}_\lambda$'s as the chaotic MC simulation goes on. The idea is to use the samples $B(x_i)$ generated in the main chaotic MC simulation to estimate $\hat{d}_\lambda$'s continuously. Therefore we get progressively better estimates of $\hat{d}_\lambda$'s and improve the decay rate. See Algorithm 2.

Algorithm 2: Progressive Approximate Super-Efficient Algorithm

1 $x \sim \rho$;   `// Draw a seed from the invariant pdf`

2 $S \leftarrow 0, D_\lambda \leftarrow 0$ for each $\lambda \in \Lambda_\omega$;   `// Initialize accumulators`

3 while *#iteration* $< N$ **do**

4 $x \leftarrow T(x)$;   `// Compute the next state`

5 $S \leftarrow S + B(x)$;

6 $D_\lambda \leftarrow D_\lambda + F_\lambda^{(L)}(x)B(x)$ for each $\lambda \in \Lambda_\omega$.

7 end

8 return $\left(S - \sum_{\lambda \in \Lambda_\omega} D_\lambda \langle f_{\lambda,0} \rangle_N \right)/N$;

5.1 Implementation Issues

5.1.1 Fast Generation of Compensators

One of the most important steps of the ASE algorithm is the estimation of the coefficients

$$d_\lambda = \sum_{j=0}^{\infty} \langle B(x), f_{\lambda,j}(x) \rangle. \tag{5.7}$$

Define the K partial sum of the basis functions as

$$F_\lambda^{(K)}(x) := \sum_{j=0}^{k-1} f_{\lambda,j}(x). \tag{5.8}$$

The coefficient d_λ can be approximated by

$$\hat{d}_\lambda^{(K)} := \left\langle B(x_k), F_\lambda^{(K)}(x_k) \right\rangle_n. \tag{5.9}$$

In the PASE algorithm, we need to evaluate (5.9) repeatedly. This can be challenging especially when K is large. In this section, we present a fast way of computing (5.9). Recall that a dynamical system has the Lebesgue spectrum if the basis function $f_{\lambda,j}(x)$ satisfies the condition

$$f_{\lambda,j}(T(x_n)) = f_{\lambda,j+1}(x_n). \tag{5.10}$$

By using the above property, the partial sum $F_\lambda^{(K)}(x_n)$ and $F_\lambda^{(K)}(x_{n+1})$ can be written as

$$F_\lambda^{(K)}(x_n) = f_{\lambda,0}(x_n) + f_{\lambda,1}(x_n) + \cdots + f_{\lambda,K-2}(x_n) + f_{\lambda,K-1}(x_n), \tag{5.11}$$

$$F_\lambda^{(K)}(x_{n+1}) = f_{\lambda,1}(x_n) + f_{\lambda,2}(x_n) + \cdots + f_{\lambda,K-1}(x_n) + f_{\lambda,K}(x_n). \tag{5.12}$$

Therefore $F_\lambda^{(K)}(x_n)$ can be written as

$$F_\lambda^{(K)}(x_{n+1}) = F_\lambda^{(K)}(x_n) - f_{\lambda,0}(x_n) + f_{\lambda,K}(x_n). \tag{5.13}$$

This is to say that once we have computed $F_\lambda^{(K)}(x_0)$, $F_\lambda^{(K)}(x_n)$ can be computed easily regardless of K for all n. The procedure is summarized in ALGORITHM III.

Algorithm 3: Fast Compensator Generation

1   $x \leftarrow x_0$;   `// Generate an initial state.`

2   $F \leftarrow F_\lambda^{(K)}$;   `// Compute the partial sum (5.8).`

3   **Loop**

4       $F \leftarrow F - f_{\lambda,0}(x) + f_{\lambda,k}(x)$;   `// Compute F recursively`

5       $x \leftarrow T(x)$;   `// Generate the next state.`

6   **EndLoop**

5.1.2   Generating Chaotic Sequence

As we have seen from the previous section, generating compensators can be implemented very efficiently: we only need to evaluate two terms $f_{\lambda,0}(x_n)$ and $f_{\lambda,K}(x_n)$ for each invariant class λ as in (5.13). Thus, the real question is how to evaluate these terms. In this section, we consider the doubling map and present a fast algorithm based on the one-sided Bernoulli shift. Note that this method is applicable to any dynamical systems that have topological conjugacy relation [69] with the doubling map, such as the Chebyshev dynamical system with $p = 2$.

Implementing a doubling map is particularly simple using a digital computer. Recall the doubling map is defined as

$$T_2(x) = (2x) \bmod 1. \tag{5.14}$$

Consider a real number $x \in (0, 1)$, which has the binary representation

$$x = 0.b_1 b_2 \ldots, \tag{5.15}$$

where b_k's are either 0 or 1. Applying T_2 on x is equivalent to performing a left shift to (5.15), i.e.

$$T_2(x) = 0.b_2 b_3 \ldots. \tag{5.16}$$

If we want to implement such an operation using a digital computer, the first problem we will encounter is that the computer can only store a finite number of bits, say L bits of x. If we apply the mapping T_2 on x for L times, all the L bits will be flushed to the left and result in zero output. More specifically, let

$$\underline{x} := 0.b_1 b_2 \ldots b_L \tag{5.17}$$

be the L-bit representation of x in (5.15). We use the notation $T_2^n(x)$ to mean applying T_2 on x for n times. We have the following:

$$
\begin{aligned}
\underline{x} &= 0. & b_1 & \; b_2 & \ldots & b_{L-1} & b_L \\
T_2(\underline{x}) &= 0. & b_2 & \; b_3 & \ldots & b_L & 0 \\
&\quad \vdots \\
T_2^{L-1}(\underline{x}) &= 0. & b_L & \; 0 & \ldots & 0 & 0 \\
T_2^L(\underline{x}) &= 0. & 0 & \; 0 & \ldots & 0 & 0
\end{aligned}
\tag{5.18}
$$

Note that the numerical error between x and its finite binary representation $\underline{x}$ is bounded by $0 \leq x - \underline{x} \leq 2^{-L}$. Let $x_0 \in (0, 1)$, define $x_k = T_2^k(x_0)$. The error between x_k and $T_2^k(\underline{x_0})$ is bounded by

$$0 \leq x_k - T_2^k(\underline{x_0}) \leq 2^{-L+k} \wedge 1, \tag{5.19}$$

69

where $x \wedge y$ is $\min\{x, y\}$. This means that the naive implementation of T_2 leads to a numerical disaster: after applying T_2 for L times, the relative error $\frac{x_L - T_2^L(\underline{x_0})}{x_L}$ is always 100%. The problem stems from the fact that digital computers can only store finite number of bits. On the other hand, storing an irrational number requires infinitely many bits.

A trick to get around this problem is to "generate" the lost bit after applying T_2: suppose we store the finite binary version $\underline{x_0}$ of an irrational number $x_0 \in (0, 1)$. Each time we apply T_2 on the previous value, we add the term $b2^{-L}$ to compensate for the lost bit b. Starting from $\underline{x_0}$, we have

$$\underline{x_1} := \underline{T_2(x_0)} = T_2(\underline{x_0}) + b_{L+1}2^{-L}. \tag{5.20}$$

By adding the term $b_{L+1}2^{-L}$, we restore the truncated version $\underline{x_1}$ of x_1. Similarly, we can restore the truncated version $\underline{x_2}$ of x_2 by

$$\underline{x_2} = T_2(\underline{x_1}) + b_{L+2}2^{-L}. \tag{5.21}$$

The general step is

$$\underline{x_n} = T_2(\underline{x_{n-1}}) + b_{L+n}2^{-L}. \tag{5.22}$$

This is what we called the randomized doubling procedure, and we denoted the operation in (5.22) by

$$T_2^*(\underline{x_{n-1}}) = T_2^{n*}(\underline{x_0}) = \underline{x_n}. \tag{5.23}$$

The error of the randomized doubling procedure is

$$0 \leq x_n - T_2^{n*}(\underline{x_0}) \leq 2^{-L}, \tag{5.24}$$

which is always bounded by 2^{-L} regardless of n, in contrast to the exponentially

large error in (5.19) of the naive implementation. The remaining problem is how to generate the "lost bits" b_{L+k} for $k = 1, 2, \ldots$. If we select $x_0 \in (0, 1)$ at random, then b_k's form a Bernoulli process, i.e. b_k's are independent to each other and have the same chance to be 0 or 1. Therefore, the problem becomes how to generate an infinitely stream of independent bits. From practical point of view, we don't need an infinitely long sequence of bits. Suppose that we will apply T_2 at most M times on x_0, it suffices to generate M independent bits. For example, the Linear Feedback Shift Register (LFSR) of length m is a simple algorithm to generate high quality, period $2^m - 1$ pseudo-random bits. Besides doubling x, we also need to double the number of the form λx as in (5.10) when $\lambda \neq 1$.
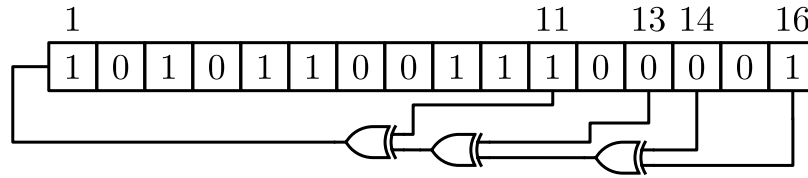
Figure 5.4: The example of a 16-bit linear feedback shift register. By connecting the 11th, 13th, 14th and 16th bit to the XOR gates it is able to produce a binary sequence of length $2^{16} - 1$, which can be used to generate the "loss bits".

Let

$$\lambda = e_0 + e_1 2 + e_2 2^2 + \cdots + e_n 2^n \tag{5.25}$$

be the binary representation of $\lambda \in \mathbb{N}$, where $e_i \in \{0, 1\}$. λx can be written as

$$\lambda x = e_0 x + e_1 T_2(x) + e_2 T_2^2(x) + \cdots + e_n T_2^n(x) \mod 1, \tag{5.26}$$

and $T_2(\lambda x)$ can be written as

$$T_2(\lambda x) = e_0 T_2(x) + e_1 T_2^2(x) + e_2 T_2^3(x) + \cdots + e_n T_2^{n+1}(x) \mod 1. \tag{5.27}$$

A straightforward way of implementing (5.26) and (5.27) on a digital computer is

to replace $T_2^n(x)$ by $T_2^{n*}(\underline{x})$:

$$T_2(\lambda x) \approx e_0 T_2^*(\underline{x}) + e_1 T_2^{2*}(\underline{x}) + e_2 T_2^{3*}(\underline{x}) + \cdots + e_n T_2^{n+1*}(\underline{x}) \bmod 1. \qquad (5.28)$$

Clearly, if we implement (5.28) directly, it would be very inefficient because we need to perform numerous randomized doubling procedures. A better approach is to exploit the fact that the LSB generated by $T_2^{k*}(\underline{x})$ for $k = 1, 2, \ldots, n-1$ have already been generated before. For example, suppose we want to compute $10x$ from doubling $5x$. Let x be given by (5.15). Since $5x = x + 4x$, we can imagine there are two shift registers S1 and S2 that hold the values of x and $4x$, respectively (the first and the second row of Fig. 5.5).
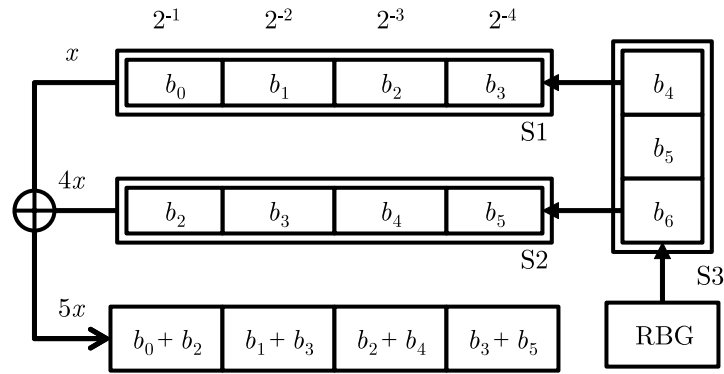
Figure 5.5:   Illustration of doubling the number $5x$: before doubling.
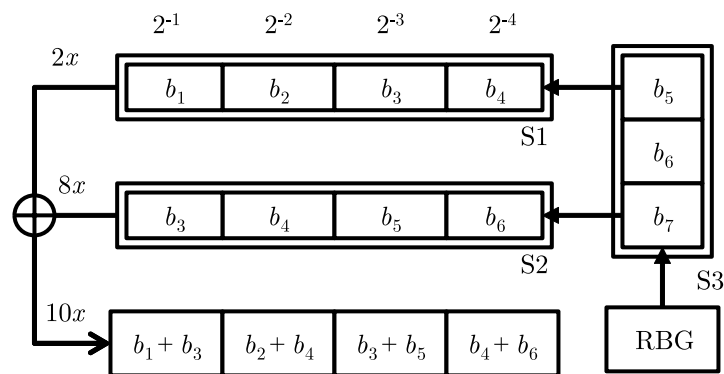
Figure 5.6:   Illustration of doubling the number $5x$: after doubling.

In addition, we introduce a shift register S3 that stores the previously generated

bits (the right most column of Fig. 5.5). The cache in the bottom of Fig. 5.5 stores the sum of x and $4x$. In the next cycle, S1 and S2 shift in their corresponding LSB from S3, and S3 shifts in the bit b_7 produced by the random bit generator (RBG). See Fig. 5.6. Effectively, we don't need the shift registers S1 and S2 to store the values of x and $4x$. The entire operation can be implemented as shown in Fig. 5.7.
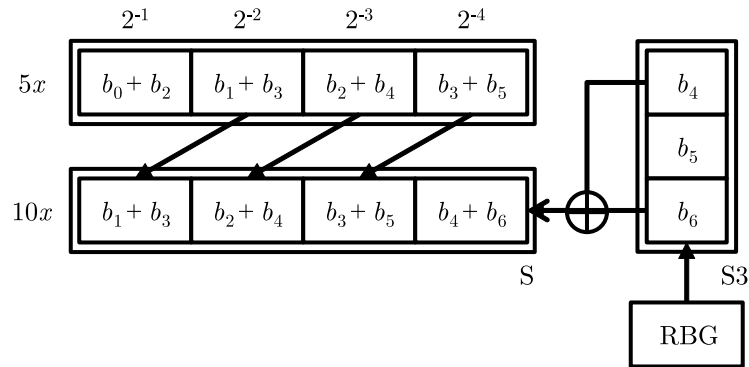
Figure 5.7: The actual doubling process for $5x$.

In general, we only need a shift register S to hold the current value of $10x$ and an extra shift register S3 to store the previously generated random bits.

The procedure of doubling the number λx is summarized in Algorithm 4.

Algorithm 4: Randomized Doubling

    input: The multiplier $\lambda := e_0 + e_1 2 + \ldots + e_n 2^n$.

1   $\boldsymbol{b} \leftarrow (b_0, b_1, \ldots, b_n)$;   // Initialize buffer with random bits.

2   **Loop**

3      $s \leftarrow \sum_{i=0}^{n} e_i b_i$;   // Calculate the LSB.

4      $x \leftarrow (x << 1) + 2^{-L} s$;   // Left shift x.

5      $\boldsymbol{b} \leftarrow (\boldsymbol{b} << 1) + (0, 0, \ldots, X)$;   // Left shift the buffer and generate a new bit X.

6   **EndLoop**

Note that the numerical error of (5.28) is given by

$$0 \le T_2(\lambda x) - e_0 T_2^*(\underline{x}) + e_1 T_2^{2*}(\underline{x}) + e_2 T_2^{3*}(\underline{x}) + \cdots + e_n T_2^{n+1*}(\underline{x}) \bmod 1 \le \log_2(\lambda) 2^{-L}. \tag{5.29}$$

For a given λ the error can be made arbitrarily small by increasing the number of bits L, and there is no error propagation.

5.1.3 Parallel Implementation

It is possible to implement the parallel algorithm of the PASE in various ways. We argue that PASE is particularly suitable for heterogeneous computing based on the assumption that the most computationally intensive task of the simulation is the evaluation of the integrand $B(x)$. Define $\mathbf{B} = (B(x_1), B(x_2), \ldots, B(x_M))^T$ and $\boldsymbol{j}_\lambda = (F_\lambda^{(K)}(x_1), F_\lambda^{(K)}(x_2), \ldots, F_\lambda^{(K)}(x_M))$ for each $\lambda \in \Lambda_0$, where $F_\lambda^{(K)}(x)$ is the K partial sum of $f_\lambda(x)$ as defined in (5.8). Recall that the estimate $\hat{d}_\lambda$ can be computed as the inner product

$$\hat{d}_\lambda = \left\langle B(x) F_\lambda^{(K)}(x) \right\rangle_M = \mathbf{B}^T \boldsymbol{j}_\lambda. \tag{5.30}$$

By linearity of the time average operator, the integral can be written as

$$\left\langle \tilde{B}(x) \right\rangle = \langle B(x) \rangle - \sum_\lambda \hat{d}_\lambda \langle f_{\lambda,0} \rangle. \tag{5.31}$$

Using the matrix notation, (5.31) can be expressed as

$$\left\langle \tilde{B}(x) \right\rangle = \frac{1}{M} \left(\mathbf{B}^T \mathbf{1} - \mathbf{d}^T \boldsymbol{j} \right), \tag{5.32}$$

where $\mathbf{1} = (1, 1, \ldots, 1)^T$ is an M-vector of unit entries, $\mathbf{d}^T = \mathbf{B}^T \left(\boldsymbol{j}_{\lambda_1}, \ldots, \boldsymbol{j}_{\lambda_\omega} \right)$ and $\boldsymbol{j} = (\langle f_{\lambda_1,0} \rangle, \ldots, \langle f_{\lambda_\omega,0} \rangle)^T$. Based on the assumption that the most computationally intensive task is the evaluation of $\mathbf{B}$, it is reasonable to assign the task

to powerful CPUs, which can execute complex instructions. On the other hand, the task of constructing $\boldsymbol{j}$ and $\boldsymbol{j}$ consists of lots of similar and lightweight computations, which can be computed efficiently by special-purpose processors such as Graphics Processing Units (GPU). See Algorithm 5.

Algorithm 5: Parallel PASE

1 Generate x_0;

2 **repeat**

3 $\quad$ Generate $x_1, \ldots, x_M$ from x_0;

4 $\quad$ **in CPU :**

5 $\qquad$ $\boldsymbol{B} \leftarrow (B(x_1), \ldots, B(x_M))^T$;

6 $\qquad$ $S \leftarrow S + \boldsymbol{B}^T \mathbf{1}$;

7 $\qquad$ Send $\boldsymbol{B}$ to GPU.

8 $\quad$ **end**

9 $\quad$ **in GPU :**

10 $\qquad$ $\boldsymbol{F} \leftarrow (F_{\lambda_j}^{(K)}(x_i))_{ij}$;

11 $\qquad$ $\boldsymbol{f} \leftarrow \boldsymbol{f} + \left(\sum_{m=1}^{M} f_{\lambda_i,0}(x_m) \right)_i$;

12 $\qquad$ $\boldsymbol{d} \leftarrow \boldsymbol{d} + \boldsymbol{F}^T \boldsymbol{B}$;

13 $\quad$ **end**

14 $\quad$ $x_0 \leftarrow x_M$;

15 **until** N *samples have been generated*;

16 **return** $I = \frac{1}{N} \left(S + \frac{M}{N} \boldsymbol{d}^T \boldsymbol{f} \right)$;

5.2 Conclusion

While conventional MC simulation yields the convergence rate $1/N$, SE MC has superior convergence rate $1/N^2$ for integrands of the SE type. Since most integrands are not SE, we introduce the concept of ASE. The ASE and Progressive ASE algorithms are general, and at least as fast as conventional MC simulation,

while sometimes yielding near super-efficient convergence rate. Furthermore, the introduction of the Lebesgue spectrum concept from ergodic theory allows us to systematically study the SE MC simulation. The above discussions are applicable also to multi-dimensional integrands. It is of great interest to find more applications to exploit the concept of SE and ASE.

CHAPTER 6

On The Throughput Maximization in Cellular Networks

Packet retransmission and channel feedback are two fundamental mechanisms in the modern communication systems. They improve the efficiency and robustness of communication links. Since the communication links are subject to noise and channel variation, the receiver may fail to decode a damaged packet. To recover the lost packet, the receiver may send a negative-acknowledgment (NAK) to the transmitter to request a retransmission. Combining with the damaged packet, the newly received packet may help the receiver to recover the packet, and thus enhances the reliability of the communication link. However, this added reliability comes at the cost of extra redundancy, which results in lower data throughput. To better utilize the channel resource, the transmitter relies on the channel state information (CSI) feedback by the receiver. The CSI indicates the quality of the channel, hence provides guideline for the transmitter to determine the packet size, modulation level, code rate, etc. If the channel quality is good, the transmitter can transmit a larger packet with small error rate. On the other hand, if the channel quality is poor, the transmitter may select a smaller packet size so that stronger error correction code can protect the packet. While high packet error rate results in poor efficiency, low packet error rate may indicate that the system does not properly utilize the channel resources, hence the throughout may be improved by transmitting a larger packet. From the viewpoint of data throughput, it is desirable for a system to operate at a certain packet error rate.

For example, in the 3rd and the 4th generation cellular networks, the user equipment (UE, mobile station) monitors channel quality and periodically reports CSI back to the base station (Node B). One component of CSI is the Channel Quality Indicator (CQI), which is an integer ranges from 0 to 15 for LTE and 0 to 30 for UMTS, where 0 indicating the channel is unusable and 15 (30 for UMTS) indicating the best channel condition. Based on the UE reported CQI, the Node B will choose the largest Transportation Block Size (TBS, number of information bits per packet), modulation level and code rate so that the UE can decode at a certain probability. It is recommended in [70, 6A.2.1] (UMTS) and [71, 7.2.3] (LTE) that the UE should report CQI such that the first block error rate (BLER) is around 10% under static channel. However, this 10% target BLER is by no mean throughput optimal. The exact relationship between the packet error rate and the throughput is complicated, and it depends strongly on the channel statistics.

In [72], Tao considered the throughput maximization problem by applying an offset to the CQI distribution. The offset is adaptively adjusted to achieve a given BLER target, or to maximize the throughput using the stochastic approximation algorithm.

Instead of finding an optimal offset to the CQI distribution, we consider a more fundamental question: what is the throughput maximizing CQI reporting mechanism? More generally, what is the mechanism that not only maximizes the throughput but also meets some design constraints, such as satisfying a given BLER target? Most importantly, how to achieve these goals *online*, where channel statistics and many problem-dependent factors needs to be learn on the fly?

Clearly the CQI offset approach studied by Tao [72] is a special case among all the possibilities. If we consider more general CQI reporting mechanisms, the UE potentially can achieve a much higher throughput. By formulating the problem of designing an optimal CQI reporting mechanism as a constrained optimization problem, we show that under the independent channel condition, the optimal

CQI reporting mechanism is to report CQIs according to some distribution. This distribution becomes degenerative in the unconstrained case, i.e. there exists a throughput maximizing CQI. In the BLER constrained case, we show that the optimal CQI distribution has two atoms, and derive an explicit formula for their probability mass. The solution to both the unconstrained and constrained problem depends critically on the channel statistics and the decoding capability of the UE. From a practical point of view, these conditions are unknown a priori and needs to be learned online. In the unconstrained case, since there exists an throughput maximizing CQI, the UE only needs to learn the throughput associated with each CQI, and report the optimal CQI as frequently as possible. This can be done by trying all the possible CQIs and report the CQI that yields the highest throughput. However, trying suboptimal CQIs has the adverse effect of lowering the average downlink throughput. The UE would like to identify the throughput maximizing CQI and spend minimum amount of time on suboptimal CQIs. Here the UE is facing a classical exploration and exploitation dilemma: while it is desirable to exploit the throughput maximizing CQI by reporting it as frequently as possible, it takes time to explore other CQIs before getting an accurate throughput estimate for each CQI. We propose using the Multi-Armed Bandit (MAB) framework to study the problem. In a MAB problem, an agent chooses some action to play in each time step and gets a reward associated with that action. The agent's task is to decide which action to play so that the cumulative reward is maximized. This setting is very similar to the throughput maximization problem. The UE need to choose the right CQI to report at each time step so that the average throughput is maximized. However, the notion of cumulative reward in the throughput maximization problem is different from the classical MAB problems. In the throughput maximization problem, the objective is to maximize the average throughput, which is the ratio of number of decoded bits to the number of transmission blocks. This difference needs to be taken into consideration when

designing an algorithm. Based on the classical ϵ-Greedy, Boltzmann exploration and Thompson sampling algorithm, we present three algorithms: Greedy-CQI, Boltzmann-CQI and TS-CQI, which are tailored to solve the online throughput maximization problem. We further conduct finite time performance analysis for the Greedy-CQI algorithm.

In the BLER constrained throughput maximization problem, we propose a novel Greedy-LP algorithm, which solves a sequence of linear programs and gradually converges to the optimal CQI distributions. To quantify the performance of CQI reporting mechanisms with the BLER constraint, we introduce the concept of penalized regret, and show that the Greedy-LP algorithm's penalized regret converges to zero almost surely.

Our simulation results show that the proposed unconstrained algorithms achieve up to 99% of the optimal throughput within 1000 blocks of transmissions. In the BLER constrained case, the Greedy-LP algorithm achieves the given target BLER with good accuracy and achieves 90% to 99% of the optimal throughput, depending on the fading model. Note that the UE implementation in our simulation closely mirrors commercial devices. The performance of the proposed algorithms is an indication of the potential throughput enhancement that can be realized in practice.

The chapter is organized as follows. In section 6.1 we formulate the throughput maximization problem as a moment problem with a fractional objective function. The explicit solution for both the unconstrained and BLER constrained case are derived ins section 6.2. Practical online algorithm is considered in Chapter 7.

6.1 Problem formulation

In a communication system, the receiver constantly monitors and reports the channel quality information back to the transmitter. In practice, this information

is quantized to a finite set of values known as CQI. Since higher CQI values indicate better channel quality, the communication channel can support larger packet size with high probability. In this study, we assume there is a one-to-one correspondence between the reported CQI and the packet size.

Since CQI measurement and processing takes time, there is a delay between the reported CQI and its corresponding packet. This delay causes a mismatch between CQI and TBS due to channel variation. If the channel varies slowly [1], we may predict the channel condition and report an appropriate CQI that maximize the throughput. However, if the channel varies rapidly, it is not clear what is the throughput optimizing CQI reporting strategy.

In this section, we formulate the problem of finding the optimal strategy mathematically and show that the optimal solution exists.

Let M be the maximum number of transmissions of a packet (including the first transmission). Denote the CQI reported by UE at time n by Λ_n, and let d be the time delay between CQI and its corresponding TBS.

Suppose the UE received a new packet of TBS m_i at time n. The size m_i was determined by the UE reported CQI $\Lambda_{n-d} = i$ at time $n-d$. Let Y be the number of transmissions needed to successfully decode the packet subject to the limit of M transmissions. The number of information bits decoded is a random number

$$
X = \begin{cases} m_i & \text{if the packet is eventually decoded,} \\ 0 & \text{if the packet can not be decoded after } M-1 \text{ retransmissions.} \end{cases}
$$

(6.1)

The downlink throughput T is the rate of transfered information bits over the

---

[1] By varies slowly we mean the delay is larger than the channel coherence time. Typically the CQI-TBS delay is around 8 ms to 20 ms depending on the system.

number of time slots taken. That is

$$\mathsf{T} = \frac{\mathbf{E}(\text{bits decoded})}{\mathbf{E}(\text{number of transmissions})} = \frac{\mathbf{E}(X)}{\mathbf{E}(Y)}. \tag{6.2}$$

The event $\{Y > 1\}$ indicates a block error occurs. The kth block error rate (BLER) is defined as the probability $B_k = \Pr(Y > k)$. Since BLER dependents critically on the SNR and the TBS, we denote the kth BLER as a function of TBS and SNR by

$$B_k(m, \gamma) = \Pr(Y > k \mid \text{TBS} = m, \Gamma_n = \gamma), \tag{6.3}$$

where Γ_n is the instantaneous SNR experienced by the UE at time n.

BLER and throughput are closely related. Indeed, given the SNR and TBS, the expected number of decoded bits X can be written as

$$g(m, \gamma) = \mathbf{E}(X \mid \text{TBS} = m, \Gamma_n = \gamma) = m(1 - B_M(m, \gamma)). \tag{6.4}$$

Similarly the expected number of transmissions Y can be written as

$$h(m, \gamma) = \mathbf{E}(Y \mid \text{TBS} = m, \Gamma_n = \gamma) = \sum_{k=1}^{M} k(B_{k-1}(m, \gamma) - B_k(m, \gamma)) + M B_M(m, \gamma). \tag{6.5}$$

Averaging over the SNR and the CQI, the throughput is given by

$$\mathsf{T} = \frac{\mathbf{E}(X)}{\mathbf{E}(Y)} = \frac{\int_0^\infty \sum_{i=1}^{K} g(m_i, \gamma) f_{\Lambda_{n-d}\Gamma_n}(i, \gamma) \, d\gamma}{\int_0^\infty \sum_{i=1}^{K} h(m_i, \gamma) f_{\Lambda_{n-d}\Gamma_n}(i, \gamma) \, d\gamma}, \tag{6.6}$$

where $f_{\Lambda_{n-d}\Gamma_n}(i, \gamma)$ is the joint pdf of CQI reported at time $n - d$ and SNR at time n.

A CQI reporting mechanism is a function $Q : \mathbb{R}^+ \mapsto \{1, 2, \ldots, K\}$ that maps the measured SNR to the set of possible CQI values. That is, $\Lambda_{n-d} = Q(\Gamma_{n-d})$. Our goal is to find a mapping Q^* such that the throughput T is maximized. Since

Λ_{n-d} is a function of Γ_{n-d}, the joint pdf $f_{\Lambda_{n-d}\Gamma_n}$ can be written as

$$f_{\Lambda_{n-d}\Gamma_n}(i,\gamma) = \int_{Q_i} f_{\Gamma_n\Gamma_{n-d}}(\gamma,\gamma')\,d\gamma', \qquad (6.7)$$

where $Q_i = Q^{-1}(i)$ is the range of SNRs that maps to CQI i.

To express explicitly the throughput T as a function of Q, denote the conditional expectation $\mathbf{E}(X \mid \Gamma_{n-d} = \gamma', \mathrm{TBS} = m)$ by

$$G(m,\gamma') = \int_0^\infty g(m,\gamma) f_{\Gamma_n|\Gamma_{n-d}}(\gamma|\gamma')\,d\gamma \qquad (6.8)$$

and the conditional expectation $\mathbf{E}(Y \mid \Gamma_{n-d} = \gamma', \mathrm{TBS} = m)$ by

$$H(m,\gamma') = \int_0^\infty h(m,\gamma) f_{\Gamma_n|\Gamma_{n-d}}(\gamma|\gamma')\,d\gamma, \qquad (6.9)$$

the throughput (6.6) can be written as

$$\mathsf{T}(Q) = \frac{\sum_{i=1}^K \int_{Q_i} G(m_i,\gamma') f_{\Gamma_{n-d}}(\gamma')\,d\gamma'}{\sum_{i=1}^K \int_{Q_i} H(m_i,\gamma') f_{\Gamma_{n-d}}(\gamma')\,d\gamma'}. \qquad (6.10)$$

Thus the problem of finding the optimal CQI reporting strategy can be formulated as

$$Q^* = \arg\max_Q \{\mathsf{T}(Q) \mid Q : [0,\infty) \mapsto \{1,2,\ldots,K\}\}. \qquad (6.11)$$

From the Bayesian decision theory point of view, we may interpret Γ_{n-d} as the evidence and Γ_n as the state of nature. The CQI mapping Q is a decision rule that maps from measured SNR Γ_{n-d} to an appropriate CQI. The function g in (6.4) and h in (6.5) may be interpreted as the utility and the loss function, respectively. Similarly, the function $G(m,\gamma')$ and $H(m,\gamma')$ are the Bayesian expected gain and loss function, respectively.

To get an intuitive understanding about the problem (6.11), let's consider the

special case that $M = 1$, meaning that there is no retransmission. The throughput becomes

$$\mathsf{T}(Q) = \sum_{i=1}^{K} \int_{Q_i} G(m_i, \gamma') f_{\Gamma_{n-d}}(\gamma') \, d\gamma'. \tag{6.12}$$

Clearly the throughput maximizing mapping is given by

$$Q^*(\gamma') = \arg \max_{1 \leq i \leq K} G(m_i, \gamma'), \tag{6.13}$$

which is the usual generalized Bayes rule.

6.2 Optimal solution under IID channel

In this paper, we focus on the case of fast fading channels, which leads to the condition

$$\Gamma_{n-d} \perp\!\!\!\perp \Gamma_n \quad \forall n, \tag{6.14}$$

where $\perp\!\!\!\perp$ denotes independence.

Since $\Gamma_{n-d} \perp\!\!\!\perp \Gamma_n$, Λ_{n-d} being a function of Γ_{n-d} will necessarily be independent of Γ_n. The expected number of decoded bits $G(m_i, \gamma')$ in (6.8) and the expected number of transmissions $H(m_i, \gamma')$ (6.9) becomes

$$g_i = \int_0^\infty g(m_i, \gamma) f_{\Gamma_n}(\gamma) \, d\gamma \tag{6.15}$$

and

$$h_i = \int_0^\infty h(m_i, \gamma) f_{\Gamma_n}(\gamma) \, d\gamma, \tag{6.16}$$

respectively. The throughput (6.10) can be written as

$$\mathsf{T}(Q) = \frac{\sum_{i=1}^{K} g_i \int_{Q_i} f_{\Gamma_{n-d}}(\gamma') \, d\gamma'}{\sum_{i=1}^{K} h_i \int_{Q_i} f_{\Gamma_{n-d}}(\gamma') \, d\gamma'}. \tag{6.17}$$

Note that the integral $\int_{Q_i} f_{\Gamma_{n-d}}(\gamma') \, d\gamma'$ is precisely $f_{\Lambda_{n-d}}(i)$, the probability mass function (pmf) of CQI at time $n-d$. Therefore, the problem of finding the optimal CQI reporting strategy becomes finding the optimal CQI distribution $f^*_{\Lambda_{n-d}}$:

$$\underset{f_{\Lambda_{n-d}}}{\arg\max} \quad \mathsf{T} = \frac{\sum_{i=1}^{K} g_i f_{\Lambda_{n-d}}(i)}{\sum_{i=1}^{K} h_i f_{\Lambda_{n-d}}(i)} \tag{6.18}$$

$$\text{s.t.} \quad f_{\Lambda_{n-d}} \text{ is a valid pmf on } \{1, 2, \ldots, K\}. \tag{6.19}$$

Problem (6.18) is known as the moment problem with fractional objective function. It is an optimization problem over probability distributions [73]. Given the discrete nature of the probability measure $f_{\Lambda_{n-d}}$, our problem (6.18) became an linear-fractional program [74]:

$$\max_{\boldsymbol{f} \in \mathbb{R}^K} \quad \frac{\boldsymbol{g}^T \boldsymbol{f}}{\boldsymbol{h}^T \boldsymbol{f}} \tag{6.20}$$

$$\text{s.t.} \quad \mathbf{1}^T \boldsymbol{f} = 1, \tag{6.21}$$

$$\boldsymbol{f} \geq 0, \tag{6.22}$$

where $\boldsymbol{g} = [g_1, g_2, \ldots, g_K]^T$, $\boldsymbol{h} = [h_1, h_2, \ldots, h_K]^T$ and $\boldsymbol{f} = [f_{\Lambda_{n-d}}(1), \ldots, f_{\Lambda_{n-d}}(K)]$.

The constraint (6.21) is called a moment constraint. It is either an equality or inequality constraint of the form

$$\boldsymbol{a}^T \boldsymbol{f} \lesseqgtr b \tag{6.23}$$

for some K-vector $\boldsymbol{a}$ and constant b.

In general the throughput maximization problem may have multiple moment

constraints:

$$\max_{\boldsymbol{f} \in \mathbb{R}^K} \quad \frac{\boldsymbol{g}^T \boldsymbol{f}}{\boldsymbol{h}^T \boldsymbol{f}} \tag{6.24}$$

$$\text{s.t.} \quad \boldsymbol{A}\boldsymbol{f} = \boldsymbol{b}, \tag{6.25}$$

$$\boldsymbol{B}\boldsymbol{f} \leq \boldsymbol{c}, \tag{6.26}$$

$$\boldsymbol{f} \geq 0, \tag{6.27}$$

for some matrix $\boldsymbol{A}$, $\boldsymbol{B}$ and vector $\boldsymbol{b}$ and $\boldsymbol{c}$. To ensure that $\boldsymbol{f}$ is a valid pmf, we require that the first row of $\boldsymbol{A}$ is $\mathbf{1}^T$ and the first component of $\boldsymbol{b}$ is 1.

By the Charnes-Cooper transformation [75] $\boldsymbol{x} = \boldsymbol{f}/(\boldsymbol{h}^T \boldsymbol{f})$ and $z = 1/(\boldsymbol{h}^T \boldsymbol{f})$, we may convert (6.24) into a linear program

$$\max_{\boldsymbol{x} \in \mathbb{R}^K, z \in \mathbb{R}} \quad \boldsymbol{g}^T \boldsymbol{x} \tag{6.28}$$

$$\text{s.t.} \quad \boldsymbol{A}\boldsymbol{x} = \boldsymbol{b}z, \tag{6.29}$$

$$\boldsymbol{B}\boldsymbol{x} \leq \boldsymbol{c}z, \tag{6.30}$$

$$\boldsymbol{h}^T \boldsymbol{x} = 1, \tag{6.31}$$

$$\boldsymbol{x} \geq 0, z \geq 0, \tag{6.32}$$

and the solution to the original problem (6.24) is $\boldsymbol{f} = \boldsymbol{x}/z$.

In the following subsection, we derive an explicit solution to the unconstrained throughput maximization problem and to the throughput maximization problem with block error rate constraint.

6.2.1 Unconstrained throughout maximization

We call the throughput optimization problem *unconstrained* if (6.21) is the only moment constraint. The equivalent linear program is

$$\max_{\boldsymbol{x}\in\mathbb{R}^K} \quad \boldsymbol{g}^T\boldsymbol{x} \tag{6.33}$$

$$\text{s.t.} \quad \boldsymbol{h}^T\boldsymbol{x} = 1, \tag{6.34}$$

$$\boldsymbol{x} \geq 0. \tag{6.35}$$

This simple linear program has an explicit solution $\boldsymbol{x} = \boldsymbol{e}_{i^*}/h_{i^*}$, where $\boldsymbol{e}_{i^*}$ is the i^*th unit vector in $\mathbb{R}^K$, and i^* is given by

$$i^* = \arg\max_i \frac{g_i}{h_i}. \tag{6.36}$$

Therefore, the throughput maximizing CQI distribution is

$$f_{\Lambda_{n-d}}(i) = \begin{cases} 1 & \text{for } i = i^*, \\ 0 & \text{otherwise,} \end{cases} \tag{6.37}$$

and the optimal throughput is

$$\mathsf{T}^* = \frac{g^*}{h^*}, \tag{6.38}$$

where $g^* = g_{i^*}$ and $h^* = h_{i^*}$. This result shows that the optimal CQI Λ_{n-d} under *i.i.d.* channel is a deterministic value i^* that maximize the ratio

$$\mathsf{T}_i = \frac{g_i}{h_i}. \tag{6.39}$$

The ratio T_i can be interpreted as the conditional throughput for CQI $= i$, because it is precisely the throughput that UE gets if it keeps reporting CQI $= i$.

The result may seem surprising at first but it turns out to be very intuitive:

since the channel varies so rapidly, we can not predict the instantaneous SNR in the future. Instead, we optimize the long term average of the throughput. The solution is thus some fixed value i^*. For example, under the AWGN, SNR 10dB case, the optimal CQI is 24 for our UE. Any other distribution will lead to suboptiaml performance.

6.2.2 Throughput maximization under BLER constraint

In addition to maximizing the throughput, we may want to keep the block error rate at some target β. That is, we would like to solve the following moment problem

$$\max_{Q} \quad \mathsf{T}(Q) = \frac{\mathbf{E}(X)}{\mathbf{E}(Y)} \tag{6.40}$$

$$\text{s.t.} \quad \bar{B}_1 = \beta, \tag{6.41}$$

where $\bar{B}_1 = \Pr(Y > 1)$ is the first block error rate. The problem can be formulated as a linear fractional program

$$\max_{\boldsymbol{f} \in \mathbb{R}^K} \quad \frac{\boldsymbol{g}^T \boldsymbol{f}}{\boldsymbol{h}^T \boldsymbol{f}} \tag{6.42}$$

$$\text{s.t.} \quad \boldsymbol{b}^T \boldsymbol{f} = \beta, \tag{6.43}$$

$$\mathbf{1}^T \boldsymbol{f} = 1, \tag{6.44}$$

$$\boldsymbol{f} \geq 0, \tag{6.45}$$

where

$$B_k(m_i) = \int_0^\infty B_k(m_i, \gamma) f_{\Gamma_n}(\gamma) \, d\gamma \tag{6.46}$$

is the average kth block error rate and $\boldsymbol{b} = [B_1(m_1), \dots, B_1(m_K)]^T$ is the vector of first BLERs associated with each CQI. Note that the target first BLER β is achievable if $B_1(m_1) \leq \beta \leq B_1(m_K)$. From now on we assume the target first

BLER is achievable. The equivalent linear program is

$$\max_{\boldsymbol{x} \in \mathbb{R}^K} \quad \boldsymbol{g}^T \boldsymbol{x} \tag{6.47}$$

$$\text{s.t.} \quad \boldsymbol{h}^T \boldsymbol{x} = 1, \tag{6.48}$$

$$(\boldsymbol{b} - \beta \mathbf{1})^T \boldsymbol{x} = 0, \tag{6.49}$$

$$\boldsymbol{x} \geq 0. \tag{6.50}$$

From the theory of linear program, we know that the optimal solution $\boldsymbol{x}^*$ of (6.47) has at most two nonzero entries because there are exactly two equality constraints (6.48) and (6.49) [76]. That is, we only need to consider the basic solution $\boldsymbol{x}$, where all but some ith and jth entry are zero. We refer to this candidate solution the (i, j)th basic solution, and it must satisfy

$$\begin{pmatrix} h_i & h_j \\ b_i - \beta & b_j - \beta \end{pmatrix} \begin{pmatrix} x_i \\ x_j \end{pmatrix} = \begin{pmatrix} 1 \\ 0 \end{pmatrix}. \tag{6.51}$$

After some algebra, it can be shown that the throughput associated with the (i, j)th basic solution is

$$\mathsf{T}_{ij} = \frac{\begin{vmatrix} g_i & g_j \\ b_i - \beta & b_j - \beta \end{vmatrix}}{\begin{vmatrix} h_i & h_j \\ b_i - \beta & b_j - \beta \end{vmatrix}}, \tag{6.52}$$

where $|\cdot|$ is the determinant function. Note that not all the basic solutions are feasible, since $\boldsymbol{x}$ must be non-negative. Observe that the components of $\boldsymbol{b}$ are non-decreasing, thus there will be a number k_0 such that $b_{k_0} - \beta \leq 0$ and $b_{k_0+1} - \beta \geq 0$. In order for the (i, j)th basic solution to be feasible, we must have $i \leq k_0$ and $j > k_0$. This observation leads to the following conclusion: the optimal

throughput to (6.24) is given by

$$\mathsf{T}_{\mathrm{c}}^* = \max_{i \le k_0, j > k_0} \mathsf{T}_{ij}, \tag{6.53}$$

where the subscript c stands for constrained, and the optimal CQI distribution is

$$f_{\Lambda_{n-d}}(i) = \begin{cases} \frac{b_{j^*} - \beta}{b_{j^*} - b_{i^*}} & \text{for } i = i^*, \\[2mm] \frac{\beta - b_{i^*}}{b_{j^*} - b_{i^*}} & \text{for } i = j^*, \\[2mm] 0 & \text{otherwise}, \end{cases} \tag{6.54}$$

where

$$(i^*, j^*) = \arg \max_{i,j} \mathsf{T}_{ij} \tag{6.55}$$

is the index of the optimal basic feasible solution.

Unlike the unconstrained problem (6.28), where a single deterministic optimal CQI exists, the solution (6.54) suggests that there is no single CQI that will maximize the throughput and meet the BLER constraint at the same time. It is a CQI distribution that achieves this.

CHAPTER 7

Online Throughput Maximization Algorithms

7.1 Online algorithm for unconstrained maximization

From section 6.2.1, we know that the optimal CQI reporting policy under the *i.i.d.* channel condition is always reporting some fixed value i^* such that the conditional throughput T_{i^*} (6.39) is the maximized. Our C++ based HSDPA simulator showed up to 80% throughput gain[1] using the genie-aided optimal CQI compare to the legacy CQI algorithm, which reports CQI based on instantaneous SNR.

However, in practice we do not know i^* before hand. To harvest the huge gain of reporting the optimal CQI, we need an online algorithm that learns the conditional throughput T_i for each i, and reports the optimal CQI i^* with high probability.

One simple strategy is to learn the conditional throughput T_i for each i during a training phase, and then apply the best estimated CQI index $\hat{i}^*$ afterward. However, this strategy will always have a non-zero probability of finding and locking at a suboptimal CQI, and it is not possible for UE to determine if the CQI $\hat{i}^*$ is suboptimal since the UE no longer explores other possibilities.

The challenge here is the classical exploration and exploitation dilemma: in

---

[1] Note that the throughput gain over the legacy algorithm is not a good performance metric. It depends strongly on the performance of the baseline algorithm. This makes comparing different algorithms on difference version of UE difficult. A better performance metric is to use the regret (7.3), which is defined as the gap between the maximal achievable throughput and the algorithm's average throughput. This metric is independent of the baseline algorithm.

order to find the optimal CQI i^* with high confidence, the UE needs to explore all CQIs with sufficient amount of samples. However, exploring suboptimal CQIs means losing the opportunity of exploiting the optimal CQI. We propose using the multi-arm bandit (MAB) framework to model and study the problem.

In a MAB problem, the agent takes an action $a \in \mathcal{A}$ at each time step t and the environment generates a reward associated with the action. The agent's goal is to maximize the overall reward by properly choosing the actions to play.

Under this setting, it is clear that the UE's action is to report a CQI $I_t \in \{1, 2, \ldots, K\}$, where the time step t corresponds to the tth new packet transmission. After Node B transmitted the packet $Y_{I_t,t}$ times, UE decodes $X_{I_t,t}$ bits. The aggregate reward generated by the system up to time n is given by the throughout

$$\mathsf{T}(n) = \frac{\sum_{t=1}^{n} X_{I_t,t}}{\sum_{t=1}^{n} Y_{I_t,t}}. \tag{7.1}$$

The UE's goal is to find a policy $\pi_t : \mathcal{H}_{t-1} \mapsto \mathcal{A}$ at each time step t that maps from the history $\mathcal{H}_{t-1} = \{(I_n, X_{I_n}, Y_{I_n})\}_{n=1}^{t-1}$ to a CQI I_t, such that the expected throughput

$$\bar{\mathsf{T}}(n) = \frac{\mathbf{E}(\sum_{t=1}^{n} X_{I_t,t})}{\mathbf{E}(\sum_{t=1}^{n} Y_{I_t,t})} \tag{7.2}$$

is maximized. Equivalently, the UE would like to minimizes the regret

$$R_n = \mathsf{T}^* - \bar{\mathsf{T}}(n), \tag{7.3}$$

which is the gap between the optimal throughput T^* (6.38) and the expected throughput.

Note that $g_i = \mathbf{E}(X_{i,t})$ and $h_i = \mathbf{E}(Y_{i,t})$ from (6.15) and (6.16). Let $g^* =$

$\mathbf{E}(X_{i^*,t})$, $h^* = \mathbf{E}(Y_{i^*,t})$, and

$$T_i(n) = \sum_{t=1}^{n} 1\{I_t = i\} \tag{7.4}$$

be the number of times that UE reports CQI $= i$ up to time n. The regret can be written as

$$R_n = \frac{g^*}{h^*} - \frac{\sum_{i=1}^{K} \mathbf{E}(T_i(n))g_i}{\sum_{i=1}^{K} \mathbf{E}(T_i(n))h_i} = \frac{\sum_{i=1}^{K} \mathbf{E}(T_i(n))(g^* h_i - g_i h^*)}{\sum_{i=1}^{K} \mathbf{E}(T_i(n))h^* h_i}. \tag{7.5}$$

A MAB algorithm is said to have zero regret if its regret converges to zero asymptotically [77]. Suppose the expected number of reporting suboptimal CQI $i \neq i^*$ can be bounded by

$$\mathbf{E}(T_i(n)) \leq q_i(n) \tag{7.6}$$

for some function $q_i(n)$, then the average regret (7.5) in our problem can be bounded by

$$R_n \leq \frac{\sum_{i=1}^{K} C_i \log(n) \Delta_i h^* h_i}{\sum_{i=1}^{K} \mathbf{E}(T_i(n))} \leq \frac{M^2}{n} \sum_{i=1}^{K} q_i(n) \Delta_i, \tag{7.7}$$

where $\Delta_i = \mathsf{T}^* - \mathsf{T}_i$ is the difference between the optimal throughput and the conditional throughput T_i. This shows that if a policy has sublinear upper bounds $q_i(n)$ for each i, then it has zero regret.

From the *i.i.d.* channel assumption, it is clear that $(X_{i,t}, Y_{i,t})_{t=1}^{\infty}$ is a sequence of *i.i.d.* random pairs for each i. Thus our problem can be categorized as the stochastic type of MAB problem [78], where the reward associated with each action is independent to each other and also independent to time. However, the definition of our regret (7.3) is different from the classical MAB regret. In classical MAB problems, the overall reward is the sum of instantaneous reward. In our problem, the reward (7.1) is the ratio between the sum of the number of decoded bits and the sum of the number of transmissions taken. Because of the difference in the definition of the regret, we can not directly apply MAB algorithms to our

problem. Based on four popular MAB algorithms, we present the following modified algorithms that are tailored to solve our throughput maximization problem with unknown block error distributions. We also provide an upper bound for the Greedy-CQI algorithm.

7.1.1 Greedy-CQI

The ϵ-Greedy algorithm achieves the exploration by reporting CQI randomly with probability ϵ and achieves exploitation by reporting the CQI with highest estimated throughput with probability $1 - \epsilon$. See Algorithm 6. Clearly, if ϵ is kept fixed, the regret R_n will not decrease to zero. It is shown in [79] that $\epsilon = C/n$ is sufficient to produce $O(\log(n))$ regret for some properly chosen C. By modifying the Chernoff-Hoeffding bound, we proved that the modified ϵ-Greedy algorithm has a logarithmic regret upper bound.

Theorem 6. *The expected time spent on reporting suboptimal CQIs of the Greedy-CQI algorithm is upper bounded by*

$$\mathbf{E}(T_j(n)) = O(\log(n)) \tag{7.8}$$

for each j.

Proof. See Appendix. $\qquad\square$

Algorithm 6: Greedy-CQI algorithm.

    input: $c > 0$ and $0 < d < \min_{j \neq i^*} \Delta_j$.

1   **for** $n = 1, 2, \ldots$ **do**

2      $\epsilon_n \leftarrow \min \left\{ 1, \frac{cK}{d^2 n} \right\}$.

3   Report CQI $i \sim \begin{cases} \arg\max_j \hat{\mathsf{T}}_j & \text{with probability } 1 - \epsilon_n, \\[2mm] \text{Uniform} & \text{probability } \epsilon_n. \end{cases}$

4   Receive (X_i, Y_i).

5      $\hat{g}_i \leftarrow \hat{g}_i + \frac{1}{n}(X_i - \hat{g}_i)$.

6      $\hat{h}_i \leftarrow \hat{h}_i + \frac{1}{n}(Y_i - \hat{h}_i)$.

7      $\hat{\mathsf{T}}_i \leftarrow \hat{g}_i / \hat{h}_i$.

8   **end**

7.1.2   UCB

The family of Upper Confidence Bound (UCB) algorithms compute a reward upper bound for each arm i by adding a bias factor B_i on top of estimated reward $\hat{r}_i$. The agent then reports the arm with the highest upper bound. Carefully chosen bias factor helps UCB to achieve the exploration-exploration balance. [79] proved a $O(\log(n))$ regret upper bound for UCB-1. By applying lemma (7.26), we can also bound the regret of our throughput maximization problem logarithmically. However, the bound appears to be rather loose. Empirical results suggest that UCB algorithm does not perform well compare to other methods.

7.1.3   Boltzmann-CQI

Boltzmann Exploration, also known as SoftMax method, is an MAB algorithm that reports arms based on the Boltzmann distribution. More specifically, at each

step n, the agent reports arm i with probability

$$p_i = \frac{\exp\left(\frac{\hat{\mathsf{T}}_i}{\tau_n}\right)}{\sum_{j=1}^{K} \exp\left(\frac{\hat{\mathsf{T}}_j}{\tau_n}\right)}, \tag{7.9}$$

where temperature τ_n is a user defined sequence that resembles the temperature parameter in simulated annealing [80–82], and $\hat{\mathsf{T}}_i$ is the estimated conditional throughput for CQI $= i$.

Algorithm 7: Boltzmann-CQI algorithm.

    input: a non-increasing sequence $\tau_n > 0$ for $n = 1, 2, \ldots$.

1 $\hat{\mathsf{T}}_1 = \hat{\mathsf{T}}_2 = \ldots = \hat{\mathsf{T}}_K = 0$.

2 for $n = 1, 2, \ldots$ **do**

3   Report CQI i with probability $p_i = \frac{\exp(\frac{\hat{\mathsf{T}}_i}{\tau_n})}{\sum_{j=1}^{K} \exp(\frac{\hat{\mathsf{T}}_j}{\tau_n})}$ for each $i = 1, \ldots, K$.

         $\epsilon_n \leftarrow \min\left\{1, \frac{cK}{d^2 n}\right\}$.

4   Receive (X_i, Y_i).

5 $\hat{g}_i \leftarrow \hat{g}_i + \frac{1}{n}(X_i - \hat{g}_i)$.

6 $\hat{h}_i \leftarrow \hat{h}_i + \frac{1}{n}(Y_i - \hat{h}_i)$.

7 $\hat{\mathsf{T}}_i \leftarrow \hat{g}_i / \hat{h}_i$.

8 end

7.1.4 TS-CQI

The philosophy of Thompson Sampling (TS) is that the agent should take action a_i with probability p_i that matches the probability of action a_i being optimal. More specifically, let r be the reward, a_i be the ith action, and $\{p(r|a_i, \theta)\}_{i,\theta}$ be some parametric model. At step n, the agent takes action a_i with probability

$$p_i = \int \mathbf{1}\{\mathbf{E}(r \mid a_i, \theta, \mathcal{H}_{n-1}) = \max_j \mathbf{E}(r \mid a_j, \theta, \mathcal{H}_{n-1})\} p(\theta|\mathcal{H}_{n-1}) \, d\theta, \tag{7.10}$$

where $p(\theta|\mathcal{H}_{n-1})$ is the posterior probability of θ given the history $\mathcal{H}_{n-1}$ of all the previous actions and rewards. In general it is difficult to compute p_i. Fortunately we do not need to evaluate the probability explicitly. If we sample θ from the posterior distribution $p(\theta|\mathcal{H}_{n-1})$ and take action

$$a = \arg\max_{a_i} \mathbf{E}(r \mid a_i, \theta, \mathcal{H}_{n-1}), \tag{7.11}$$

then the probability of taking action a_i will be exactly p_i. This simple rule can be interpreted as performing a one-sample Monte Carlo simulation of (7.10). After getting a reward from the action, the agent update the posterior distribution $p(\theta|\mathcal{H}_n)$ and repeat the same process. TS can be implemented very efficiently if the prior distribution $p(\theta)$ is chosen to be the conjugate prior for the likelihood function $p(r|a_i, \theta)$.

Based on the spirit of the Thompson sampling algorithm, we proposed the TS-CQI algorithm to solve the online throughput maximization problem. We define the posterior throughput at time n as

$$\hat{\mathsf{T}}(n|I_n = i, \boldsymbol{\theta}, \mathcal{H}_{n-1}) = \frac{\sum_{t=1}^{n-1} X_{I_t,t}\mathbb{1}\{I_t = i\} + \mathbf{E}(X_{i,n} \mid \boldsymbol{\theta})}{\sum_{t=1}^{n-1} Y_{I_t,t}\mathbb{1}\{I_t = i\} + \mathbf{E}(Y_{i,n} \mid \boldsymbol{\theta})}, \tag{7.12}$$

where $\theta_{ik} = \Pr(Y_{i,n} = k)$ is the probability that it takes exactly k times for UE to decode a packet of TBS m_i, for $i = 1, \ldots, K$ and $k = 1, \ldots, M$, and $\theta_{i0} = \Pr(X_{i,n} = 0)$ is the probability that the packet of TBS m_i is lost after M transmissions. From (6.4) and (6.5), it is clear that

$$\mathbf{E}(X_{i,n} \mid \boldsymbol{\theta}) = m_i(1 - \theta_{i0}) \tag{7.13}$$

and

$$\mathbf{E}(Y_{i,n} \mid \boldsymbol{\theta}) = \sum_{k=1}^{M} k\theta_{ik} + M\theta_{i0}. \tag{7.14}$$

For each CQI $= i$, the likelihood function $p((X_{i,t}, Y_{i,t})|\boldsymbol{\theta})$ is a categorical distribution with $M + 1$ possible values: $(m_i, 1), \ldots (m_i, M)$ and $(0, M)$. It is natural to choose the prior distribution $p(\boldsymbol{\theta}) \sim \prod_i \text{Dir}(\boldsymbol{\alpha}_i)$ to be the Dirichlet distribution with the hyperparameter $\boldsymbol{\alpha}_i = [\alpha_{i0}, \ldots, \alpha_{iM}]$ [83–85]. The hyperparameter $\alpha_{ik} - 1$ represents the number of the occurrence that it takes k transmissions to decode a packet of size m_i for $k = 1, \ldots, M$, and $k = 0$ represents the event that the packet is lost. The hyperparameters can be selected according to our prior knowledge. If such information is not available, we can initialize $\alpha_{ik} = 1$ for all i and k. We summarize the TS algorithm in Algorithm 8.

Algorithm 8: TS-CQI algorithm.

    input: α_{ik} for $i = 1, \ldots, K$ and $k = 0, \ldots, M$.

1 $\hat{\mathsf{T}}_1 = \hat{\mathsf{T}}_2 = \ldots = \hat{\mathsf{T}}_K = 0$.

2   **for** $n = 1, 2, \ldots$ **do**

3   **for** $i = 1, 2, \ldots, K$ **do**

4   Sample $[\theta_{i0}, \theta_{i1}, \ldots, \theta_{iM}] \sim \text{Dir}(\boldsymbol{\alpha}_i)$ for $i = 1, \ldots, K$.

5   Compute $X_i = m_i(1 - \theta_{i0})$ and $Y_i = \sum_{k=1}^{M} k\theta_{ik} + M\theta_{i0}$.

6 $\hat{\mathsf{T}}_i \leftarrow \frac{\sum_{t=1}^{n-1} X_{I_t,t} 1\{I_t = i\} + X_i}{\sum_{t=1}^{n-1} Y_{I_t,t} 1\{I_t = i\} + Y_i}$.

7   **end**

8   Report CQI $i = \arg\max_j \hat{\mathsf{T}}_j$.

9   Receive (X_i, Y_i).

10 $\alpha_{iY_i} \leftarrow \begin{cases} \alpha_{iY_i} + 1 & \text{if } X_i \neq 0, \\ \alpha_{i0} + 1 & \text{otherwise.} \end{cases}$

11 **end**

7.2   Online algorithm for constrained maximization

In this section, we consider the online algorithm for the throughput maximization problem (6.40) with the first BLER constraint $\bar{B}_1 = \beta$ for some $\beta \in (0, 1)$.

The main challenge of the online constrained problem (6.40) is that the space of actions $\mathcal{A}$ is an uncountable set, where each action is a CQI distribution with two atoms $\{i, j\} \subset \{1, 2, \ldots, K\}$. Contrary to the unconstrained problem, where the optimal CQI distribution is degenerative, the space of action is isomorphic to the finite set $\{1, 2, \ldots, K\}$.

A suboptimal strategy is to consider some finite subspace $\mathcal{B} \subset \mathcal{A}$ and apply a MAB algorithm on $\mathcal{B}$. However, it is not clear how to properly select a subspace $\mathcal{B}$, and the algorithm will almost never find the optimal solution.

Another challenge of applying MAB methodology to the constrained problem is that there is no natural notion of regret, because we not only want to maximize the throughput but also want to keep BLER at a certain level. A plausible approach may be adding the deviation of the first BLER $\bar{B}_1$ from the target β as a penalty term to the throughput. More specifically, we define the penalized throughput at time n to be

$$\bar{\mathsf{T}}^{(\phi)}(n) = \bar{\mathsf{T}}(n) - \phi\left(\bar{B}_1(n) - \beta\right), \tag{7.15}$$

where $\bar{\mathsf{T}}(n)$ is the expected throughput (7.2) without penalty, and ϕ is some non-negative penalty function continuous at 0 that satisfies $\phi(0) = 0$, and

$$\bar{B}_1(n) = \frac{\sum_{t=1}^{n} 1\{Y_{I_t,t} > 1\}}{n} \tag{7.16}$$

is the average first BLER up to time n. The penalized regret is defined as

$$R_n^{(\phi)} = \mathsf{T}_c^* - \mathsf{T}^{(\phi)}(n), \tag{7.17}$$

where T_c^* is the constrained optimal throughput (6.53). Thus, for any nontrivial penalty function, if an algorithm has zero penalized regret, the throughput $\bar{\mathsf{T}}$ must converge to T_c^* and the BLER must converge to β.

In this section, we propose the Greedy-LP algorithm, which has zero penalized-

regret, and the CQI distribution converges to the optimal distribution.

7.2.1 Greedy-LP

Based on the spirit of ϵ-Greedy algorithm, we propose the Greedy-LP algorithm, which performs exploration by randomly reporting CQI with a diminishing probability ϵ_n and performs exploitation by reporting CQI with probability distribution $\hat{\boldsymbol{f}}_n$, which is the solution to the linear program (6.47) using the estimated problem data $(\hat{\boldsymbol{g}}_n, \hat{\boldsymbol{h}}_n, \hat{\boldsymbol{b}}_n)$.

More specifically, let

$$S = L(\boldsymbol{g}, \boldsymbol{h}, \boldsymbol{b}, \beta) \tag{7.18}$$

be the set of optimal solutions to (6.47) with data $(\boldsymbol{g}, \boldsymbol{h}, \boldsymbol{b})$. At each step n, UE estimated the problem data $\hat{\boldsymbol{g}}_n = [\hat{g}_i(n)]_i$, $\hat{\boldsymbol{h}}_n = [\hat{h}_i(n)]_i$ and $\hat{\boldsymbol{b}}_n = [\hat{b}_i(n)]_i$ from the history $\mathcal{H}_{n-1}$ by

$$\hat{g}_i(n) = \frac{\sum_{t=1}^{n-1} X_{i,t} 1\{I_t = i\}}{T_i(n-1)}, \tag{7.19}$$

$$\hat{h}_i(n) = \frac{\sum_{t=1}^{n-1} Y_{i,t} 1\{I_t = i\}}{T_i(n-1)}, \tag{7.20}$$

$$\hat{b}_i(n) = \frac{\sum_{t=1}^{n-1} 1\{Y_{i,t} > 1, I_t = i\}}{T_i(n-1)}, \tag{7.21}$$

and compute a CQI distribution $\hat{\boldsymbol{f}}_n \in L(\hat{\boldsymbol{g}}_n, \hat{\boldsymbol{h}}_n, \hat{\boldsymbol{b}}_n, \beta)$. With probability $1 - \epsilon_n$, the UE reports a CQI by sampling the distribution $\hat{\boldsymbol{f}}_n$. Otherwise the UE reports

100

a CQI randomly. See Algorithm 9.

Algorithm 9: Greedy-LP algorithm.

    input: Target first BLER $\beta \in (0,1)$.

            A non-increasing sequence $0 < \epsilon_n \leq 1$ for $n = 2, 3, \ldots$.

            Initial problem data $\hat{\boldsymbol{g}} = [\hat{g}_i]_i$, $\hat{\boldsymbol{h}} = [\hat{h}_i]_i$ and $\hat{\boldsymbol{b}} = [\hat{b}_i]_i$.

1 **for** $n = 1, 2, \ldots$ **do**

2   Report CQI $i \sim \begin{cases} \hat{\boldsymbol{f}} \in L(\hat{\boldsymbol{g}}, \hat{\boldsymbol{h}}, \hat{\boldsymbol{b}}) & \text{with probability } 1 - \epsilon_n, \\ \text{Uniform} & \text{probability } \epsilon_n. \end{cases}$

3   Receive (X_i, Y_i).

4      $\hat{g}_i \leftarrow \hat{g}_i + \frac{1}{n}(X_i - \hat{g}_i)$.

5      $\hat{h}_i \leftarrow \hat{h}_i + \frac{1}{n}(Y_i - \hat{h}_i)$.

6      $\hat{b}_i \leftarrow \hat{b}_i + \frac{1}{n}(\mathbb{1}\{Y_i > 1\} - \hat{h}_i)$.

7 **end**

Note that there is no need to use a general purpose linear program solver to find the estimated CQI distribution $\hat{\boldsymbol{f}}_n$. The UE can use the explicit formula (6.54) to compute $\hat{\boldsymbol{f}}_n$, where the support of the distribution is $(i^*, j^*) = \arg\max_{i,j} \mathsf{T}_{ij}$. Thus, at each step the UE only needs to maintain a sorted list of $\{\mathsf{T}_{ij}\}_{ij}$ and extract the index (i^*, j^*) of the maximum element to find the support of the distribution $\hat{\boldsymbol{f}}_n$. Since there are only K elements in $\{\mathsf{T}_{ij}\}_{ij}$ get changed at each step, maintaining a sorted list can be done efficiently using merge sort.

One caveat of this approach is that the solution to a linear program is in general not continuous with respect to the problem data, which means a small perturbation in the estimated problem data may lead to an abrupt jump of the solution [86]. Fortunately, if the underlying linear program is regular (both the primal and dual problem has nonempty and bounded optimal set), then the estimated CQI distribution $\hat{\boldsymbol{f}}_n$ does converge to the optimal distribution $\boldsymbol{f}^*$ as UE collects more samples. We state the result formally in Theorem 7.

Theorem 7. *If both the linear program (6.28) and its dual has nonempty and*

bounded optimal set, then the Greedy-LP has zero penalized-regret (7.17), and the distribution $\hat{\boldsymbol{f}}_n$ converges almost surely to the optimal distribution $\boldsymbol{f}^*$.

Proof. The main idea of the proof is that the estimated problem data $(\hat{\boldsymbol{g}}_n, \hat{\boldsymbol{h}}_n, \hat{\boldsymbol{b}}_n)$ will converge to the actual value $(\boldsymbol{g}, \boldsymbol{h}, \boldsymbol{b})$ under appropriate assumptions. By a continuity result of linear programing due to Robinson, the estimated CQI distribution $\hat{\boldsymbol{f}}_n$ converges to the optimal distribution $\boldsymbol{f}^*$. Consequently, the average throughput will converge to the optimal throughput and the BLER will converge to β.

First we will show that the estimated problem data converge to the actual problem data. Let $\bar{g}_i(k) = \frac{\sum_{t=1}^{k} X_{i,t}}{k}$, $\bar{h}_i(k) = \frac{\sum_{t=1}^{k} Y_{i,t}}{k}$ and $\bar{b}_i(k) = \frac{\sum_{t=1}^{k} 1\{Y_{i,t} > 1\}}{k}$. Clearly $\bar{g}_i(k)$, $\bar{h}_i(k)$ and $\bar{b}_i(k)$ converge almost surely to g_i, h_i and b_i, respectively, as k goes to infinity. Let $\{I_t^R = i\}$ be the event that CQI $= i$ at time t due to exploration, i.e. $\Pr(I_t^R = i) = \epsilon_t/K$, and $T_i^R(n) = \sum_{t=1}^{n} 1\{I_t^R = i\}$. Clearly we have $T_i^R(n) \leq T_i(n)$ for each i and n. As a result of Borel-Cantelli lemma, $T_i^R(n) \to \infty$ almost surely because the events $\{I_t^R = i\}$ are independent and $\sum_{t=1}^{\infty} \epsilon_t = \infty$. This implies $T_i(n) \to \infty$ almost surely. Thus $\hat{g}_i(n) = \bar{g}_i(T_i(n-1))$ converges to g_i for each i, which implies that $\hat{\boldsymbol{g}}_n$ converges almost surely to $\boldsymbol{g}$. Similarly $\hat{\boldsymbol{h}}_n \to \boldsymbol{h}$ and $\hat{\boldsymbol{b}}_n \to \boldsymbol{b}$.

Secondly, we will show the estimated CQI distribution $\hat{\boldsymbol{f}}_n$ converges to the optimal distribution $\boldsymbol{f}^*$. By assumption, the original linear program and its dual problem has nonempty and bounded optimal set (known as the regularity condition), from Robinson [87, Theorem 1], there exist an $\epsilon_0 > 0$ and some number K such that $d(\hat{\boldsymbol{f}}_n, S) \leq K\epsilon$ whenever $\max\{\|\hat{\boldsymbol{g}}_n - \boldsymbol{g}\|, \|\hat{\boldsymbol{h}}_n - \boldsymbol{h}\|, \|\hat{\boldsymbol{b}}_n - \boldsymbol{b}\|\} \leq \epsilon < \epsilon_0$. That is, the estimated CQI distribution can be made arbitrarily close to an optimal distribution if the estimated problem data is close enough to the actual problem data. Here $d(x, A) = \inf\{d(x, y) \mid y \in A\}$ denotes the shortest distance from a point x to a set A.

Finally, note that $\mathbf{E}(X_{I_n,n}) = \boldsymbol{g}^T(\epsilon_n \mathbf{1}^T/K + (1 - \epsilon_n)\mathbf{E}(\hat{\boldsymbol{f}}_n))$ is bounded between 0 and the max TBS m_K. Since $\hat{\boldsymbol{f}}_n$ converges to $\boldsymbol{f}^*$ a.s. and $\epsilon_n \to 0$, the expected value $\mathbf{E}(X_{I_n,n})$ will converge to $\boldsymbol{g}^T\boldsymbol{f}^*$. By Kolmogorov's strong law, $\sum_{t=1}^n X_{I_t,t}/n \to \boldsymbol{g}^T\boldsymbol{f}^*$ almost surely. Similarly, $\sum_{t=1}^n 1\{Y_{I_t,t} > 1\}/n \to \beta$ and $\sum_{t=1}^n X_{I_t,t}/n \to \boldsymbol{h}^T\boldsymbol{f}^*$ almost surely as n goes to infinity. This implies the penalized-regret converges to zero almost surely. □

It is not difficult to see that our problem is regular: the primal problem (ref) has a nonempty and bounded optimal set because the problem is feasible and has bounded feasible region. This is the consequence of $\boldsymbol{h} \geq \mathbf{1}$ and $\boldsymbol{b} - \beta\mathbf{1}$ has both positive and negative components. On the other hand, in order for the dual problem of (ref) to have an unbounded optimal set, we must have $B_1(m_i) = \beta$ for all $i = 1, 2, \ldots, K$, which almost never happens.

7.3 Simulation

We apply the Greedy-CQI, Boltzmann-CQI and TS-CQI algorithms developed in section 7.1 to the unconstrained throughput maximization problem (6.18), and apply the Greedy-LP algorithm developed in section 7.2 to the constrained throughput maximization problem (6.40). We consider the AWGN, VA30 and VA120 channel models, with SNR ranges from 0dB to 20dB.

Note that these algorithms are applicable whenever the instantaneous SNR satisfies the independence condition (6.14). We assume the maximum number of packet re-transmission is 4, which means $M = 5$. During the initialization phase, the UE will report CQI from 1 to 30 once to get an coarse estimate of the conditional throughput for each CQI.

7.3.1 Unconstrained throughput maximization

The performance metric R_n/T^* is the throughput regret (7.3) normalized by the optimal throughput T^* (6.38). For Greedy-CQI, we choose $c = d = 10$. For Boltzmann-CQI, we choose the temperature sequence $\tau_n = 50$ for all n. For TS-CQI, we choose the prior distribution to be Dirichlet with zero pseudo-counts. We average over 5,000 realizations. The error bars indicates the interquartile range.

Under AWGN, Boltzmann-CQI outperforms other tested algorithms by a large margin. It has less than 0.5% of normalized regret across the whole geometry range after 1000 new packet transmissions. See Fig. 7.1.
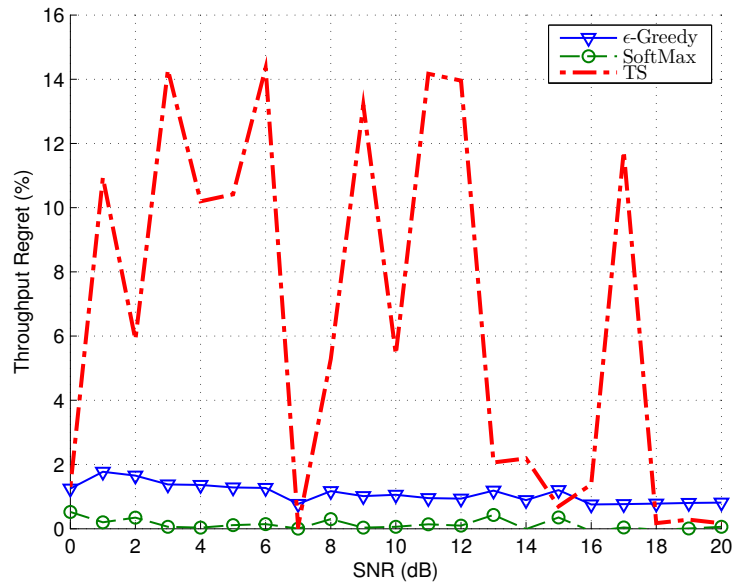

Figure 7.1: Average throughput regret after 1000 new packet transmissions under AWGN.

The throughput regret for Greedy-CQI is under 2% for all geometries. TS-CQI performs the worst. In some geometries, TS-CQI has regret comparable to Boltzmann-CQI, but in general its normalized average regret can be as high as 15%.

TS-CQI performs much better under VA30 and VA120, see Fig. 7.2 and Fig. 7.3, respectively.
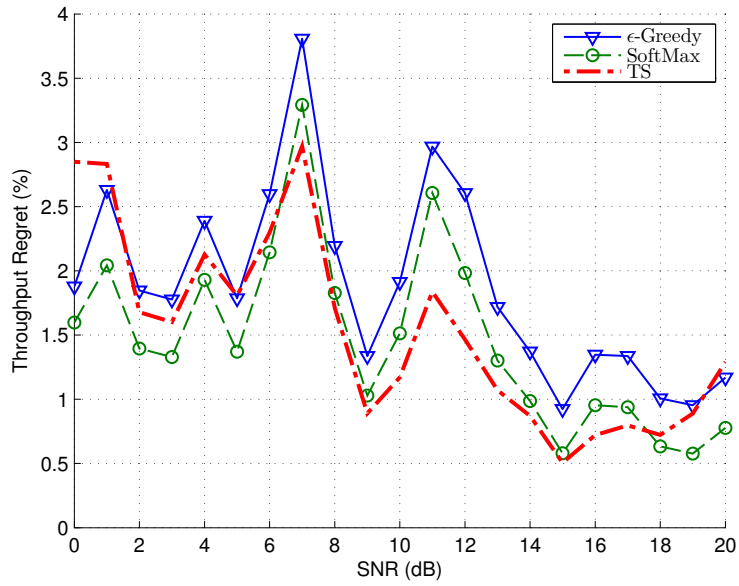
Figure 7.2: Average normalized regret after 1000 new packet transmissions under VA30. Error bar indicates interquartile range.
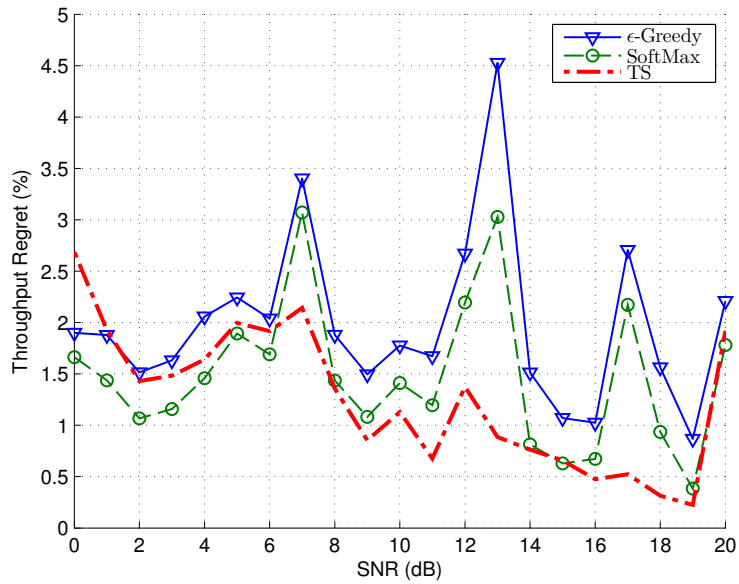

Figure 7.3: Average normalized regret after 1000 new packet transmissions under VA120.

In fact, from middle to high geometry, TS-CQI has the lowest regret among the tested algorithms. We plot the throughput for each algorithms over time in Fig. 7.4 under VA30 15dB. It can be seen that TS behaves more exploratory in

the beginning and learns about the optimal CQI very quickly after about 100 new packet transmissions.
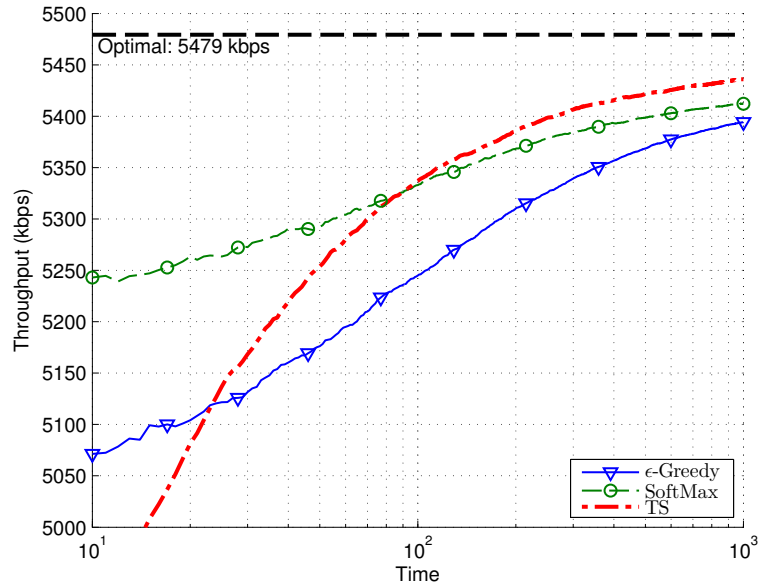
Figure 7.4: The throughput over time under VA30 15dB for each algorithms. The gap between the throughput of each algorithm and the optimal throughput is the throughput regret.

7.3.2 BLER constrained throughput maximization

We set the target first BLER to be $\beta = 0.1$. The performance metric $R_n^{(\phi)}/\mathsf{T}_c^*$ is the penalized regret (7.17) normalized by the constrained optimal throughput (6.53), where the penalty function is defined as

$$\phi(x) = x\mathsf{T}_c^* 1\{x > 0\}. \tag{7.22}$$

Results are averaged over 1,000 realizations. The BLER curve converges to $\beta = 10\%$ at around the 100th packet transmission.
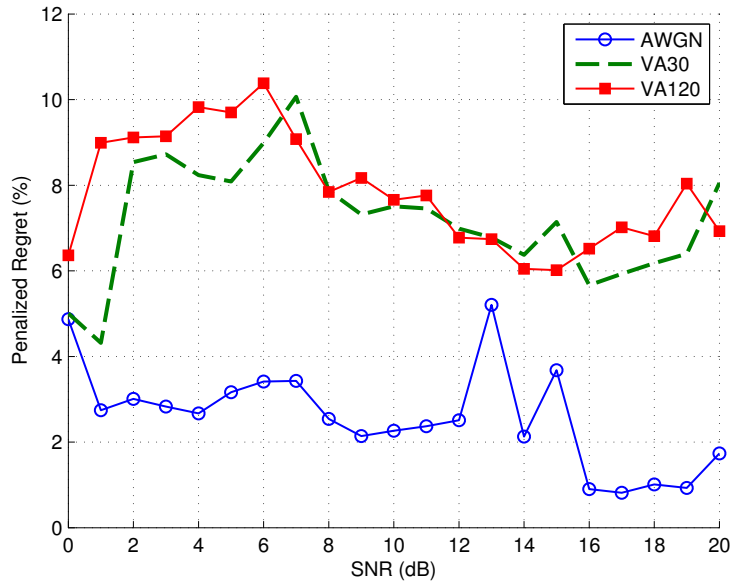
Figure 7.5: The penalized average regret at the 1,000th packet transmission for AWGN, VA30 and VA120.
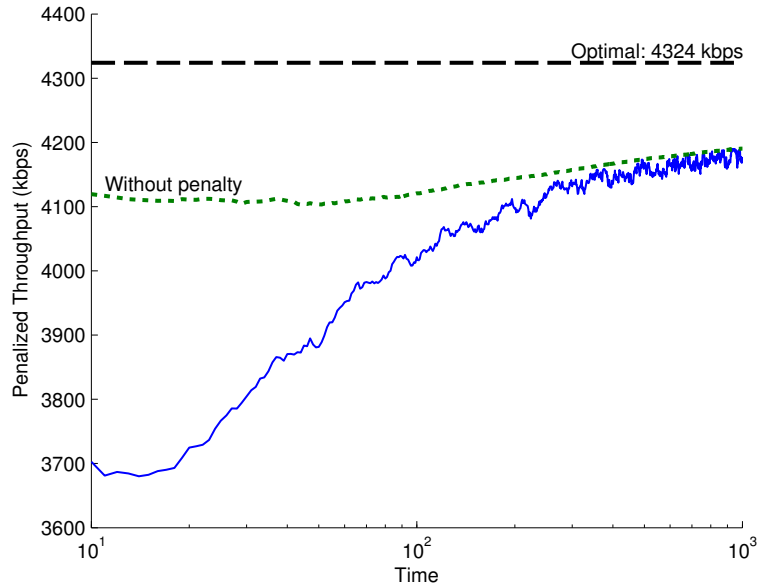
Figure 7.6: The penalized throughput $\mathsf{T}^{(\phi)}(n)$ over time under VA120 14dB. The penalized throughput (solid curve) is the throughput without penalty (dotted curve) minus the penalty function ϕ. The gap between them is proportional to the deviation between the target BLER β and the actual BLER $\bar{B}_1(n)$. As number of sample increases, Greedy-LP produces CQI distribution that has BLER very close to the 10% target, hence the gap is diminishing.

107

7.4 Conclusion

In this paper, we investigated the UE throughput maximization problem. We characterized the optimal CQI reporting scheme for both the unconstrained and the BLER constrained scenario under the independent channel condition. We derived the optimal solution as a function of channel statistics and UE's decoding capability. In practice, these conditions are unknown a priori and need be learned online. We proposed using the multi-armed bandit framework to study the trade-off between learning the conditional throughput of each CQI and exploiting the throughput maximizing CQI. We presented three algorithms, Greedy-CQI, Boltzmann-CQI and TS-CQI to solve the unconstrained online throughput maximizing problem, and we also provided a regret upper bound for the Greedy-CQI algorithm. For the BLER constrained throughput maximization problem, we presented the Greedy-LP algorithm and proved that it has zero penalized regret. From our extensive simulations, we found that Boltzmann-CQI algorithm can achieve up to 99% of optimal throughput for all test cases after 1000 new packet transmission and more than 95% of optimal throughput after 100 new packet transmissions. The Greedy-LP can achieve 90%-99% of the optimal throughput while satisfying the BLER constrain.

7.5 Appendix

Lemma 1. *Suppose $\{(X_i, Y_i)\}_{i=1}^{\infty}$ are pairs of i.i.d. random variables with mean (μ_X, μ_Y). $X_i \in [0, m]$ and $Y_i \in \{1, 2, \ldots, M\}$. Let $S_X = \sum_{i=1}^{n} X_i$ and $S_Y = \sum_{i=1}^{n} Y_i$. For all $n \in \mathbb{N}$ and $\delta > 0$, the following bound holds:*

$$\Pr\left(\frac{S_X}{S_Y} \geq \frac{\mu_X}{\mu_Y} + \delta\right) \leq \exp\left(-\frac{2\delta^2 n}{M^2(m+\delta)^2}\right). \tag{7.23}$$

Proof. Define $Z_i = X_i - \gamma Y_i$ and $S_Z = \sum_{i=1}^{n} Z_i$. Note that $Z_i \in [-M\gamma, m - \gamma]$

108

almost surely.

$$\Pr\left(\frac{S_X}{S_Y} \geq \gamma\right) = \Pr(\overbrace{S_X - \gamma S_Y}^{S_Z} \geq 0) \tag{7.24}$$

$$= \Pr(S_Z - \mathbf{E}(S_Z) \geq -\mathbf{E}(S_Z)) \tag{7.25}$$

$$\leq \exp\left(-\frac{2n^2(\mu_X - \gamma\mu_Y)^2}{n(m + \gamma(M-1))^2}\right) \tag{7.26}$$

$$= \exp\left(-\frac{2n\mu_Y^2\delta^2}{(m + \gamma(M-1))^2}\right) \tag{7.27}$$

$$\leq \exp\left(-\frac{2n\delta^2}{M^2(m+\delta)^2}\right). \tag{7.28}$$

The inequality (7.26) follows from Chernoff-Hoeffding bound. By substituting $\gamma = \frac{\mu_X}{\mu_Y} + \delta$ and use the fact that $\mu_Y \geq 1$ and $\mu_X \leq m$, we get (7.28). $\qquad\square$

CHAPTER 8

Conclusion

In this dissertation, we considered the exceedingly general spherically invariant random process (SIRP) as a unifying framework for studying the wireless communication fading channels. We showed that the family of SIRP distributions is the entropy maximizer under the spherical invariant constraint. We proposed the use of Fox H-functions to parameterize the family of SIRP distributions. This allowed us to express many important distributions by a simple parametric form, such as Weibull, Nakagami-m and Generalized Gamma distributions. In addition, we studied the important issue of modeling uncertainty, where only limited knowledge of the underlying fading channel statistics is known. The moment space methodology was proposed to characterize the uncertainty range of the system performance. Using the SIRP decomposition, we transformed the infinite dimensional optimization problem into a univariate moment problem, which can be solved by performing a series of numerical integrations.

Since Monte Carlo simulation is widely used for numerical integration, we introduce the Super-Efficient Monte Carlo simulation methodology to improve the convergence rate of Monte Carlo simulation. While conventional Monte Carlo simulation yields the convergence rate $1/N$, our Super-Efficient Monte Carlo simulation has a superior convergence rate $1/N^2$ for integrands of the Super-Efficient type. However, we do not often see Super-Efficient integrands. We thus introduce the concept of Approximate Super-Efficient (ASE) and proposed the Progressive ASE algorithm. The Progressive ASE algorithm is applicable to general inte-

grands, and yields near super-efficient convergence rate. Furthermore, we proved the necessary and sufficient condition for Super-Efficiency using the concept of Lebesgue spectrum from the ergodic theory; and designed an efficient numerical method to generate chaotic sequences. It is of great interest to find more applications to exploit the concept of Super-Efficiency and the Progressive ASE algorithm.

Finally, as an application to the moment space methodology, we studied the downlink throughput maximization problem in cellular networks. We proved that the optimal channel feedback strategy under fast fading channels is memoryless and derived an explicit formula for its probability mass function. Inspired by the multi-armed bandit problem, we proposed several algorithms to solve the online version of the throughput maximization problem, and provided convergence analysis. The proposed algorithms achieved up to 99% of the performance upper bound within 1000 new packet transmissions.

References

[1] K. Y. Ezio Biglieri and C.-A. Yang, "Fading models from spherically invariant processes," *Communications, IEEE Transactions on*, p. to appear, 2015.

[2] C.-A. Yang, K. Yao, and E. Biglieri, "Superefficient monte carlo simulations," in *Simulation Technologies in Networking and Communications: Selecting the Best Tool for the Test* (S. K. Al-Sakib Khan Pathan, Muhammad Mostafa Monowar, ed.), ch. 3, pp. 69–93, CRC Press, Taylor & Francis, October 2014.

[3] F. Yilmaz and M.-S. Alouini, "A unified mgf-based capacity analysis of diversity combiners over generalized fading channels," *Communications, IEEE Transactions on*, vol. 60, pp. 862–875, March 2012.

[4] F. Yilmaz and M.-S. Alouini, "A novel unified expression for the capacity and bit error probability of wireless communication systems over generalized fading channels," *Communications, IEEE Transactions on*, vol. 60, pp. 1862–1876, July 2012.

[5] K. Yao, "A representation theorem and its applications to spherically-invariant random processes," *Information Theory, IEEE Transactions on*, vol. 19, pp. 600–608, Sep 1973.

[6] K. Yao, "Spherically invariant random processes: Theory and applications," in *Communications, Information and Network Security* (V. K. Bhargava, H. V. Poor, V. Tarokh, and S. Yoon, ed.), pp. 315–331, Springer, 2003.

[7] K. Umeno, "Chaotic monte carlo computation: A dynamical effect of random-number generations," *Japanese Journal of Applied Physics*, vol. 39, pp. 1442–1456, Mar. 2000.

[8] I. Blake and J. B. Thomas, "On a class of processes arising in linear estimation theory," *Information Theory, IEEE Transactions on*, vol. 14, pp. 12–16, Jan 1968.

[9] A. Vershik, "Some characteristic properties of gaussian stochastic processes," *Theory of Probability & Its Applications*, vol. 9, no. 2, pp. 353–356, 1964.

[10] G. Wise and J. Gallagher, N.C., "On spherically invariant random processes (corresp.)," *Information Theory, IEEE Transactions on*, vol. 24, pp. 118–120, Jan 1978.

[11] H. Brehm, *Combinatorial Theory*, vol. 969 of *Lecture Notes in Mathematics*, ch. Description of spherically invariant random processes by means of g-functions, pp. 39–73. Springer Berlin Heidelberg, 1982.

[12] R.-Z. Li, K.-T. Fang, and L.-X. Zhu, "Some qq probability plots to test spherical and elliptical symmetry," *Journal of Computational and Graphical Statistics*, vol. 6, no. 4, pp. 435–450, 1997.

[13] A. Gualtierotti, "Some remarks on spherically invariant distributions," *Journal of Multivariate Analysis*, vol. 4, no. 3, pp. 347–349, 1974.

[14] S. T. Huang, *Nonlinear analysis of spherically invariant processes and its ramifications.* PhD thesis, University of North Carolina at Chapel Hill, September 1975.

[15] S. T. Huang and S. Cambanis, "Spherically invariant processes: Their nonlinear structure, discrimination, and estimation," *Journal of Multivariate Analysis*, vol. 9, pp. 59–83, March 1979.

[16] T. W. Anderson and K.-T. Fang, "On the theory of multivariate elliptically contoured distributions and their applications," Tech. Rep. 54, Dept. of Statistics, Stanford University, May 1982.

[17] J. P. Burg, *Maximum Entropy Spectral Analysis.* PhD thesis, Stanford University, May 1975.

[18] T. M. Cover and J. A. Thomas, *Elements of Information Theory (Wiley Series in Telecommunications and Signal Processing).* New York: Wiley-Interscience, 2006.

[19] P. Halmos, *Measure Theory.* Graduate Texts in Mathematics, Springer New York, 1976.

[20] R. Muirhead, *Aspects of Multivariate Statistical Theory.* Wiley Series in Probability and Statistics, Wiley, 2005.

[21] K. Zografos, "On maximum entropy characterization of pearson's type ii and vii multivariate distributions," *Journal of Multivariate Analysis*, vol. 71, no. 1, pp. 67–75, 1999.

[22] V. Aalo and J. Zhang, "Average error probability of optimum combining with a co-channel interferer in nakagami fading," in *Wireless Communications and Networking Confernce, 2000. WCNC. 2000 IEEE*, vol. 1, pp. 376–381 vol.1, 2000.

[23] A. Abdi, H. Barger, and M. Kaveh, "Signal modelling in wireless fading channels using spherically invariant processes," in *Acoustics, Speech, and Signal Processing, 2000. ICASSP '00. Proceedings. 2000 IEEE International Conference on*, vol. 5, pp. 2997–3000 vol.5, 2000.

[24] R. W. Grubbström and O. Tang, "The moments and central moments of a compound distribution," *European Journal of Operational Research*, vol. 170, no. 1, pp. 106–119, 2006.

[25] J. Bilmes, "A gentle tutorial of the em algorithm and its application to parameter estimation for gaussian mixture and hidden markov models," tech. rep., International Computer Science Institute, Berkeley, CA, April 1998.

[26] G. McLachlan and T. Krishnan, *The EM algorithm and extensions*, vol. 382. John Wiley & Sons, 2007.

[27] G. McLachlan and D. Peel, *Finite mixture models.* John Wiley & Sons, 2004.

[28] M. Patzold, U. Killat, and F. Laue, "An extended suzuki model for land mobile satellite channels and its statistical properties," *Vehicular Technology, IEEE Transactions on*, vol. 47, pp. 617–630, May 1998.

[29] P. Butzer and S. Jansche, "A direct approach to the mellin transform," *Journal of Fourier Analysis and Applications*, vol. 3, no. 4, pp. 325–376, 1997.

[30] M.-J. Ho and G. Stuber, "Co-channel interference of microcellular systems on shadowed nakagami fading channels," in *Vehicular Technology Conference, 1993., 43rd IEEE*, pp. 568–571, IEEE, 1993.

[31] B. M. Project, H. Bateman, A. Erdélyi, and U. S. O. of Naval Research, *Tables of Integral Transforms: Based, in Part, on Notes Left by Harry Bateman.* No. v. 2 in Tables of Integral Transforms: Based, in Part, on Notes Left by Harry Bateman, McGraw-Hill, 1954.

[32] R. J. Sasiela, *Electromagnetic wave propagation in turbulence: evaluation and application of Mellin transforms*, vol. PM171 of *SPIE Press Monograph.* SPIE Publications, 2 ed., May 2007.

[33] M. Yacoub, "The κ-μ distribution and the η-μ distribution," *Antennas and Propagation Magazine, IEEE*, vol. 49, pp. 68–81, Feb 2007.

[34] J. F. Paris, "Statistical characterization of κ-μ shadowed fading," *Vehicular Technology, IEEE Transactions on*, vol. 63, no. 2, pp. 518–526, 2014.

[35] X. Wang and N. C. Beaulieu, "Switching rates of two-branch selection diversity in κ-μ and α-μ distributed fadings," *Wireless Communications, IEEE Transactions on*, vol. 8, pp. 1667–1671, April 2009.

[36] J. Proakis, *Digital Communications.* McGraw-Hill series in electrical and computer engineering : communications and signal processing, McGraw-Hill, 2001.

[37] A. A. Kilbas, *H-transforms: Theory and Applications.* CRC Press, 2004.

[38] H. Soury, F. Yilmaz, and M.-S. Alouini, "Average bit error probability of binary coherent signaling over generalized fading channels subject to additive generalized gaussian noise," *Communications Letters, IEEE*, vol. 16, pp. 785–788, June 2012.

[39] H. Soury, F. Yilmaz, and M.-S. Alouini, "Error rates of m-pam and m-qam in generalized fading and generalized gaussian noise environments," *Communications Letters, IEEE*, vol. 17, pp. 1932–1935, October 2013.

[40] Y. A. Brychkov, O. Marichev, and A. Prudnikov, "Integrals and series, vol 3: more special functions," *Gordon and Breach science publishers*, 1986.

[41] F. Yilmaz and M.-S. Alouini, "Product of the powers of generalized nakagami-m variates and performance of cascaded fading channels," in *Global Telecommunications Conference, 2009. GLOBECOM 2009. IEEE*, pp. 1–8, Nov 2009.

[42] Z. Wang and G. B. Giannakis, "A simple and general parameterization quantifying performance in fading channels," *Communications, IEEE Transactions on*, vol. 51, pp. 1389–1398, August 2003.

[43] E. Biglieri, *Coding for Wireless Channels*. Springer US, 1 ed., 2005.

[44] Y. Dhungana and C. Tellambura, "Uniform approximations for wireless performance in fading channels," *Communications, IEEE Transactions on*, vol. 61, pp. 4768–4779, November 2013.

[45] P. Flajolet, X. Gourdon, and P. Dumas, "Mellin transforms and asymptotics: Harmonic sums.," *Theor. Comput. Sci.*, vol. 144, no. 1&2, pp. 3–58, 1995.

[46] H. White, *Asymptotic theory for econometricians*. Academic press, 2014.

[47] S. Benedetto and E. Biglieri, *Principles of Digital Transmission: With Wireless Applications*. Information Technology: Transmission, Processing and Storage, Springer US, 2006.

[48] S. Cotton and W. Scanlon, "Higher order statistics for the κ-μ distribution," *Electronics Letters*, vol. 43 (22), no. 22, pp. 1215–1217, 2007.

[49] N. Youssef, T. Munakata, and M. Takeda, "Fade statistics in nakagami fading environments," in *Spread Spectrum Techniques and Applications Proceedings, 1996., IEEE 4th International Symposium on*, vol. 3, pp. 1244–1247 vol.3, Sep 1996.

[50] E. Biglieri and N. Alrajeh, "The robustness of coding and modulation for body-area networks," *Communications and Networks, Journal of*, vol. 16, pp. 264–269, June 2014.

[51] I. Ioannou, C. D. Charalambous, and S. Loyka, "Outage probability under channel distribution uncertainty," *Information Theory, IEEE Transactions on*, vol. 58, no. 11, pp. 6825–6838, 2012.

[52] M. G. Kreĭn and A. A. Nudel'man, *The Markov moment problem and extremal problems: ideas and problems of PL Čebyšev and AA Markov and their further development*. American Mathematical Society, 1977.

[53] I. Popescu, "A semidefinite programming approach to optimal-moment bounds for convex classes of distributions," *Mathematics of Operations Research*, vol. 30, pp. 632–657, August 2005.

[54] E. Biglieri, "Probability of error for digital systems with inaccurately known interference (corresp.)," *Information Theory, IEEE Transactions on*, vol. 30, pp. 443–446, Mar 1984.

[55] T. Koch, "Coherent fading channels: The best and the worst fading laws are discrete," tech. rep., ETH, Zürich, Switzerland, 2007.

[56] W. Feller, *An Introduction to Probability Theory and its Applications*, vol. II. Wiley, New York, 1971.

[57] R. Y. Rubinstein, *Simulation and the Monte Carlo method*. Wiley series in probability and mathematical statistics, Wiley, 1981.

[58] K. Yao, "An approximate superefficient mc method is better than classical mc method." An Approximate Superefficient MC Method is Better Than Classical MC Method, 2009.

[59] J. Hammersley and D. Handscomb, *Monte Carlo methods*. Methuen & Co., 1964.

[60] D. E. Knuth, *The Art of Computer Programming, Volume 2 (3rd Ed.): Seminumerical Algorithms*. Boston, MA, USA: Addison-Wesley Longman Publishing Co., Inc., 1997.

[61] M. Matsumoto and T. Nishimura, "Mersenne twister: a 623-dimensionally equidistributed uniform pseudo-random number generator," *ACM Trans. Model. Comput. Simul.*, vol. 8, pp. 3–30, Jan. 1998.

[62] C. Moler, *Numerical Computing with Matlab*. Society for Industrial and Applied Mathematics, 2004.

[63] V. I. Arnol'd, *Ergodic problems of classical mechanics*, vol. 50. New York: Benjamin, 1968.

[64] J. Auslander and J. A. Yorke, "Interval maps, factors of maps, and chaos.," *Tohoku Math. J. (2)*, vol. 32, pp. 177–188, 1980.

[65] A. Lasota and M. Mackey, *Chaos, fractals, and noise: stochastic aspects of dynamics.* Applied mathematical sciences, Springer-Verlag, 1994.

[66] K. Petersen, *Ergodic Theory.* Cambridge Studies in Advanced Mathematics, Cambridge University Press, 1989.

[67] E. Biglieri, "Some notes on "superefficient" monte carlo methods." 2009.

[68] K. Umeno, "Numerical integration equipment, numerical integration method, and program," August 2005.

[69] K. Alligood, T. Sauer, and J. Yorke, *Chaos: An Introduction to Dynamical Systems.* Chaos: An Introduction to Dynamical Systems, New York, NY, 1997.

[70] 3GPP, "Physical layer procedures (fdd)," TS 25.214 version 9.8.0 Release 9, 3rd Generation Partnership Project (3GPP), March 2012.

[71] 3GPP, "Evolved universal terrestrial radio access (e-utra); physical layer procedures," TS 36.213 version 12.5.0 Release 12, 3rd Generation Partnership Project (3GPP), April 2015.

[72] T. Cui, F. Lu, A. Goteti, V. Sethuraman, S. Rao, and P. Subrahmanya, "Throughput optimization in high speed downlink packet access (hsdpa)," in *Communications, 2009. ICC '09. IEEE International Conference on*, pp. 1–5, June 2009.

[73] J. R. Birge and R. J.-B. Wets, "Computing bounds for stochastic programming problems by means of a generalized moment problem," *Mathematics of Operations Research*, vol. 12, no. 1, pp. 149–162, 1987.

[74] E. Bajalinov, *Linear-Fractional Programming Theory, Methods, Applications and Software.* Applied Optimization, Springer US, 2013.

[75] A. Charnes and W. W. Cooper, "Programming with linear fractional functionals," *Naval Research Logistics Quarterly*, vol. 9, no. 3-4, pp. 181–186, 1962.

[76] D. Bertsimas and J. Tsitsiklis, *Introduction to Linear Optimization.* Athena Scientific, 1st ed., 1997.

[77] J. Vermorel and M. Mohri, "Multi-armed bandit algorithms and empirical evaluation," in *Machine Learning: ECML 2005*, pp. 437–448, Springer, 2005.

[78] S. Bubeck and N. Cesa-Bianchi, "Regret analysis of stochastic and non-stochastic multi-armed bandit problems," *arXiv preprint arXiv:1204.5721*, 2012.

[79] P. Auer, N. Cesa-Bianchi, and P. Fischer, "Finite-time analysis of the multiarmed bandit problem," *Machine Learning*, vol. 47, no. 2-3, pp. 235–256, 2002.

[80] N. Cesa-Bianchi and P. Fischer, "Finite-time regret bounds for the multiarmed bandit problem.," in *ICML*, pp. 100–108, Citeseer, 1998.

[81] S. Kirkpatrick, "Optimization by simulated annealing: Quantitative studies," *Journal of statistical physics*, vol. 34, no. 5-6, pp. 975–986, 1984.

[82] V. Černỳ, "Thermodynamical approach to the traveling salesman problem: An efficient simulation algorithm," *Journal of optimization theory and applications*, vol. 45, no. 1, pp. 41–51, 1985.

[83] S. Kotz, N. Balakrishnan, and N. L. Johnson, *Dirichlet and Inverted Dirichlet Distributions*, ch. 49, pp. 485–527. John Wiley & Sons, Inc., 2005.

[84] T. S. Ferguson, "Prior distributions on spaces of probability measures," *The annals of statistics*, pp. 615–629, 1974.

[85] I. J. Good, *The estimation of probabilities: An essay on modern Bayesian methods*, vol. 30. MIT press, 1965.

[86] R. Meyer, *Continuity properties of linear programs.* University of Wisconsin-Madison. Computer Sciences Department, 1979.

[87] S. M. Robinson, "A characterization of stability in linear programming," *Operations Research*, vol. 25, no. 3, pp. 435–447, 1977.